Development and Application of Microfluidic Single-Cell Polymerase Chain Reaction

by

Adam White

B.Sc. (Honours Physics), The University of British Columbia, 2007
M.A.Sc. (Biomedical Engineering), The University of British Columbia, 2010

A THESIS SUBMITTED IN PARTIAL FULFILLMENT OF
THE REQUIREMENTS FOR THE DEGREE OF

Doctor of Philosophy

in

The Faculty of Graduate and Postdoctoral Studies

(Genome Science & Technology)

The University of British Columbia

(Vancouver)

December 2015

Abstract

Methods for single-cell analysis are critical to revealing cell-to-cell variability in biological systems, such as during development or onset of disease, where the characteristics of heterogeneity and minority cell populations are obscured by population-averaged measurements. Analysis of individual cells has been limited due to challenges associated with small amounts of starting material, combined with the cost and throughput required to examine large numbers of cells. Microfluidic approaches are well suited to single-cell analysis, providing increased sensitivity, economy of scale, and automation.

This thesis presents the development and application of microfluidic technology for single cell gene expression analysis. The foundational contribution of this work is an integrated microfluidic device capable of performing high-precision RT-qPCR measurements of gene expression from hundreds of single cells per run. This device executes all steps of single cell processing including cell capture, cell lysis, reverse transcription, and quantitative PCR. This device is further expanded upon by integrating the single cell and nucleic acid processing capabilities with final measurement of cDNA by high-density digital PCR. The direct quantification of single molecules by digital PCR has advantages over RT-qPCR in the measurement of low abundance transcripts, as well as obviating the need for relative abundance measurements or calibration standards. This technology is demonstrated in over 5,000 individual cell measurements of mRNA, microRNA, and single nucleotide variant detection in a variety of cell types. Finally, this technology is applied to study the performance of lipid nanoparticles in delivery of RNA, and manipulation of gene expression in cells. The microfluidic integration of cell and nucleic acid processing established in this thesis permits analysis of hundreds of single cells in parallel, while improving work flow and reducing technical variation compared to samples prepared in microliter volumes. Ultimately, this advances the tools available for precisely measuring transcripts in single cells, and has application in research and clinical settings.

Preface

The work presented in this thesis is part of a collaborative effort to develop and apply microfluidic systems for single cell analysis, and has resulted in co-authored publications.

A version of Chapter 2 has been published: Adam K. White, Michael VanInsberghe, Oleh Petriv, Mani Hamidi, Darek Sikorski, Marco A. Marra, James M. Piret, Sam Aparicio, and Carl L. Hansen, *High-Throughput Microfluidic Single-Cell RT-qPCR*, Proceedings of the National Academy of Sciences, 2011. AKW and MV contributed equally. AKW and MV designed and fabricated microfluidic devices. AKW, MV, OP, and MH performed on-chip experiments and analyzed data. MV developed image analysis code. OP and MH developed OCT4 assays and performed off-chip experiments. DS performed hESC differentiation experiments and mRNA FISH measurements. CLH, SA, MM, and JP designed research. AKW, MV, and CLH wrote the manuscript.

A version of Chapter 3 has been published: Adam K. White, Kevin A. Heyries, Colin Doolin, Michael VanInsberghe, and Carl L. Hansen, *High-Throughput Microfluidic Single-Cell Digital PCR*, Analytical Chemistry, 2013. AKW and KAH contributed equally. CLH designed research. AKW, KAH, CD and MV designed and fabricated devices. AKW, KAH, and CD performed experiments. AKW, KAH, CD, and MV analyzed data. AKW, KAH and CLH wrote the manuscript.

A manuscript for publication based on Chapter 4 is in preparation: *Single Cell Analysis of Lipid Nanoparticle RNA Delivery.* This work is a collaboration with Precision Nanosystems, who provided lipid nanoparticles. I performed all experiments, and designed all experiments with input from Precision Nanosystems (specifically Aysha Ansari, David Zwaenepoel, Colin Walsh, Euan Ramsay and James Taylor) and Carl Hansen. Darek Sikorski and James Piret provided tissue culture support.

Table of Contents

Appendices

List of Figures

Acknowledgements

I would first like to thank my supervisor, Dr. Carl Hansen, who has been a fantastic advisor since the end of my undergraduate degree in Physics, and throughout my graduate degrees in Biomedical Engineering and now Genome Science and Technology. It has been been a long journey! Carl, thank you for supporting my development, and sharing your ambition and passion for excellence. Working with you was a privilege, and I am forever grateful for the many opportunities you provided me to enrich my experience.

I also wish to thank my committee members, Drs. James Piret, Sam Aparicio, and Martin Hirst for their insight and support of my PhD work. Jamie, thank you for your long-time support of my career. I have benefited greatly from your optimism and thoughtful perspectives on everything from experimental design to career and life decisions. I wish to thank Dr. Sam Aparicio for his enthusiasm to harness microfluidic technology for single-cell genomics, and providing many ideas for how microfluidic technology could be used for scientific inquiry. Sincere thanks to Dr. Martin Hirst for his invaluable input since the beginning of this project, and for the scientific rigor he brings to all our discussions. I would also like to thank my collaborator, Dr. Marco Marra, for being one of the visionaries to create the interdisciplinary Genome Science and Technology program, and for his role in pushing microfluidics for single-cell genomics. I am very grateful to NSERC, MSFHR, Genome BC, and CIHR for supporting my research endeavours.

Special thanks to all my colleagues in the Hansen lab over the years for both their friendship and their helpful scientific discussions. In particular, I would like to acknowledge the exceptional team I was part of in developing the microfluidic systems presented in this thesis: Michael VanInsberghe, Kevin Heyries, and Calum Doolin. We shared many failures, but ultimately achieved our goals. Their contribution to this work is enormous. I would like to thank fellow "assassins" Hans Zahn and Georgia Russell for sharing their enthusiasm for single-cell microfluidics. My sincere gratitude is extended Anupam Singhal, Jens Huft, Kaston Leung, Veronique Lecualt,

Darek Sikorski, and Tim Leaver for all their support of my research and life pursuits. We all started around the same time, and it was fun to share in the excitement of building novel devices to solve biological problems. Thank you Bertin Wong, Adam Quiring, Mani Hamidi, Marketa Ricicova, and Oleh Petriv for enriching life in the Hansen lab. It would not have been the same without you. I have also greatly appreciated all the advice I have received from Marijn van Loenhout on careers and navigating academia. Thanks to Darek Sikorski for patiently teaching me how to culture embyronic stem cells, and for that Pearl Jam concert ticket. I would also like to thank Navid Ghaffari, Blanche Lo, Judy Booth, and Chris Sherwood for always making me feel welcome in the Piret lab. Chris, thank you for everything you do to keep the tissue culture facilities working, and all your help in setting up different cell cultures.

Thanks to the fantastic collaborators from Precision Nanosystems: Aysha Ansari, David Zwaenepoel, Colin Walsh, Euan Ramsay and James Taylor. Working with you, I greatly enjoyed taking this project in new directions and learning more about biotechnology entrepreneurship and gene therapy. I particularly want to thank Aysha Ansari for her patience with trying to get primary neurons to work in my microfluidic device.

I would also like to thank Dr. Connie Eaves, Karen Lambie, and Gloria Shaw from the Stem Cell Assay Lab at the BC Cancer Agency for taking a chance on an inexperienced physics co-op student back in 2003. That 8 month experience introduced me to lab work, and greatly contributed to launching me down this interdisciplinary research path.

Thanks to my dear friends Mike, Dana, Paul, Yichwin, Luke, Sabrina, Julia, Emilie, Martha, Ingrid and Sophie for your support despite the distance separating us. Finally, I thank my family: their love and encouragement has been invaluable to my success. I could not have done this without you.

Chapter 1

Introduction[1]

1.1 Introduction

This dissertation describes the engineering and application of novel microfluidic devices for high-throughput single-cell gene expression analysis. In particular, work has focused on the microfluidic integration of components for single-cell handling, nucleic acid processing, and measurement of transcripts by performing reverse transcription followed by polymerase chain reaction (PCR). Considerable advances have been made in developing microfluidic technology for single-cell PCR, and in demonstrating this technology in biological applications benefiting from single-cell analysis. Here I review literature relevant to the development of single-cell gene expression analysis with particular emphasis on microfluidic systems. The specific aims of this thesis are provided at the end of the chapter.

1.2 Why Measure Gene Expression?

The cells of all organisms inherit genetic instructions that govern their behaviour. This complete set of genetic instructions (the genome) is composed of DNA and contains the code for genes. Cell differences arise in part as a result of different genes being actively (or not) expressed. There are also regulatory mechanisms that affect the functionality of an expressed gene. Gene expression is the process by which genetic information is transcribed from DNA into RNA, and this RNA is translated into proteins (or processed into bioactive non-coding RNA). These proteins are chief components of the complicated molecular interactions inside a cell, performing tasks including catalysis of chemical reactions, intra- and extra-cellular signaling, and main-

[1]This chapter is an updated version of the introductory chapter from *Microfluidic Technology for High-Throughput Single Cell Gene Expression Analysis*, by Adam White, University of British Columbia, 2010. This version is updated with references and discussion of recent advancements in microfluidics and single cell analysis.

taining structural integrity. In order to maintain life, the type of proteins, abundance, and timing of gene expression is tightly regulated. A single gene can have profoundly different functions depending on the timing, location, and amount of gene expression [1]. Gene expression is regulated at the levels of transcription, RNA processing, translation, post-translational modifications, and degradation, allowing cells to respond to their environment. The transcriptome, encompassing all RNA transcripts of the cell, represents all proteins that are actively being synthesized and thus provides a unique signature of cell state. Thus, measuring transcripts allows for directly studying cellular processes and variation.

1.3 Transcriptional Variability Between Single Cells

Much of our biomolecular knowledge of cells and cell tissue is the result of gene expression measurements of transcription. However, transcription measurements are traditionally performed on bulk samples of large numbers (thousands to millions) of cells. The transcriptional variability between individual cells is obscured by ensemble averaging. Heterogeneity is an ever present feature of biological systems, and cellular heterogeneity has been observed in cell types ranging from bacteria to mammals. The sources of transcriptional variability between single cells include the stochastic nature of transcription, different stages of cell cycle, differentiation, and disease.

Although heterogeneity between two individual cells can arise through differences in the genome, even isogenetic cells exhibit variability in transcript expression. These differences may occur through several different mechanisms. The molecular kinetics involved in gene expression make it a stochastic process, subject to noise [2, 3]. This results in bursts of expression and apparently random fluctuations that contribute to phenotypic variation through various feedback mechanisms [2, 3].

Gene expression will also naturally vary between cells in different stages of the cell division cycle. Cell division is initiated by external stimuli such as growth factors, and progression through the stages of division is governed by two classes of regulatory molecules, cyclins, and cyclin-dependent kinases [4]. Cyclin-dependent kinases are constitutively expressed in cells whereas cyclins are synthesised at specific stages of the cell cycle [5, 6]. The duration of time spent in different stages of the cell cycle varies, and cell populations divide asynchronously [7]. This asynchronous division

results in transcriptional variability between cells. For this reason many studies often go to great effort to synchronize cell cultures, or arrest cells in a specific phase [5, 8].

Transcriptional variability is also particularly significant in cells undergoing differentiation. Through differentiation, it is hypothesized that stem cells or progenitor cells asymmetrically divide in order to generate many different cell types. For example, a single embryonic stem cell develops into a multicellular organism including muscle cells, brain cells, and skin cells, all of which are characterized by very distinct transcriptional programs. Asymmetric division results in cells that express different genes, giving them different behaviour and diverging fates [9]. In many cases, the phenotype of stem cells and cells undergoing differentiation is not well defined. For example, current state-of-the-art enrichment strategies result in a population of hematopoietic stem cells in which approximately 50% are capable of reconstituting the blood of mice, as determined by a functional assay [10]. Therefore, bulk analysis of hematopoietic stem cells obscures the relevant sub population.

Transcription differences between cells can also arise due to the onset of disease. Diseases such as cancer often have their origin in a single cell [11]. Environmental exposures, or the accumulation of genetic mutations through multiple cell lineages can lead to pronounced heterogeneity in the tumor cells which is manifest as aberrant gene expression [12–14].

1.4 Types of Transcripts Defining Cellular State

The two classes of RNA transcripts that determine cell state are messenger RNA (mRNA), which code for proteins, and non-coding RNA such as microRNA (miRNA) which act as regulators of gene expression.

RNA is transcribed from DNA which is subsequently processed into mRNA, and genetic information is encoded in the sequence of nucleotides. This nucleic acid is translated into protein according to codons, consisting of three bases each, which encode for specific amino acids. mRNA consists of a 5' cap, a coding region containing the codons for translation, 5' and 3' untranslated regions, and a 3' poly-adenine tail. A typical mammalian cell contains thousands of different types of proteins in varying abundance. Proteins involved in metabolic functions, and structural integrity of the cell are generally found in high abundance, and are often referred to as housekeeping genes. Although less abundant, mRNA transcripts also produce proteins involved

in intra- and extracellular signaling, as well as transcription factors. Transcription factors are proteins involved in the process of transcribing DNA into RNA, and play a significant role in regulating gene expression. Transcription factors have DNA-binding domains that give them the ability to bind to specific sequences of DNA called enhancer or promoter sequences. Some transcription factors bind to a DNA promoter sequence near the transcription start site and help form the transcription initiation complex. Other transcription factors bind to regulatory sequences, such as enhancer sequences, and can either stimulate or repress transcription of the associated gene.

Non-coding RNAs such as transfer RNA (tRNA) and ribosomal RNA (rRNA) are known to be essential in translating mRNA into protein. However, several varieties of short, non-coding RNAs such as small nucleolar RNA (snoRNA), and small interfering RNA (siRNA) are increasingly being shown to play important roles in regulating gene expression. In particular, microRNAs (miRNA) have been found to be regulators of gene expression and are drivers in development and cancer [15]. Discovered in 1993, miRNA are a species of small (approximately 22 nucleotides) non-protein coding RNA. Primary miRNA transcripts are transcribed as stemloop structures that are then processed by a protein complex known as the Microprocessor complex (consisting of the nuclease Drosha and the double-stranded RNA binding protein Pasha) into shorter structures [16]. Further processing is performed in the cytoplasm by the endonuclease Dicer, which cleaves the stemloop to form the mature miRNA [16]. Interaction with Dicer initiates the formation of the RNA-induced silencing complex (RISC), responsible for the gene silencing observed due to miRNA expression and RNA interference [16]. This RISC-integrated miRNA strand regulates gene expression by binding to complementary mRNA molecules and inhibiting translation or inducing degradation (by argonaute proteins of the RISC complex). Hundreds of miRNA species are known in humans, and their short sequence length of the critical 5' seed region makes them complementary to hundreds of mRNA transcripts that can potentially be targeted for regulation [17]. Recent research has revealed tissue-specific distributions of miRNAs appearing at different stages of mammalian development. In particular, Chen and colleagues demonstrated that overexpression of a select few miRNAs (e.g. miR-181a) can influence hematopoiesis [18], and Calin et al. provided evidence for miRNA involvement in cancer by determining that miR-15a and miR-16a are down regulated in over 68% of chronic lymphocytic leukemia patients [19].

These findings suggest the potential application of using miRNA expression profiles to identify those miRNAs involved in human cancer development. Importantly for the current work, single cell measurements of miRNA in highly purified cell populations have been found to exhibit low cell-cell variability, suggesting that miRNA may be a very useful biomarker of cellular state [20].

1.5 Techniques for Single Cell Measurements of Gene Expression

Early changes in cell state are first revealed in the transcriptome, where quantitative measurements with single molecule sensitivity are possible by both imaging and RT-PCR techniques. This section reviews the current state-of-the-art for single cell measurements of transcription.

1.5.1 Molecular Imaging

Fluorescent in situ hybridization (FISH) is a technique for detecting specific DNA sequences in fixed cells. FISH uses fluorescent microscopy to image fluorescently labeled probes that bind to DNA with similar sequences. In 1998, Femino et al. modified FISH and digital imaging techniques in order to detect single RNA molecules [21]. Specifically, multiple oligodeoxynucleotide probes were synthesized with five fluorochromes per molecule. The probes, each about 50 nucleotides long, are designed to hybridize to adjacent locations on the mRNA target such that their collective fluorescence becomes visible as a diffraction-limited spot. Single molecules are measured by processing images acquired from a series of focal planes through a hybridized cell. Combinations of these probes labeled with spectrally distinct colours have been used to measure up to 11 genes simultaneously [22]. Raj et al. improved upon this technique by probing each mRNA species with 48 or more short, singly labeled oligonucleotide probes [23], which improved the ability to resolve single transcripts. This technique has been applied in two studies looking at the effect of variable gene expression on cell fate [24] and response [25]. By counting transcripts of the genes in a network in individual *Caenorhabditis elegans* embryos (up to 200-cell stage), Raj et al. showed that the expression of an otherwise redundant gene (*end-1*) becomes highly variable in *skn-1* mutants and that this variation is subjected to a threshold,

producing an ON/OFF expression pattern of the master regulatory gene of intestinal differentiation [25]. Beyond quantifying mRNA in single cells, mRNA-FISH reveals the location of the transcript inside fixed cells [23]. Also, the spatial organization of gene expression among fixed cells can be assessed. Similar hybridization techniques have also been combined with rolling circle amplification for in situ detection of mRNA [26–28].

Although mRNA-FISH has been successfully applied [24, 25, 29], the system has not been widely adopted. One reason for this is the difficulty in synthesizing heavily labeled oligonucleotides [23]. Additionally, mRNA-FISH requires a long protocol involving fixing cells, hybridizing probes, washing unbound probes, and taking stacks of images using fluorescent microscopy. This procedure requires highly specialized and expensive equipment and reagents. Processing the stack of focal plane images requires exhaustive deconvolution and is computationally intensive [23]. Furthermore, it is challenging to unambiguously identify all the fluorescent spots as mRNA molecules as it is impossible to determine whether the detection of an individual probe arises from legitimate binding to the target mRNA or from nonspecific binding [23]. The use of multiple probes bound to a single transcript also presents challenges in distinguishing between closely related sequences. Small RNA species, such as miRNAs, are too short to accommodate multiple probes, making them refractory to analysis by FISH. Throughput of mRNA-FISH is limited by cost, labour intensive protocols, and imaging.

1.5.2 RNA-Sequencing

The deep coverage provided by next-generation sequencing has recently permitted a direct approach to single cell gene expression measurements by sequencing RNA, known as RNA-Seq or whole transcriptome shotgun sequencing (WTSS) [30]. There are many different approaches to RNA-Seq. In one example, mRNA is captured on poly(T) coated magnetic beads prior to reverse transcription. The cDNA is then fragmented, size selected, and sequenced [31]. The deep coverage allows expression levels to be estimated based on the extent to which a sequence is detected [32]. RNA-Seq has recently been applied to single cells of the inner cell mass from human embryonic stem cell development [33]. This study looked at expression dynamics of 385 genes in 74 single cells [33]. Further improvements in instrumentation, bioinformatics approaches, and optimized reagent kits (such as the template-switching method from

Clonetech) [34, 35] are rapidly establishing the coupling of whole transcriptome RNA amplification from single cells with high-throughput sequencing [36–38]. The primary advantage of RNA-Seq is that it permits analysis of much of the transcriptome, particularly mRNAs. The major limitation to this approach is representation bias, which makes RNA-Seq poorly suited to diagnostics or other applications where the abundance of a given molecular species is in question [39]. Further bottlenecks in single cell transcriptome sequencing are cost (although sequencing costs are rapidly dropping), and sample preparation. In one of the early single cell RNA sequencing studies from 2010, small numbers of single cells were laboriously isolated by mouth pipetting[33], limiting high-throughput application. However, droplet-based approaches and flow sorting are increasingly addressing this limitation.

1.5.3 Quantitative PCR Methods

Reverse transcription quantitative polymerase chain reaction (RT-qPCR) provides a powerful and sensitive method for quantitative analysis of transcript levels, and has been extensively applied to single cell analysis [40–47]. RT-qPCR is based on the traditional polymerase chain reaction (PCR), which is a method for specifically and exponentially amplifying DNA starting from as little as a single copy [48]. In RT-qPCR, the first strand of DNA is synthesized from a RNA template through a process called reverse transcription (RT). Oligonuclotides (primers) designed to be complementary to the transcript of interest are used to specifically transcribe the RNA into a complementary DNA (cDNA). After first strand synthesis, real-time quantitative PCR (qPCR) is performed similar to conventional PCR, however a fluorescent reporter probe is added to the reaction. During the annealing stage of the PCR, both probe and primers anneal to the DNA target. A variety of molecular probes have been developed for RT-qPCR including intercalating dyes [49], molecular beacons [50], scorpion probes [51], and hydrolysis probes. Fluorescence (Forster) resonance energy transfer (FRET) probes are perhaps the most commonly used [52]. These probes consist of a dual labeled DNA oligo, having a fluorophore and a quencher at the 5' and 3' ends respectively, that is complementary to an internal region of the amplicon. In close proximity, the quenching molecule prevents detection of the fluorescent molecule by absorbing energy from the reporter through a process called Forster resonance energy transfer (FRET) [53, 54]. Following annealing, the polymerization of a new DNA strand is initiated from the PCR primers. Upon reaching

the oligonuceotide of the probe, the exonuclease activity of the polymerase degrades the probe, physically separating the fluorophore from the quenching moeity, and resulting in an increase in fluorescence. Fluorescence is detected through the use of photodetectors or a charge coupled device (CCD). Monitoring the fluorescent signal of the PCR reaction allows for quantitative measurements of transcript levels [55, 56].

The specificity, sensitivity, dynamic range, and quantitative accuracy make RT-qPCR the most common technique for gene expression analysis [57]. RT-qPCR is sensitive enough to detect transcripts at the level of single cells, and a number of different strategies for single cell RT-qPCR have been reported [40–43, 45–47, 58]. Bengtsson et al. used RT-qPCR to reveal lognormal distributions of mRNA in single cells of pancreatic islets of Langerhans [40]. RT-qPCR is also able to target small RNAs, such as miRNAs, through the use of a stem-loop RT primer that yields a longer cDNA strand for annealing qPCR primers and probes [59]. This stem loop primer system has been used to perform highly multiplexed miRNA transcript measurements in single embryonic stem cells [60, 61]. However, the application of RT-qPCR to large numbers of single cells has been limited in part due to the high cost of probes and reagents. Addtionally, laborious techniques such as mouth pippetting, micropipetting, and FACS are used to isolate single cells for RT-qPCR reactions [45, 46]. The latter, although automated, requires careful optimization and calibration which make it difficult or impossible to confirm single cell capture.

Microfluidic lab-on-chip technology has enabled digital PCR (dPCR), whereby single DNA molecules are quantified by compartmentalizing a sample into thousands of nano- or pico-liter PCR reactions. The sample is diluted such that each reaction chamber has a high probability of containing 1 or 0 molecules. After PCR in the presence of a fluorescent probe, each reaction chamber in the array will be either fluorescent if the PCR reaction was successful, or not fluorescent if the reaction did not occur (i.e. no DNA template present). An end-point image of the array of reaction chambers can be used to detect DNA in a on/off (digital) format. Digital PCR has advantages over conventional quantitative PCR in that the measurement is absolute, and no reference gene or calibration curve is needed for comparison. This means PCR assays with different efficiencies can be directly quantified and compared. Furthermore, by spatially isolating each PCR reaction, contributions from contaminant or non-specific reactions are limited. This can reduce the chance of competing reactions leading to a false-positive in the case of interrogating a single nucleotide variant. Dig-

ital PCR has been applied to quantify expression of transcription factors in a limited number of single cells, following FACS isolation of single cells and RNA processing (lysis, RT reaction) in tubes [62]. More recently, the advent of commercial devices for performing dPCR in (nanoliter) droplets is facilitating widespread adoption of this technique in a variety of applications [63, 64]. The small reaction volumes in dPCR provide a 1000-fold reduction in reagent consumption cost, while providing single molecule sensitivity. However, the bottleneck in single cell dPCR remains laborious single cell isolation and sample preparation.

1.6 Integrated Microfluidic Technology for Single Cell Gene Expression Analysis

Microfluidic systems offer a number of advantages for single cell analysis of gene expression. A challenge in single cell RT-qPCR is the limited starting material [46]. Microfluidics improve reaction sensitivity by reducing the volume of reactions, thereby increasing the concentration of template. Reducing reaction volumes also decreases costly reagent consumption. Microfluidic devices are automatable and highly scalable, permitting high-throughput and cost-effective application. Furthermore, the precise fluid handling capability of microfluidic systems is ideal for delicate manipulation of single cells and the assembly of reactions with low technical variability.

1.6.1 Multilayer Soft Lithography

The microfluidic technology developed in this thesis is based on a fabrication technique called multilayer soft lithography (MSL) [65]. In MSL, silicon wafers covered in photoresist are exposed to UV light through a micro-patterned photomask. This mask determines the pattern of features on the wafer after the resist is developed. For example, a typical negative resist such as SU8 consists of a non-photosensitive substrate, a photosensitive cross-linking agent, and a coating solvent. Crosslinks form when the photoresist is exposed to UV light, and the resist polymerises. This exposed photoresist is now insoluble in a developer solution, while unexposed sections of the photoresist are subsequently washed away by the developer. Using different photoresists (and coating spin speeds), wafers can be fabricated with features of varying heights and shapes.

These patterned wafers are used as replica molds for slabs of polydimethylsiloxane (PDMS) that are stacked on top of each other. Replica molding allows low cost production of multiple chips from a single silicon master. Bonding between layers is achieved by complementary off-ratio stochiometric mixing of the potting prepolymer component (A) and hardener component (B) of the room temperature vulcanizing PDMS for each slab. For example, the normal stochiometric ratio of masses A:B is 10:1. Bonding can be achieved between PDMS layers of A:B components, such as 20:1 and 5:1.

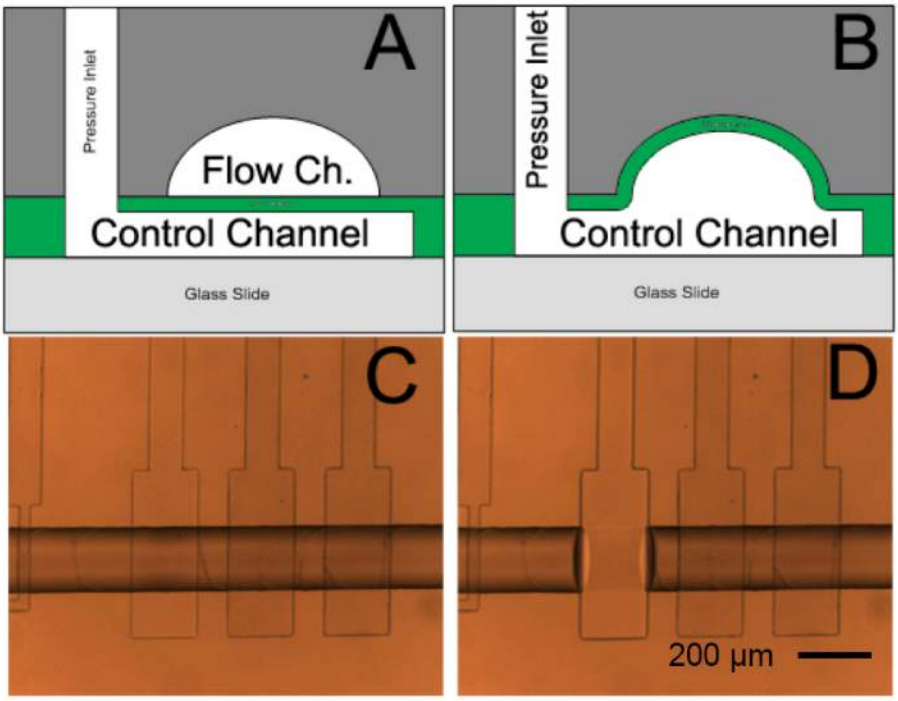

Figure 1.1: Valves in MSL. (A) A schematic profile of valve geometry in MSL devices. (B) Applying pressure to fluid in a 'control' channel deflects the membrane with the 'flow' channel to effectively valve the 'flow' line. These valves can be integrated into devices as a peristaultic pump, shown in inverse microscope images with all valves off (C), and one valve on (D).

A simple microfluidic device can be created from a 'control' wafer, and a 'flow' wafer [65]. A thick slab of PDMS (with excess hardener) molded to the features of the 'flow' wafer can be peeled from the 'flow' wafer and bonded to a thin layer of PDMS (with excess potting prepolymer) molded to the 'control' wafer. After bonding, this double-slab of PDMS can be peeled from the 'control' wafer, punched with holes for

fluid inlets/outlets, and bonded to a blank layer of PDMS to close the bottom of the 'control' layer channels. Applying pressure (controlled off-chip by solenoids) on the fluid in a control line can deflect the membrane between orthogonally crossing channels in the adjacent 'flow' layer, effectively valving the flow channel (Figure 1.1). Microfluidic devices integrate thousands of these valves (100 extmum x 100 extmum) in order to partition channels, direct fluid flow, and build active structures such as peristaltic pumps and mixers [65, 66].

1.6.2 Review of Microfluidic Technology for Single Cell Analysis

The past decade has seen a surge of efforts to manipulate and analyze individual cells in controllable lab-on-a-chip devices [67, 68]. As microfluidic technology has matured, many of the functionalities required for single cell gene expression analysis, such as cell trapping or nucleic acid detection, have been demonstrated in forms ranging from proof-of-concept to commercial products [29, 69]. Fitting these pieces of the puzzle together into a single integrated microfluidic device for high throughput, cost effective single cell gene expression analysis remains the current challenge.

1.6.2.1 Cell Manipulation

Single cell manipulation and isolation is a task well suited to micro-scale devices, and a number of distinct strategies have been demonstrated. In particular, physical trapping, encapsulation in droplets, and dielectrophoresis trapping techniques show great potential for single cell analysis.

Physical trapping of single cells in microfluidic devices has been accomplished through integration of microwells [70], cups [71–75], weirs [76, 77], and active valving [78–80]. Wheeler et al. designed a microfluidic device capable of passively isolating and trapping a single cell from a bulk suspension by positioning a square-cup "dock" with small drain channels at the stagnation point of a T-junction [75]. Similar strategies have explored different cup shapes [74, 77], and densely arraying the traps for large-scale experiments [72]. Skelley et al. developed a device for cell pairing that featured 6,000 physical cell traps made of polydimethylsiloxane (PDMS) [81]. The cell traps were densely arrayed (in an area of 8 mm by 4 mm) within a flow-through channel. Each cell trap consisted of a capture cup, and support pillars on either side

of the capture cup to allow flow into and under the trap. The pillar heights were designed to be slightly smaller than the cell diameter in order to trap a cell upon entering the capture cup. The obstruction provided by a trapped cell impedes fluid flow through the cell trap resulting in subsequent cells flowing past to be captured by unoccupied cell traps. Skelley et al. observed that the trap spacing in the array was critical for efficient capture without clogging. With optimal column spacing of 1-1.5 cell diameters (~20 µm), and a row spacing of 20-50 µm, Skelley et al. captured 70 - 90% of cells entering the array [81]. This physical cell-trapping array is a highly parallel and scalable technique.

Microfluidic technology for generating monodisperse droplets of aqueous phase solution inside an inert oil have been applied to the encapsulation of single cells. Once encapsulated inside a droplet, the droplet acts as an individual test tube, and reagents (other droplets) can be combined, and reactions can be carried out. Koster et al. developed a microfluidic device to encapsulate individual cells in picoliter aqueous drops in a carrier fluid at rates of up to 250 Hz [82]. In addition to cells remaining viable for up to 6 hours incubating inside 33 pL droplets, the small volumes of the drops enables the concentrations of secreted molecules such as antibodies to rapidly attain detectable levels. One limitation to this system is variability in the number of cells per drop due to stochastic cell loading. However, Edd et al. solved this issue by designing a high aspect-ratio microchannel that hydrodynamically focuses cells to be evenly spaced as they travel within the channel [83]. Thus, individual cells enter the drop generator with the frequency of drop formation. Encapsulation of cells within picolitre-size monodisperse drops provides new means to perform large-scale quantitative biological studies on a single-cell basis.

Microfluidic devices integrated with active electronics have been used manipulate cells with electric fields. This approach offers the advantage that the cells are not physically contacted. In dielectrophoretic cell trapping, a non-uniform electric field is generated, and the force applied to the cell depends on the dipole induced within the cell. Voldman et al. used four monolithic pillars within a microfluidic channel as electrodes to create a quadropole dielectrophoresis cell trap [84]. Dielectrophoresis can be selective in only trapping particular cell types, such as selecting white blood cells instead of erythroctyes [84]. In addition, the traps can be switched 'on' or 'off' to facilitate cell recovery or subsequent manipulation. Alternatively, optical tweezers have also been combined with microfluidic devices for single cell manipulation [85–88].

1.6.2.2 RNA Processing

Techniques such as RT-qPCR and sequencing often require RNA manipulations including purification or reverse transcription into cDNA before further analysis. Single cell capture, lysis, and reverse transcription have been implimented in a microfluidic rotary mixer that that may be injected with cell sample, reagents, and output RT product [78]. The throughput is limited to one cell, however. Bontoux et al. applied this system to neuronal progenitors, followed by template switching PCR in a tube, and reported the detection of 5000 genes in each cell (corresponding to the expected total number of genes expressed) by microarray analysis [78]. However, due to the low reported correspondence between different cells and the lack of data analysis it is unclear how much of this signal was specific. Interestingly, Bontoux et al. reported that the RT reaction was more efficient in nanoliter volumes inside the microfluidic device compared to microliter volume reactions in tubes [78].

Zhong et al. reported a microfluidic device capable of purifying mRNA from 20 single cells using oligo(dT) beads, followed by recovery for off-chip qPCR [89]. Individual cells were stochastically isolated by partitioning a cell suspension between physical microvalves. A chemical buffer was mixed with the sample fluid to lyse the cell. The cell lysate was pushed through a column of beads functionalized with short sequences of deoxy-thymine nucleotides on the surface. The oligo(dT) strand binds the poly-A tail of mRNA transcripts, thereby capturing the mRNA from the cell while the remaining contents are washed away. By performing reverse transcription of the purified mRNA on the microfluidic device, Zhong et al. demonstrated a ~4-fold increase in reverse transcription reaction efficiency (measured by cDNA yield) compared to performing the reaction in conventional tubes [89]. Measurement of 3 transcripts in 54 single hESCs revealed a heterogeneous population [89], further underscoring the need for discrete cell analysis. The throughput of this system is limited by stochastic cell loading, and challenges recovering the samples from the device for off-chip analysis.

1.6.2.3 Gene Expression Analysis

Microfluidic devices employing arrays of thousands of nanolitre micro-reactors have been used by researchers for highly multiplexed, as well as single molecule quantitative analysis of cDNA prepared from single cell samples. Digital PCR is performed in a microfluidic "Digital Array" whereby a 7.5 µl sample is partitioned into 1,200 isolated

reaction chambers ("wells"), before PCR [62]. The sample is diluted such that each reaction chamber has high probability of containing a single template molecule, or zero, allowing absolute quantification of single molecules by counting the number of fluorescent reaction wells after PCR amplification. Warren et al. used FACS to sort 116 individual cells using hematopoietic differentiation markers to select cells representing hematopietic stem cells (HSC), common lymphoid progenitors (CLP), two sub-populations of common myeloid progenitors (CMP), and megakaryocyte-erythroid progenitors (MEP) [62]. Following off-chip reverse transcription, abundance of transciption factor PU.1 was quantified using digital PCR. Warren et al. were able to show differential expression of PU.1 between flk+ and flk- CMPs with single cell (and single molecule) resolution.

Integrated fluidic circuits for digital PCR have been commercialized by Fluidigm, which also offers a Dynamic Array chip for quantitative analysis by highly multiplexed real-time PCR. Following conventional (off-chip) sample preparation (including reverse transcription and pre-amplification of cDNA), the Dynamic Array combines 48 samples with 48 assays, to perform 2,304 real-time PCR reactions, each 10 nL in volume (also available as 96 samples by 96 assays). In addition to fluid handling advantages, performing the equivalent multiplexing real-time PCR experiments in conventional microliter volumes quickly becomes cost prohibitive. This multiplexing allows for large-scale gene expression profiling, starting with small samples such as single cells.

The Biomark Dynamic Array (Fluidigm Corporation) technology has been leveraged to study cellular development from zygote to blastocyst stage fertilized mouse embryos [90]. In 2010, Guo et al. investigated expression of 48 genes in a survey of 500 single cells from 8, 16, 32, and 64 -cell stage embryos [90]. By tracking multiple expression markers, Guo et al. revealed at least three distinct developmental expression patterns, and associate these with development of cells forming the trophectoderm (TE), the primitive endoderm (PE), and the epiblast (EPI) [90]. Furthermore, Id2 and Sox2 were identified as the earliest markers of outer and inner cells, respectively. These results illustrate the power of single cell gene expression analysis to provide insight into developmental mechanisms [91], and this technique is applicable to other biological systems [92]. The coupling of single cell isolation by flow cytometry, followed by RNA processing and final multiplexed qPCR in these microfluidic arrays has since become well established for analyzing hundreds to low thousands of cells for

large assay panels [93]. Importantly, these studies have uncovered clinically relevant cellular heterogeneity in diseases such as cancer. In 2011, Dalerba et al. used single-cell microfluidic RT-qPCR to identify distinct cell populations within colon cancer tissues, and showed that the different gene expression signatures are predictive of patient survival and clinical outcomes [94]. Single-cell analysis has also uncovered that a subset of breast tumor cells exhibit increased expression of genes associated with reactive oxygen species scavenging, contributing to tumor radioresistance [95].

1.6.2.4 State of the Art: Integrated Systems for Cell Manipulation and RNA Analysis

The above examples demonstrate the single cell handling, nucleic acid processing, and analysis capabilities of microfluidic devices, however complete integration of all sample processing and analysis into a single device remains a pursuit of active research. This was particularly true at the outset of the work presented in this thesis. At that time, the only device to integrate all components of single cell isolation, RNA processing, and final measurement of gene expression was from Toriello et al., who developed an integrated microfluidic device for single cell gene expression analysis capable of capturing a single cell, cell lysis and reverse transcription of contained mRNA, followed by amplification and detection of product of interest [96]. The device features a nanoliter metering pump, and DNA capture pads to catch functionalized single cells. An integrated heating element is used for cell lysis, followed by RT-PCR. The 200 nL PCR chamber is coupled to capillary electrophoresis for size-based measurement of products. Each device is capable of measuring 4 single cells in parallel, and is used to measure variable siRNA knockdown of the GAPDH gene in 8 individual Jurkat cells [96]. Other efforts towards microfluidic integration of single cell gene expression analysis in droplet [97] or micro-well [98] systems have suffered from lysate inhibition of RT-qPCR reactions, reducing the sensitivity, precision, and robustness of these measurements. These devices demonstrated the feasibility of a microfluidic approach to single cell expression analysis, however further development was still needed for microfluidic based methods to become routine in single cell analysis.

Here we present the first microfluidic device to achieve integration of all components for single cell gene expression analysis, such as single cell trapping, washing, lysis, reverse transcription and quantitative PCR measurements, at high-throughput (for the time) of hundreds of cells per run. In the course of my thesis work developing

and applying this technology, the field of microfluidics and single-cell gene expression analysis has advanced considerably. In particular, through publishing to disseminate knowledge, and licensing intelectual property, this work contributed to the development of a commercial microfluidic product (the C1, from Fluidigm Corp.) that integrates single cell trapping with nucleic acid processing with recovery of single-cell products for downstream assessment by sequencing or highly paralel PCR (such as on the Biomark Dynamic Array). The C1 currently has a throughput of up to 96 cells per run. The C1 device has been gaining popularity [36, 99], enabling single-cell genomics and transcriptomics studies in a variety of applications [38, 100, 101].

In addition to integrated microfluidic devices using successive physical chambers for reactions [102], micro-wells [103, 104] and droplet-based [105] approaches have also made advances. In a technique called Drop-seq, thousands of cells were separated into nano-liter sized aqueous droplets [106]. Each droplet was used to associate a different molecular identifier, or barcode, for transcripts originating from the encapsulated cell [107]. This allowed all of the cells to be sequenced together, while retaining transcripts' cell of origin. Drop-seq has enabled the studies with over 44,000 single cell transcriptomes sequenced [106], the highest throughput reported to date. Molecular imaging techniques such as mRNA-FISH have been combined with *in situ* RNA sequencing to look at a highly multiplexed number of genes while preserving spatial information of where the transcripts are located within the cell [108, 109]. These single cell gene expression analysis methods are beginning to deliver on the promise of single cell genomics, but improving on these techniques remains an active area of research.

1.7 Research Objective

Transcription measurements with single cell resolution are critical to understanding variable responses in immunity, measuring stochastic noise in gene expression, and assessing the disease and developmental state of heterogeneous populations. Current methods for measuring transcript levels in single cells include reverse transcription followed by quantitative polymerase chain reaction (RT-qPCR), single molecule counting using digital PCR or hybridization probes, and next generation sequencing. Widespread adoption of these techniques has been limited by challenges isolating single cells, high reagent costs, low sensitivity, and difficulties in accurately measuring low abundance transcripts. Microfluidic systems offer a number of advantages for single cell analysis of gene expression by providing economy of scale, automation and parallelization, and increased sensitivity in small volume reactions. Furthermore, the precise fluid handling capability of microfluidic systems is ideal for delicate manipulation of single cells.

This thesis is focused on the development of new technologies for single cell analysis with the following goals:

1. Develop a microfluidic system for PCR-based transcription measurements in single cells.

2. Apply this technology to explore transcriptional heterogeneity in single cells.

1.7.1 Specific Aims

1. Development of an integrated microfluidic device for high-throughput single-cell RT-qPCR

2. Development of an integrated microfluidic device for high-throughput single-cell digital PCR

3. Application of single-cell digital RT-PCR to study the use of lipid nanoparticles for RNA delivery.

Integrating single cell capture, lysis, and reverse transcription, with final measurement of transcripts by digital PCR will permit analysis of hundreds of single cells in parallel, while improving work flow and reducing technical variation compared to

samples prepared in microliter volumes. Thus, microfluidic single-cell digital PCR represents a significant advancement to the tools available for precisely measuring transcripts in single cells, and has application in research and clinical settings.

Chapter 2

High-Throughput Microfluidic Single-Cell RT-qPCR[1]

2.1 Overview

A long-sought milestone in microfluidics research has been the development of integrated technology for scalable analysis of transcription in single cells. Here we present a fully integrated microfluidic device capable of performing high-precision RT-qPCR measurements of gene expression from hundreds of single cells per run. Our device executes all steps of single cell processing including cell capture, cell lysis, reverse transcription, and quantitative PCR. In addition to higher throughput and reduced cost, we show that nanoliter volume processing reduced measurement noise, increased sensitivity, and provided single nucleotide specificity. We apply this technology to 3300 single cell measurements of i) miRNA expression in K562 cells, ii) co-regulation of a miRNA and one of its target transcripts during differentiation in embryonic stem cells, and iii) single nucleotide variant detection in primary lobular breast cancer cells. The core functionality established here provides the foundation from which a variety of on-chip single cell transcription analyses will be developed.

2.2 Introduction

Single cells represent the fundamental unit of biology; however, the vast majority of biological knowledge has emerged as a consequence of studying cell populations and not individual cells. Inevitably, there are fundamental and applied questions, such as those relating to transcriptional control of stem cell differentiation, intrinsic

[1] A version of this chapter has been published: Adam White, Michael VanInsberghe, Oleh Petriv, Mani Hamidi, Darek Sikorski, Marco A. Marra, James M. Piret, Sam Aparicio, and Carl L. Hansen, *High-Throughput Microfluidic Single-Cell RT-qPCR*, Proceedings of the National Academy of Sciences, 2011.

noise in gene expression, and the origins of disease, that can only be addressed at the single cell level. For example, single cell analysis allows for the direct measurement of gene expression kinetics, or for the unambiguous identification of co-regulated genes, even in the presence of de-synchronization and heterogeneity that could obscure population-averaged measurements. Similarly, single cell methods are vital in stem cell research and cancer biology, where isolated populations of primary cells are heterogeneous due to limitations in purification protocols, and it is often a minority cell population that is the most relevant. High-throughput single cell measurement technologies are therefore of intense interest and have broad application in clinical and research settings.

Existing methods for measuring transcript levels in single cells include RT-qPCR[46], single molecule counting using digital PCR[62] or hybridization probes[23, 26], and next generation sequencing[30]. Of these, single cell RT-qPCR provides combined advantages of sensitivity, specificity, and dynamic range, but is limited by low throughput, high reagent cost, and difficulties in accurately measuring low abundance transcripts[58].

Microfluidic systems provide numerous advantages for single cell analysis: economies of scale, parallelization and automation, and increased sensitivity and precision that comes from small volume reactions. Considerable effort over the last decade has been directed towards developing integrated and scalable single cell genetic analysis on chip[67, 110]. Thus, many of the basic functionalities for microfluidic single cell gene expression analysis have been demonstrated in isolation, including cell manipulation and trapping[75, 81], RNA purification and cDNA synthesis[78, 79, 89], and microfluidic qPCR[90] following off-chip cell isolation cDNA synthesis and preamplification. In particular, microfluidic qPCR devices (Biomark Dynamic Array, Fluidigm) have recently been applied to single cell studies[20, 95]. Although these systems provide a high-throughput qPCR readout, they do not address the front end sample preparation and require single cell isolation by FACS or micropipette followed by off-chip processing and pre-amplification of starting template prior to analysis. The critical step of integrating all steps of single cell analysis into a robust system capable of performing measurements on large numbers of cells has yet to be reported. A single demonstration of an integrated device for directly measuring gene expression in single cells was described by Toriello et al., combining all steps of RNA capture, PCR amplification, and end-point detection of amplicons using integrated capillary electrophoresis[96]. Despite the engineering complexity of this system, throughput was limited to four

cells per run, cell capture required metabolic labeling of the cells, and the analysis was not quantitative. Thus, there remains an unmet need for microfluidic technologies capable of scalable and quantitative single cell genetic analysis.

Here we describe an integrated microfluidic device for high-throughput RT-qPCR analysis of mRNA and miRNA expression at a throughput of hundreds of single cells per experiment. We show that this technology provides a powerful tool for scalable single cell gene expression measurements with improved performance, reduced cost, and higher sensitivity as compared to analysis in µL volumes. This technology represents the first implementation of robust and high-throughput single cell processing and amplification of nucleic acids on a chip, thereby achieving a major milestone in microfluidic biological analysis.

2.3 Methods

2.3.1 Device Fabrication and Operation

Microfluidic devices were fabricated by multilayer soft lithography[65, 66]. Planar silicon molds were defined by photolithography, using photomasks designed with CAD software (AutoCAD, Autodesk Inc.), and printed on transparency films at a resolution of 20,000 dots per inch (CAD/Art services). The control mold was fabricated using SU8-2025 photoresist (Microchem, USA) to deposit valve features 24 µm in height. The flow mold was fabricated with three lithographic steps. First, the channels for reagent injection, and connections between chambers were fabricated using 13 µm high SPR220-7 photoresist (Shipley, USA). The SPR channels were rounded to facilitate valve closure by incubation at 115 °C for 15 minutes. A hard bake at 190 °C for 2 hours was used to prevent SPR photoresist erosion during addition of subsequent layers. Second, the cell trap features were defined in 14 µm SU8-2010 photoresist (Microchem, USA). Finally, the large chambers and fluidic bus lines were constructed using 150 µm high SU8-100 photoresist. All photoresist processing was performed according to manufacturer specifications.

Microfluidic devices were cast from these molds in polydimethylsiloxane (PDMS, RTV615, General Electric, USA). Each device consists of a three layer elastomeric structure with a blank bottom layer, a middle control layer with channels that act as valves by pushing up and pinching closed channels in the above flow layer. The

molds were first treated with chlorotrimethylsilane (TMCS, Aldrich) vapor for 2 min to prevent PDMS from bonding to the photoresist structures. The flow layer was made by pouring a mixture of PDMS (5 parts RTV615A : 1 part RTV615B) onto the flow mold, degassing, and then baking for 60 min at 80 °C. A thin control layer was made by spin coating the control mold with PDMS (20 parts RTV615A : 1 part RTV615B) at 1800 rpm and baking for 45 min at 80 °C. After baking, the PDMS of the flow layer was peeled from the flow mold and aligned to the control layer. Following a 60 min bake at 80 °C, the bonded two layer structure was separated from the control mold, and channel access holes were punched. A blank layer (without channels) was prepared by spinning PDMS (20 parts RTV615A : 1 part RTV615B) on a blank wafer (2000 rpm) and baking 45 min at 80 °C. The bonded flow and control structure was mounted on to the blank layer, and baked for 3 hours at 80 °C. Finally, the three layer bonded structure was removed from the blank mold, diced into individual devices, and these were each bonded to clean glass slides by baking overnight at 80 °C.

The device operation requires control of 9 pneumatic valves and may be operated using a simple manifold of manual valves. For the current study a semi-automated implementation was used in which microfluidic valves were controlled by solenoid actuators (Fluidigm Corp., San Francisco) controlled through a digital input output card (NI-DAQ, DIO-32H, National Instruments) operated using LabView drivers (National Instruments). Tygon tubing connected the solenoids to the microfluidic device by 20 gauge stainless steel pins (Small Parts Inc.) fitted into the control line ports. Krytox (DuPont) oil was used as the fluid in the control lines, and the valves were actuated with 30 psi pressure.

2.3.2 Single Cell Transcript Measurements by Heat Lysis and 2-step RT-qPCR

The device was primed by flowing PBS containing 0.5 mg/mL bovine serum albumin (BSA) and 0.5 U/µL RNase Inhibitor through all channels, while keeping the RT, and PCR chambers empty and isolated by valves. The BSA helped prevent cells from adhering to channel walls. After priming, but prior to cell loading, all valves were closed. A single cell suspension was injected into the device by applying pressure (∼2-3 psi) to microcapillery pipette tips plugged into the sample inlets. The sample inlets

were first dead-end filled against an inlet valve to prevent air bubbles from entering the device. The sample inlet valves, cell chamber valves and outlet valve were opened to allow the cell suspension to flow through the sample channels. Cells were loaded into the device suspended in culture media (directly from culture). Cell loading concentrations were kept between 5×10^5 cells/mL and 1×10^6 cells/mL, resulting in over 80% occupancy of cell traps with single cells in 1-2 min at a flow rate of approximately 20 nL/s. Lower concentrations were found to require proportionately longer times to achieve high occupancy of trapped single cells. Concentrations greater than 2×10^6 cells/mL were found to occasionally clog the inlet port or the channel at trap locations. A peristaltic pump was integrated into the device for controlling the flow rate, however pressure driven flow was used for the current study.

After injecting the cell suspension and trapping single cells the cell sample inlet valve was closed, and the cells were washed by flushing the line with the PBS solution used to prime the device. This removed untrapped single cells, extracellular RNA, and debris. Following on-chip washing, the cell chamber valves were closed to partition the cell loading channel and isolate individual cell reactors. Visual inspection of the cell capture chambers with a microscope was used to confirm and count the number of cells in each chamber. The cells were lysed by placing the microfluidic device onto a flatbed thermocycler and heating to 85 °C for 7 minutes (and then cooled to 4°C).

Reverse transcription (RT) was performed in the device by using the ABI High Capacity Reverse Transcription kit[59], with the addition of a surfactant to prevent adsorption of nucleic acids and proteins to PDMS surfaces (2 µL 10× Reverse Transcription Buffer, 4 µL 5X RT stem-loop miRNA primer from ABI, 1 µL 100mM dNTPs, 1.34 µL of 50 U/µL Multiscribe Reverse Transcriptase, 0.26 µL of 20 U/µL RNase Inhibitor, 2 µL 1% Tween 20, 9.4 µL PCR grade water). The RT mix was loaded into the device, and flushed through the reagent injection channels. RT reagent was injected into the reaction by opening the valve connecting the cell chamber to the RT chamber, and the valve connecting the cell chamber to the reagent injection line. The RT chamber was dead-end filled before closing the connection to the reagent injection line. A pulsed temperature RT protocol was carried out by placing the microfluidic device on a flatbed thermocycler (2 min at 16 °C, followed by 60 cycles of 30 seconds at 20 °C, 30 seconds at 42 °C, and 1 second at 50 °C). RT enzyme was inactivated at 85 °C (5 min), and then the device was cooled to 4 °C.

The PCR reagent was prepared with 25 µL of 2× TaqMan Universal Master Mix

(ABI), 2.5 µL 20× Real-Time miRNA assays (primers and probe, ABI), 5 µL of 1% Tween 20, and 7.5 µL of PCR grade water. The PCR reagent was flowed through the reagent injection channels to flush away the RT reagent. Valves were opened and the PCR reagent was injected to dilute the RT product into the PCR reaction chamber. After completely filling the PCR reaction chamber, the valves closing the PCR chambers were actuated, and the device was transferred to an enclosure for real-time PCR (Prototype version of Biomark Instrument, Fluidigm CA). The real-time PCR enclosure consists of a custom flatbed thermocycler, a xenon arc lamp and filter set, and a charged coupled device (CCD) imager with optics for fluorescent imaging of the entire device periodically during PCR thermocycling (see description of real-time PCR instrumentation below). PCRs were thermocycled with the following conditions: 10 min at 95 °C, followed by 50 cycles of 15 s at 95 °C and 1 min at 60 °C. Images were acquired at 60 °C.

2.3.3 Single Cell Transcript Measurements by Chemical Lysis and 1-step RT-qPCR

Measurements of mRNA transcripts (SP1, GAPDH) were performed using the Cells Direct kit (Invitrogen, USA). Operation of the microfluidic device for chemical lysis and 1-step RT-qPCR was similar to the methods described for heat lysis and 2-step RT-qPCR with several distinctions. The device was primed and cells were washed with PBS containing 0.5 mg/mL BSA. Additional RNase Inhibitor was omitted as the chemical lysis buffer (10 µL lysis resuspension buffer, 1 µL lysis enhancer solution, Invitrogen, USA) contained RNA stabilizing agents. Cell loading was the same as in the heat lysis and 2-step RT-qPCR scenario. Single cells were lysed by injecting a chemical lysis buffer through the cell capture chamber and filling the 10 nL chamber (used for RT reagent injection in the 2-step protocol). The lysis reaction was incubated at room temperature for 10 minutes, followed by heat inactivation of the lysis reagent by placing the device on a flatbed thermocycler and incubating at 70 °C for 10 minutes. The one-step RT-qPCR mix (1 µL of SuperScript III RT/Platinum Taq Mix, 25 µL of 2X Reaction Mix (with ROX reference dye), 2.5 µL of 20X Taqman Assay (primers and probes, ABI), 1 µL of 50 mM MgSO4, 5.5 µL of H2O, and 5 µL of 1% Tween 20) was then combined with the cell lysate into the final 50 nL reaction chamber. The device was transferred to the real-time PCR enclosure for temperature

Table 2.1: Heat Lysis and 2-Step RT-qPCR Protocol

Step	Description	Time
1	Prime device with PBS 0.5 mg/mL BSA and 0.5 U/µL RNase Inhibitor	1 min
2	Inject cell suspension (passive cell trapping)	1 min
3	On chip cell washing with PBS containing 0.5 mg/mL BSA and 0.5 U/µL RNase Inhibitor	1 min
4	Close valves partitioning cell loading channel and isolating single cells	30 sec
5	Count cells by visual inspection with microscope	7 mins
6	Heat lysis by placing device on flatbed thermocycler and heating to 85 °C	7 min
7	Flush fluidic bus and reagent injection lines with reagent for RT	2 min
8	Inject RT reagent through the cell capture chamber, dead-end filling the 10 nL RT chamber	1 min
9	Close reagent injection valve, creating isolated reactors combining the cell capture chamber and RT chamber	30 sec
10	Perform reverse transcription (pulsed temperature protocol) by placing device on flatbed thermocycler	2.5 hr
11	Flush fluidic bus and reagent injection lines with reagent for PCR	2 min
12	Inject PCR reagent through combined cell-capture/RT chamber into 50 nL PCR chamber	5 min
13	Close valve to PCR chamber. Allow for mixing by diffusion	40 min
14	Load device into BioMark real-time PCR system and focus camera	5 min
15	Run qPCR protocol	(varies)

control and imaging of the 1-step RT-qPCR (20 min at 50 °C for RT, followed by a hot-start at 95 °C for 2 min, and 50 cycles of 15 s at 95 °C and 30 s at 60 °C).

2.3.4 Digital PCR Experiments

For mRNA digital PCR analysis cells were washed with PBS containing 0.5 mg/mL BSA, lysed in chemical lysis buffer, reverse transcription was performed in tubes according to the protocol described above, and the resulting cDNA product was loaded into digital PCR arrays. For miRNA studies, cells were lysed in PBS containing 0.5 mg/mL BSA and 0.5 U/µL RNase inhibitor. Reverse transcription was performed using miRNA stem-loop primers (Applied Biosystems, USA) and the High Capacity cDNA Reverse Transcription kit (Applied Biosystems, USA) in 10 µL volumes. Prior

Table 2.2: Chemical Lysis and 1-step RT-qPCR Protocol

Step	Description	Time
1	Prime device with PBS 0.5 mg/mL BSA and 0.5 U/µL RNase Inhibitor	1 min
2	Inject cell suspension (passive cell trapping)	1 min
3	On chip cell washing with PBS containing 0.5 mg/mL BSA and 0.5 U/µL RNase Inhibitor	1 min
4	Close valves partitioning cell loading channel and isolating single cells	30 sec
5	Count cells by visual inspection with microscope	7 mins
6	Inject lysis reagent through the cell capture chamber, dead-end filling the 10 nL chamber	1 min
7	Close reagent injection valve, creating isolated reactors combining the cell capture chamber and lysis reservoir chamber	30 sec
8	Perform lysis at room temperature and heat inactivation of the lysis reagent at 75 °C by placing device on flatbed thermocycler	25 min
9	Flush fluidic bus and reagent injection lines with reagent for RT-qPCR	2 min
10	Inject RT-qPCR reagent through combined cell-capture/lysis chamber into 50 nL RT-qPCR chamber	5 min
11	Close valve to RT-qPCR chamber. Allow for mixing by diffusion	40 min
12	Load device into BioMark real-time PCR system and focus camera	5 min
13	Run RT-qPCR protocol	(varies)

to injection into microfluidic digital PCR arrays, RT product was added to the PCR reagent as in the on-chip 2-step RT-qPCR protocol described above. Thermal cycling of digital PCR arrays was also performed using the same protocols as described above. PDMS digital PCR arrays consisting of 765 2 nL individual PCR chambers, of similar design to those described in Warren et al.[62], were fabricated by multilayer soft lithography. After thermal cycling, positive chambers were counted and actual molecule numbers were derived based on the binomial distribution.

2.3.5 System for Real-Time PCR

The BioMark™ Reader is a commercially available real-time PCR instrument developed by Fluidigm and designed to run Fluidigm Integrated Fluidic Circuits (IFCs). The prototype version of this system allowed access to the flatbed thermocycler inside the enclosure, permitting the use of custom microfluidic devices in addition to

the intended commercial IFCs. Image Resolution and bit depth: 4 Megapixel, 16 bit; Filters: FAM (Ex 485/20, Em 525/25), VIC (Ex 530/20, Em 570/30), ROX (Ex 580/25, Em 610/15), QAS (Ex 580/25, Em 680/25); Light Source: 175 W xenon arc bulb.

2.3.6 RT-qPCR Assays

Measuring mRNA in the presence of genomic DNA requires primers designed to specifically target mature mRNA sequences. In many cases, this can be accomplished by designing intron-spanning primers. A specially designed stem-loop RT primer system (Applied Biosystems) is used for the specific targeting of mature miRNAs.

TaqMan assays for GAPDH (Applied Biosystems, Assay ID Hs99999905_m1) and miRNAs were obtained from Applied Biosystems. For GAPDH, a control experiment omitting the reverse transcriptase was performed off-chip, in microliter volumes with bulk cell lysate (at equivalent concentration of a single cell on-chip, 10^5 cells/mL), and showed no amplification after 40 cycles of PCR.

OCT4 (POU5F1) primer sequences were obtained from RTPrimerDB and synthesized by Biosearch Technologies Inc; Forward primer: ACC CAC ACT GCA GCA GAT CA, Reverse primer: CAC ACT CGG ACC ACA TCC TTC T, Probe: Quasar670-CCA CAT CGC CCA GCA GCT TGG-BHQ-2, RT primer: TTG TGC ATA GTC GCT GCT TGA T. Measurement of OCT4 in single hESCs by microfluidic RT-qPCR without reverse transcriptase showed no amplification after 40 cycles of PCR.

BHQ-Plus probes with enhanced duplex stabilization (Biosearch Technologies Inc) were used for SNV detection to allow for shorter sequence lengths and increased specificity. The SNV location for the SP1 locus was selected from Table 2 in Shah et al.[32]. Two hundred bp flanking this location on the hg18 sequence were used for assay design using Primer3. The resulting primer and probe sequences are as follows (the SNV is in bold). SP1 Mutant Probe: FAM-AGGCCAGCAAAAA**C**AAGG-BHQ-1, 5' Modification: FAM, 3' Modification: BHQ-1 Plus, Tm = 62.7 °C. SP1 WT probe: Cal Fluor-CAGGCCAGCAAAAA**G**AA-BHQ-1, 5' Modification: CAL Fluor Orange 560, 3' Modification: BHQ-1 plus, Tm = 62.1 °C. SP1 Forward Primer: CCAGACATCTGGAGGCTCATTG, Tm = 65.8 °C. SP1 Reverse Primer: TGAACTAGCTGAGGCTGGATA, Tm = 66.0 °C.

Control experiments without reverse transcriptase showed positive amplification.

Therefore the measurement of SP1 mutant and wilde-type abundance in single cells by RT-qPCR does not discriminate between mature mRNA transcript and genomic DNA.

2.3.7 Image Analysis

Fluorescence images of the entire device were taken in at least two different colors (one passive reference dye and one or more reporter dyes) after each PCR cycle and were analyzed using custom scripts written in MATLAB (MathWorks) to generate real-time amplification curves. Reaction chambers were segmented from the rest of the image using the first image of the passive reference dye. The image was manually rotated so that all of the reaction chambers were square with the edges of the image. Next, the average image intensities across each row and column were calculated and a threshold was manually set to differentiate bright areas from background. Regions containing both bright rows and bright columns were assigned to the reaction chambers.

All subsequent images were automatically aligned to this initial image by minimizing the absolute distance between the average row and column intensities of the initial image, and the one being analyzed. For each image, the intensities of the reporter and passive dyes were recorded for each reaction chamber. Real time amplification curves were generated by normalizing the intensity of each reporter dye to that of the passive dye. Linear components were removed from these curves by fitting the equation of a line to the pre-exponential region and extrapolating and subtracting the result from the entire curve. The threshold for determining CT values was automatically determined as the median normalized fluorescence value at the maximum second derivative of all amplification curves.

2.3.8 mRNA FISH

Cells grown on LABTEK chambered cover-glass were washed with PBS, fixed in 4% formaldehyde for 10 min at room temperature and permeabilized in 70% EtOH at 40 °C overnight. The next day cells were rinsed with wash buffer (15% Formamide in 2× SSC) and then hybridized with the appropriate dilution of mRNA FISH probes specific to OCT4 (see table) in hybridization solution (dextran sulfate, Yeast tRNA, NEB, BSA, 15% Formamide in 2 SSC) overnight at 30 °C. The next morning the

OCT4 hybridization solution was aspirated and cells were sequentially rinsed and incubated with wash buffer at 30 °C for 30 minutes then washed with 2× SSC. One drop (25 µL) of Slowfade GOLD antifade reagent with DAPI was then added to the cells, covered immediately with a cover slip, and imaged. Stacks of 32-64 mRNA hybridization images (spaced by 0.5 µm) were acquired for each cell using a Leica DMI 6000B inverted microscope with a 100 objective (N.A. 1.3) in DAPI and Texas Red filter spectra.

Fluorescent spots corresponding to individual mRNA molecules in each image stack were evaluated manually since automatic thresholding using previously reported algorithms were found to be unreliable. Difficulty in automating this process was attributed to inconsistent signal to noise using reported protocols and may be related to the thickness of hESC cells (∼15 µm). In addition, manual intervention was needed to ascertain the boundaries of adjacent cells. To optimize the signal to noise we systematically varied the probe concentration, incubation time, incubation temperature as well as the formamide concentration in the hybridization buffer solution.

2.3.9 Cell Culture

K562 cells were cultured in Dulbecos Modified Eagle Medium (DMEM) (Gibco) supplemented with 10% fetal bovine serum (FBS) (Gibco). Purified RNA was extracted from K562 cells using RNA MiniPrep (Qiagen, USA).

CA1S hESCs[111, 112] were propagated in mTeSR[113] basal medium (STEMCELL Technologies, Inc., Vancouver, BC, Canada), additionally supplemented with antibiotic-antimycotic (100 U/mL penicillin, 100 mg/mL streptomycin and 0.25 mg/mL amphotericin B) (Invitrogen, Carlsbad, CA, USA). Upon passaging, hESCs were washed with phosphate-buffered saline (PBS) prior to incubating with TrypLE Express (Invitrogen, Carlsbad, CA, USA) at 37 °C for 10 minutes to detach single hESCs from 4-8 day-old cultures depending on confluency. TrypLE Express was neutralized with mTeSR supplemented with antibiotic-antimycotic and suspensions were then transferred into new tissue culture dishes containing a precoated layer of 1:30 diluted Matrigel (Becton Dickinson, San Jose, CA, USA) and mTeSR supplemented with antibiotic-antimycotic. For differentiation, mTeSR was replaced with Dulbeccos modified eagle medium with 10% fetal bovine serum (FBS) 1 day after plating cells.

When harvesting hESCs for qRT-PCR, cells were incubated with TrypLE Express (Invitrogen, Carlsbad, CA, USA) at 37 °C for 20 minutes in order to produce a more

uniform single cell suspension from 4-8 day-old cultures.

Cryo-vials of primary cells isolated from a lobular breast cancer metastasis were provided by the BC Cancer Agency in accordance with ethical guidelines of the University of British Columbia. To increase viability, cells were transferred to fresh culture medium and incubated for 2 days before analyzing in the microfluidic device.

2.3.10 Transfer Efficiency Measurements

A solution containing 10 µM FAM-labeled 40-mer poly-A oligonucleotides (IDT, USA), 0.1% Tween 20, and ROX passive reference dye (from CellsDirect kit, Invitrogen, P/N 54880) diluted 100× was loaded into the cell capture chambers and sequentially pushed into the 10 nL and 50 nL chambers with water containing 0.1% Tween 20, and ROX reference dye diluted 100×. Fluorescence images acquired of FAM and ROX were used to measure the transfer of oligonucleotides from one chamber to the next. The transfer efficiency for each chamber was calculated as (Initial Signal Final Signal)/(Initial Signal), where Signal = (FAM Intensity FAM Background)/(ROX Intensity ROX Background). A conservative estimate of the lower bound of transfer efficiency was taken to be one standard deviation from the mean measurement of transfer efficiency.

2.3.11 Cell Capture Measurements

A custom microfluidic device with a linear array of cell trap geometries was fabricated using protocols described above. The device was mounted on an inverted microscope (Leica DM IRE2) and imaged in bright field using a CCD camera (Hamamatsu ORCA-ER). The device was primed with 0.05% bovine serum albumen (BSA) (Gibco) in phosphate-buffered saline (PBS) (Gibco). Prior to loading in the device, cells were washed twice in fresh culture media (Dulbecos Modified Eagle Medium (DMEM) (Gibco) supplemented with 10% Fetal Bovine Serum (Gibco)). After the final wash cells were resuspended to be at a concentration of 1 million per mL. Input sample viability was measured with the Cedex Automated Cell Counter (Roche innovatis AG).

To measure the capture efficiency, cells were pumped through the array using a downstream microfluidic peristaltic pump at a rate of approximately 1 nL/second and the number of cells that bypassed each trap before a successful trapping event

was recorded. These counts were fit using a maximum-likelihood estimator for a geometric distribution with the fitdistr function (MASS package version 7.3-6) in R (version 2.11.1). Efficiencies are reported as the probability of a successful capture for each cell.

To measure cell viability after loading, cells were loaded into the array using pressure driven flow as described above until high trap occupancy was observed. 0.2% Trypan Blue (Gibco) in PBS was then flowed over the trapped cells. Viability was calculated as the number of unstained cells divided by the total number of cells.

Cell diameter was measured from Cedex images and images of cells trapped in the microfluidic device using ImageJ (version 1.43u). A two sample t-test was used to test the hypothesis that the resulting size distributions were significantly different. The assumption of equal variance was tested using an F test. For optimized cell trap geometries the cell trapping efficiency was improved to 87% by bringing the cup within one cell diameter of the focuser and by including a small bypass shunt through the cup, similar to the cup geometry presented in Skelley et al.[81].

2.3.12 Mixing by Diffusion

Mixing of solutions by diffusion was characterized in the microfluidic device by loading fluorescently labeled 40 base poly-A oligonucleotides into the 10 nL chambers, and pushing the contents of the chamber into the adjacent 50 nL chambers. Time-lapse imaging was used to measure the evolution of the distribution of fluorescently labeled oligonuceotides in the PCR chambers over time (Figure 2.1). The standard deviation of the pixel intensities in each chamber through time was used as a metric of mixing. The resulting curves of all analyzed chambers (N = 200) were each fit to a decaying exponential using least squares regression to determine the characteristic mixing time constant. This resulted in a mean mixing time of 15.2 $\pm$ 1 minutes.

Using the Stokes-Einstein relation and assuming a random coil we estimate the diffusion constant of a 40 base oligonucleotide to be:

$$D = \frac{K_B T}{6\pi\eta R_h}, \tag{2.1}$$

where $K_B T$ is the thermal energy (4.1 pN·nm), η is the fluid viscosity ($\sim$ 0.001 kg/m·s), and R_h is the coil hydrodynamic radius (10). The hydrodynamic radius is

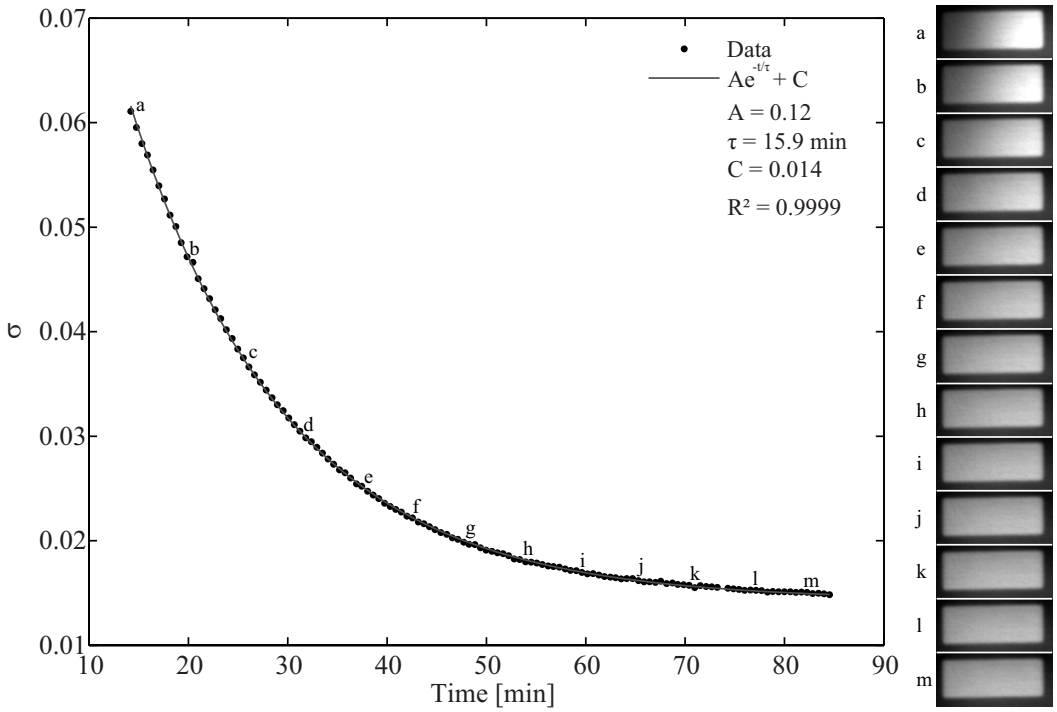

Figure 2.1: Mixing by diffusion. Plot shows the standard deviation of pixel intensity values for a chamber as a function of time following the transfer of a solution of fluorescently labelled 40 base pair poly-A oligonucleotide from the RT chamber (10 nL) to the PCR chamber (50 nL) by flushing with buffer. An exponential fit to the data to each of 200 chambers yields a mean mixing time constant of 15.2 ± 1.0 minutes. A representative time-lapse series of images from one chamber is shown on the right.

proportional to the radius of gyration R_g, and is given by

$$R_h \approx 0.5 R_g \approx 0.5(Lp/3)^{\frac{1}{2}}, \tag{2.2}$$

where L is the contour length of single stranded DNA (40 bases × 4.3 Angstroms/base) and p is the persistence length ($\sim$ 40 Angstroms)[114]. This yields a diffusion value of approximately 9.0×10^{-11} m^2s^{-1}, which is comparable to the diffusion constant of polymerase, the largest molecule in the PCR mix. Since the template solution constitutes only 1/5 of the final PCR reaction it must diffuse the longest distance to equilibrate across the chamber. Therefore, the measured diffusion time of 15.2 minutes represents an upper bound to the time constant for complete mixing of all components.

2.4 Results and Discussion

2.4.1 Device Design

An integrated microfluidic device that performs 300 parallel RT-qPCR assays and executes all steps of single-cell capture, lysis, reverse transcription, and qPCR is shown in Figure 1A. To facilitate the precise comparison of different samples and cell types, our prototype consists of 6 independent sample-loading lanes, each containing 50 cell-processing units. We resolved previously limiting technical pitfalls by the inclusion of design elements to 1) allow for efficient distribution of single cells without mechanical damage, 2) minimize background signal arising from free RNA or cell debris in the medium, and 3) avoid reaction inhibition by cell lysates in nL volumes.

In order to reduce device complexity and obviate the need for RNA purification, we optimized our device to be compatible with commercially available assays that use one-pot RT-qPCR protocols requiring only the sequential addition of reagents into a single reaction vessel. Each cell-processing unit consists of a compound chamber, formed by a cell capture chamber connected sequentially to two larger chambers for RT and qPCR (Figure 2.2B). This simple fluidic architecture allows the implementation of either heat lysis followed by two-step RT-qPCR (Figure 2.2D-I), or chemical

Figure 2.2 *(following page)*: Design and operation of the microfluidic device for single cell gene expression analysis. (A) Schematic of microfluidic device. Scale bar: 4 mm. The device features 6 sample input channels, each divided into 50 compound reaction chambers for a total of 300 RT-qPCR reactions using approximately 20 µL of reagents. Rectangular box indicates the region depicted in B. (B) Optical micrograph of array unit. For visualization, the fluid paths and control channels have been loaded with blue and red dyes, respectively. Each unit consists of (i) a reagent injection line, (ii) a 0.6 nL cell capture chamber with integrated cell traps, (iii) a 10 nL RT chamber, and (iv) a 50 nL PCR chamber. Scale bar: 400 µm. (C) Optical micrograph of two cell capture chambers with trapped single cells indicated by black arrows. Each trap includes upstream deflectors to direct cells into the capture region. Scale bar: 400 µm. (D-I) Device operation. (D) A single cell suspension is injected into the device. (E) Cell traps isolate single cells from the fluid stream and permit washing of cells to remove extracellular RNA. (F) Actuation of pneumatic valves results in single cell isolation prior to heat lysis. (G) Injection of reagent (green) for reverse transcription (RT) reaction (10 nL). (H) Reagent injection line is flushed with subsequent reagent (blue) for PCR. (I) Reagent for qPCR (blue) is combined with RT product in 50 nL qPCR chamber. Scale bar for D-I: 400 µm.

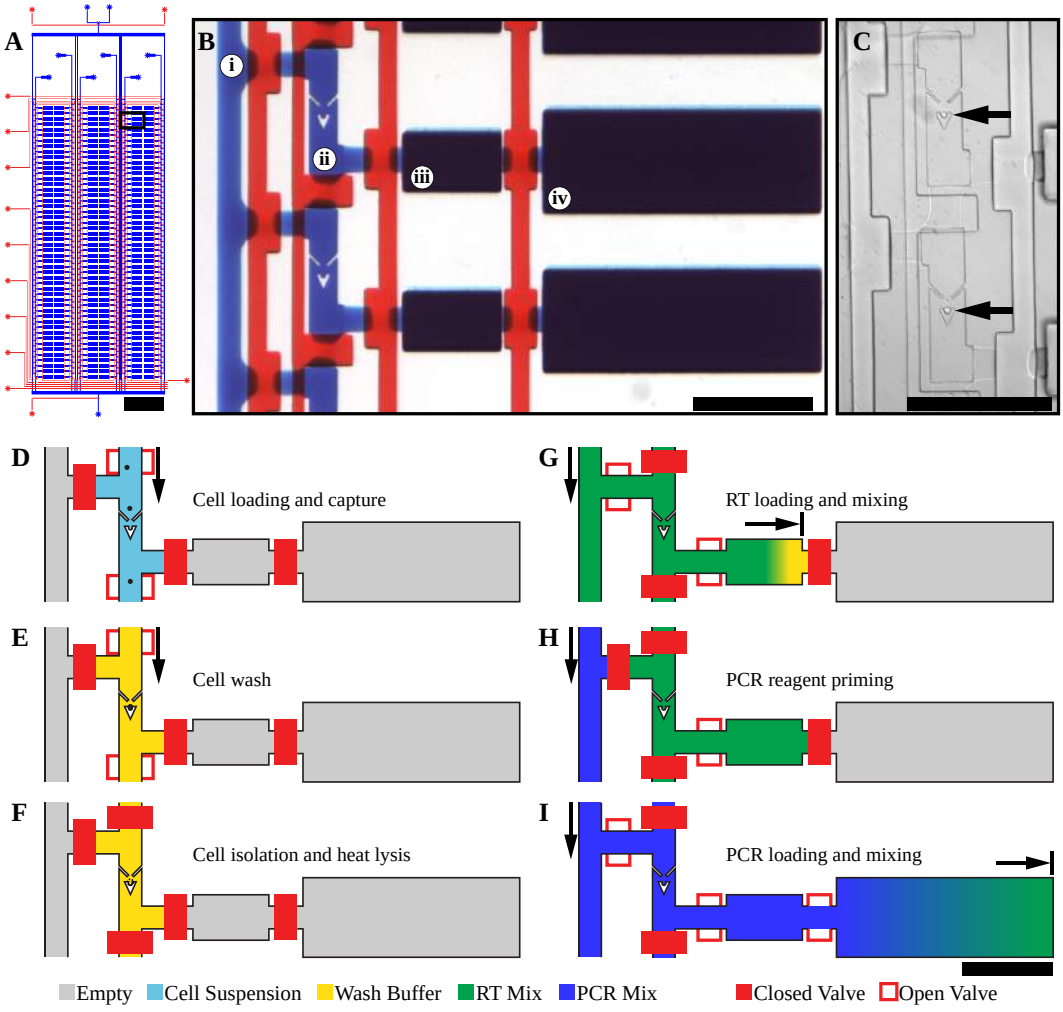
A
B
i
ii
iii
iv
C
D
Cell loading and capture
G
RT loading and mixing
E
Cell wash
H
PCR reagent priming
F
Cell isolation and heat lysis
I
PCR loading and mixing
Empty
Cell Suspension
Wash Buffer
RT Mix
PCR Mix
Closed Valve
Open Valve

lysis followed by one-step RT-qPCR. A detailed description of device operation for each of these protocols is provided in the methods section. All lanes are connected to a common feed channel which, following the completion of each reaction step, is used to inject the next reaction master mix through the upstream chambers, thereby diluting the intermediate product (cell lysate or cDNA) and assembling the next reaction mixture. This parallelization of reaction assembly in a microfluidic format ensures equal timing of all reaction steps and greatly reduces technical variability associated with pipetting and mixing steps in µL volumes. Fluorescence measurements were performed to ensure the efficient and reproducible transfer of reactants at each step, showing that losses in sample transfer are below 5%. To minimize device expense and complexity, temperature control and fluorescence detection were performed using peripheral hardware including a CCD detector mounted above a flatbed thermocycler plate.

Figure 2.3 *(following page)*: Precision and sensitivity of microfluidic RT-qPCR. (A) Fluorescence image of entire device showing 300 reactions in 6 lanes. Image is taken after 40 cycles of PCR from dilution series of purified total RNA from K562 cells. From left to right the samples are 40 pg/chamber, 5 pg/chamber, 625 fg/chamber, 78 fg/chamber, 10 fg/chamber, and no-template control (NTC). Single molecule amplification at limiting dilution results in a digital amplification pattern for 10 fg and 78 fg lanes. No amplification is observed in NTC lane (N = 50). (B) 300 real time amplification curves generated from processing sequences of images similar to (A). The threshold for determining CT values is indicated by the dashed line. (C) On-chip (black) and off-chip (blue) RT-qPCR for GAPDH from a 8× serial dilution of purified total RNA shows improved sensitivity in nL volume reactions. In the microfluidic system, CT values for the 10 fg sample correspond to single molecule amplifications detected in 19 of 50 chambers. The mean and standard deviation from single cell measurements is shown in green for both on and off-chip analysis. CT values obtained on chip correspond to a mean of 20 pg of RNA per cell. Off-chip measurements of single K562 cells washed twice in PBS and isolated by glass capillary exhibit artificially increased levels due to residual signal from debris and free RNA in the supernatant (red). Cells were transferred in approximately 2 µL of supernatant, which was measured to contain ∼20 pg of extracellular RNA. Error bars represent standard deviation of measured CT values for all amplified reactions. (D) Real-time amplification curves of GAPDH in K562 cell lysate dilutions. Inhibition of RT-PCR occurs at cell lysate concentrations beyond 10 cell equivalents per 50 nL reaction. (E) Measured CT values for GAPDH in dilution series of cell lysate. No inhibition occurs for single cell lysates.

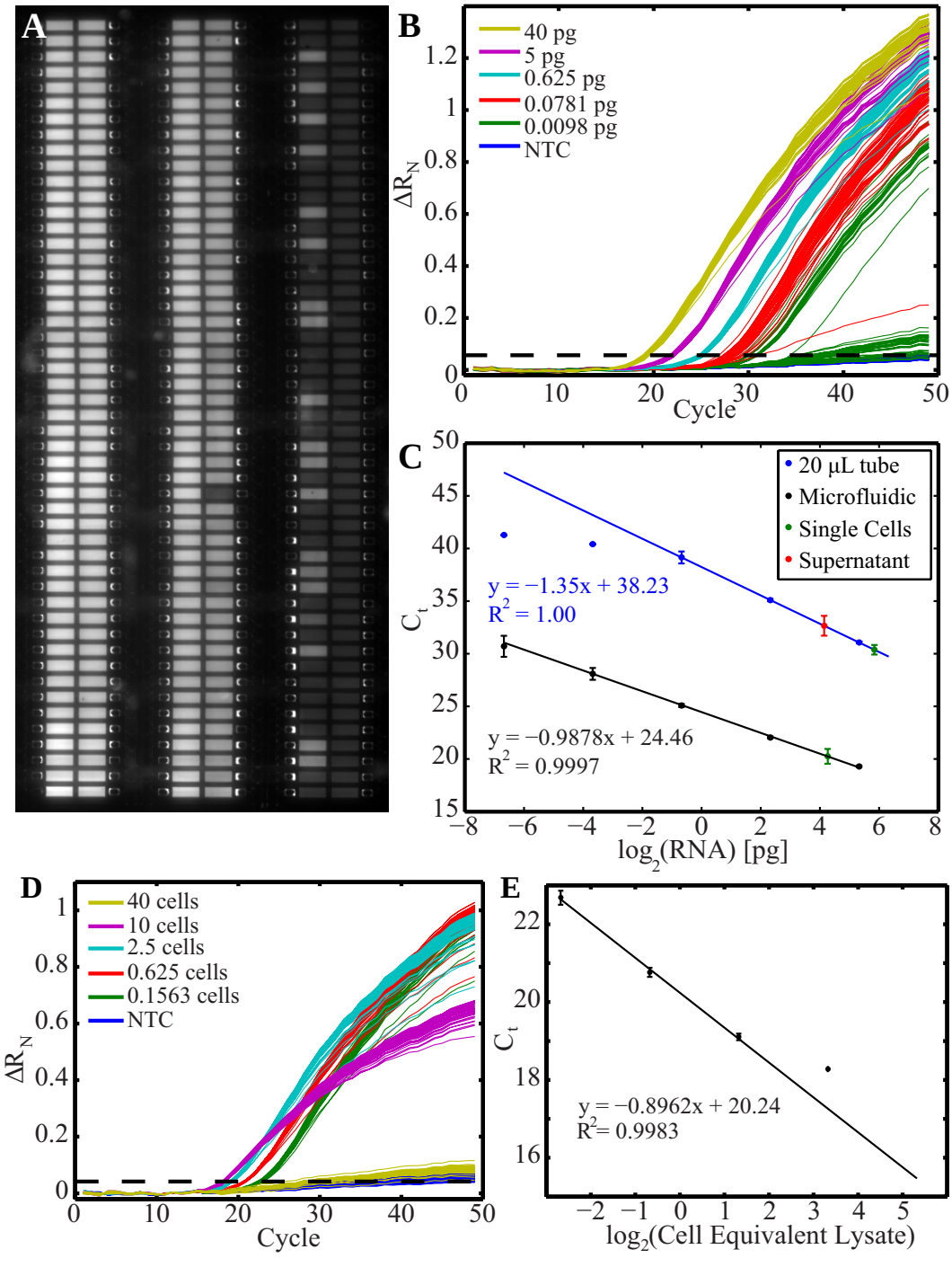
A
B
40 pg
5 pg
0.625 pg
0.0781 pg
0.0098 pg
NTC
ΔR_N
Cycle
C
20 µL tube
Microfluidic
Single Cells
Supernatant
y = −1.35x + 38.23
R^2 = 1.00
y = −0.9878x + 24.46
R^2 = 0.9997
C_t
log_2(RNA) [pg]
D
40 cells
10 cells
2.5 cells
0.625 cells
0.1563 cells
NTC
ΔR_N
Cycle
E
y = −0.8962x + 20.24
R^2= 0.9983
C_t
log_2(Cell Equivalent Lysate)

We designed our chamber volumes to ensure sufficient dilution between each processing step to avoid reaction inhibition while at the same time maintaining high template concentrations and assay sensitivity. Initial attempts to perform RT-qPCR in low nL volumes were found to produce highly variable results, including nonspecific amplification and inconsistent detection of abundant transcripts[98]. Cell lysate dilutions showed that reaction inhibition becomes significant at concentrations in excess of 0.2 cells/nL, or 10 cells per 50 nL reaction (Figure 2.3D). On the other hand, RT-qPCR measurement noise has been shown to become the dominant source of variability when starting at concentrations below 1 copy per 100 nL[58], illustrating that minimizing reaction volumes is critical for precise measurements on limited template. Finally, experiments in tubes were performed to determine that a dilution ratio of at least 5:1 (PCR mix:RT product) is optimum for PCR efficiency. We therefore designed our combined reactors to have an aggregate total volume of 60.6 nL, consisting of a 0.6 nL cell capture chamber, a 10 nL RT chamber, and a 50 nL qPCR chamber. These volumes allow for the reliable amplification of single molecules (Figure 2.3A), and result in a final template concentration of 330 ng/mL when starting from a single cell equivalent of RNA (20 pg). The use of larger volume RT and PCR chambers has the added advantage of reducing their surface to volume ratio, thereby minimizing reagent evaporation through the gas permeable device material (polydimethylsiloxane).

Another critical step towards integration was to efficiently distribute single cells into each location on the array without mechanical damage. To achieve reproducible and deterministic loading of single cells into each array element we engineered a hydrodynamic single cell trap within each capture chamber. Cell traps consisting of a single cup structure[71] were found to be highly inefficient, capturing less than 0.1% of cells passing in close proximity to the center of the channel structure. To improve capture efficiency, we incorporated upstream deflectors, located 22.5 µm from the trap, to focus cells into the central streamlines where capture is most efficient (Figure 2.4C). Using these structures we were able to achieve high single cell occupancy of array locations (Figure 2.4A-B). Over 8 separate experiments, a loading protocol of $\sim$60 seconds (10^6 cells/mL, 20 nL/s per lane) resulted in the successful isolation of single cells in 1518/1700 chambers (89.3%), with a cell capture efficiency of 5.0$\pm$0.5%. Staining with Trypan Blue™ was used to assess the viability of cells after loading and was determined to be equivalent to the viability of the input sample (97.4% viability

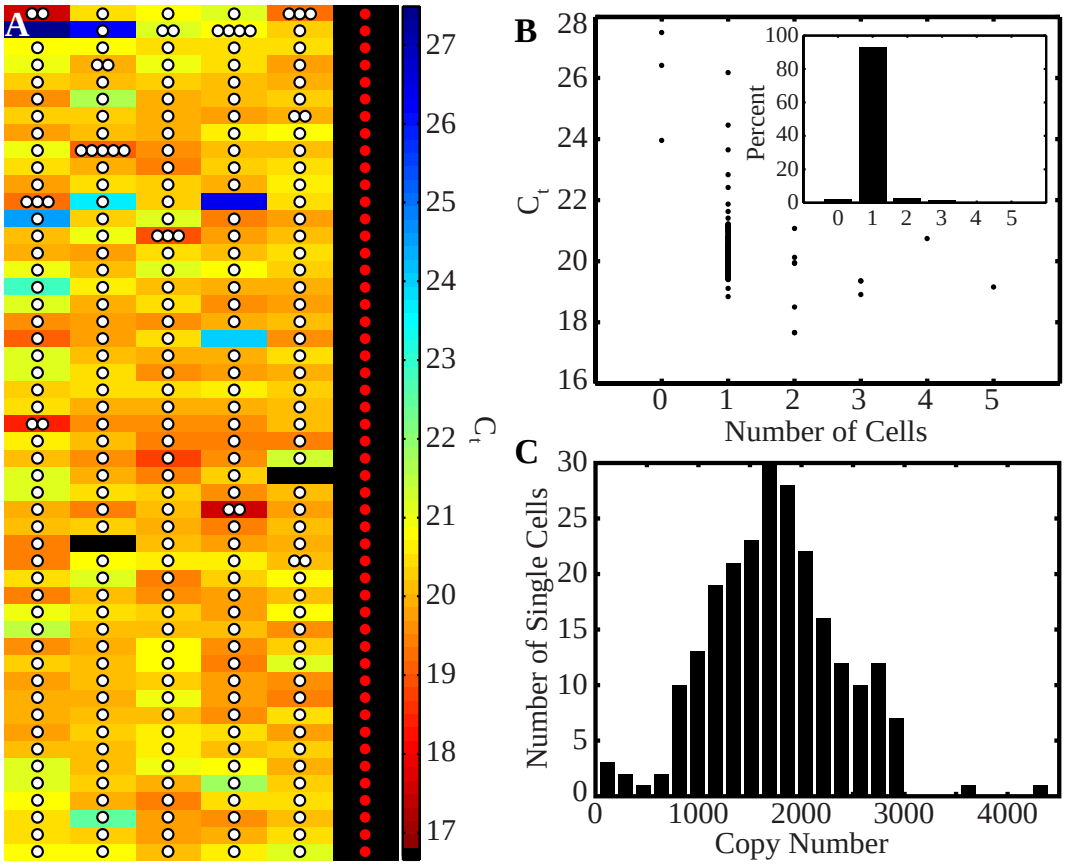

Figure 2.4: Single cell loading and transcript measurements. (A) The locations of cells in each chamber along all 6 lanes of a device, as determined by brightfield microscopy, are represented as white circles and overlaid on a heat map of CT values obtained from RT-qPCR measurements of GAPDH in K562 cells. Red circles indicate NTC. (B) Scatter plot showing CT measurements for experiment shown in (A). Histogram (inset) shows 93.2% single cell occupancy. (C) Distribution of the number of GAPDH transcripts measured in single K562 cells (N=233).

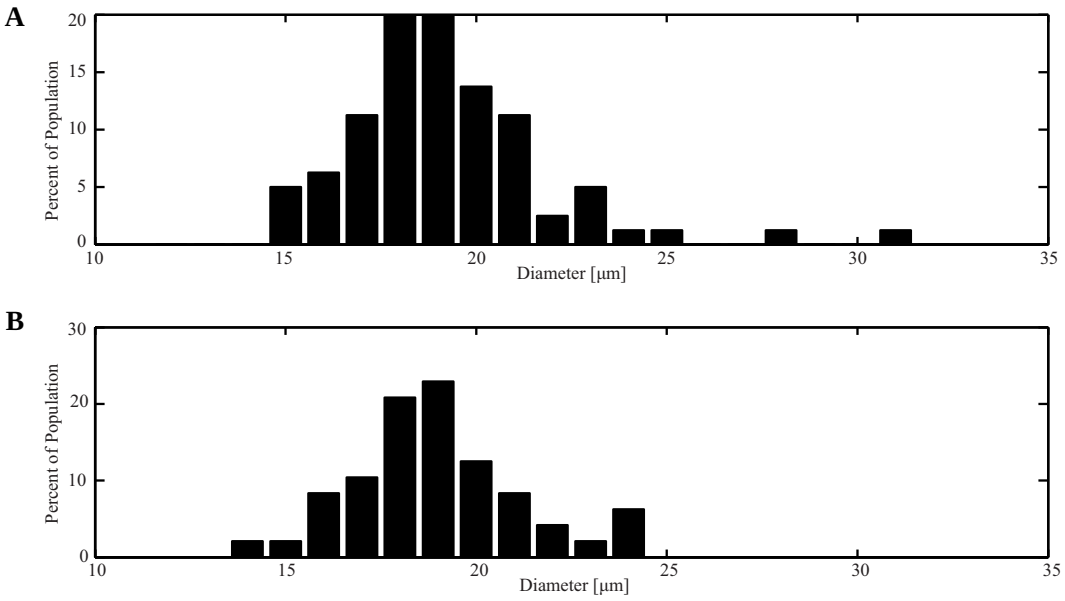

Figure 2.5: Histograms showing the size distribution of cells in original sample as measured by Cedex (A) are consistent with the size distribution of cells isolated by microfluidic traps (B). Under the assumption of spherical cell shape the distribution of diameters of trapped cells corresponds to a mean volume of 4.2 pL with a standard deviation of 2.0 pL.

vs. input 96.8%). Finally, measurements of the distribution of cell diameters prior to and after loading indicated that cell trapping did not introduce significant bias (p=0.67, two sample t-test) in selecting cells of different sizes (Figure 2.5). This cell trap geometry and loading protocol were used in all subsequent qPCR measurements presented below. Further improvement of trap and deflector geometries were found to achieve fill factors of >99% (100 single cells captured out of 100 traps analyzed) and cell capture efficiencies of 87.0±4.5%, with cell viability again matching the input sample (>98%) and not significantly biasing cell sizes (p=0.35, two-sample t-test), making this method applicable to the analysis of limited quantity samples such as rare stem cells or clinical samples.

The immobilization of cells in traps was also used for on-chip washing of cells prior to lysis to remove free RNA, cellular debris, and untrapped cells that would otherwise give rise to background signal or result in low single cell occupancy (Figure 2.7A-B). The efficiency of chamber washing, determined by loading purified RNA template (36.5 ng/µL), followed by washing and RT-qPCR analysis, was >99.99% (1.1×10^4 copies measured without wash, 0 copies detected after washing) (Figure S2C). In addition, RT-qPCR measurements testing different cell loading and washing protocols demonstrated that on-chip washing allows for loading directly from culture medium with low background as compared to off-chip wash steps followed by analysis in µL volumes (Figure 2.3C). Importantly, on-chip washing allows for lysis within seconds of washing, thereby minimizing spurious transcriptional responses that may arise from sequential medium exchange and spin steps.

2.4.2 Validation of Integrated Single Cell RT-qPCR

We first tested the sensitivity and precision of RT-qPCR in our device by performing measurements of GAPDH expression over an 8-fold dilution series of total RNA, ranging from 40 pg (∼2 cell equivalents) to 10 fg (∼1/2000 cell equivalents). RNA was purified from K562 cells, a BCR-ABL positive human cell line derived from a patient with chronic myeloid leukemia (20) (Figure 2.3A-C). The efficiency of amplification was determined over the four highest template concentrations (40 pg, 5 pg, 625 fg, 78.125 fg) as the slope from a linear least squares fit of log2(C) vs. CT, and was found to be 0.988±0.055. The standard deviation of CT values was less than 0.15 at the three highest concentrations (s.d.=0.08, 0.10, 0.14 for the 40 pg, 5 pg, and 625 fg samples respectively), indicating uniform amplification across the

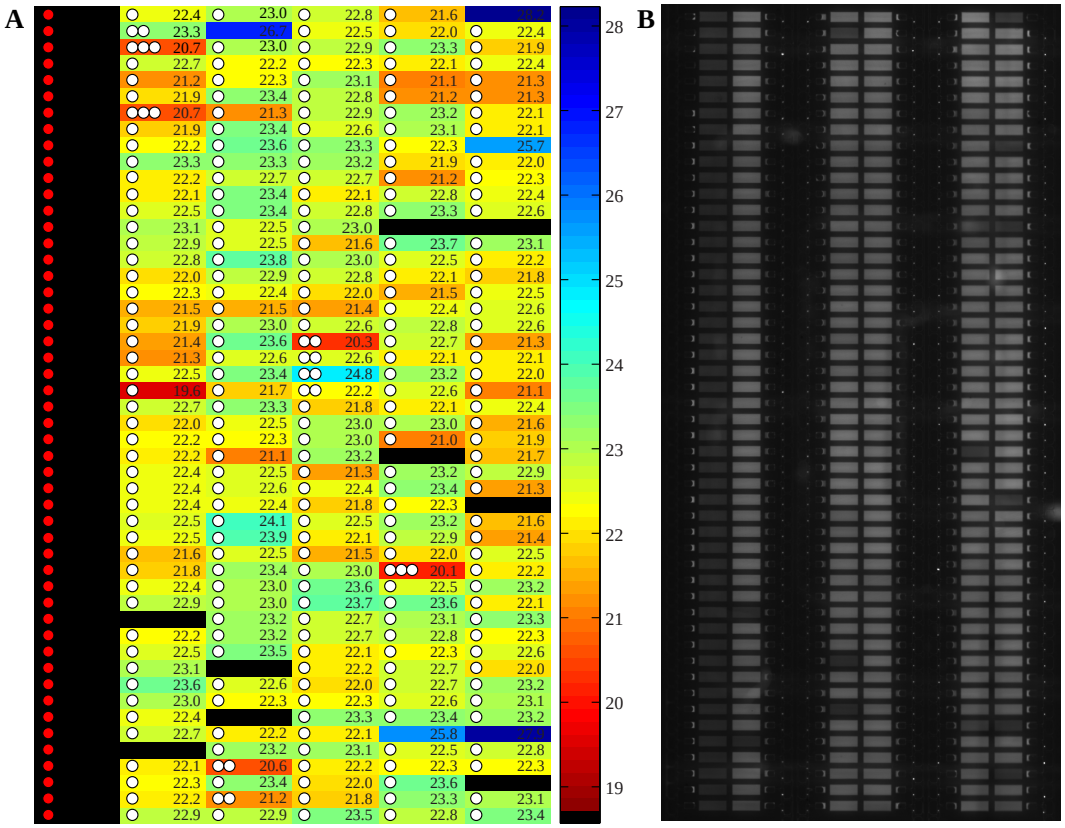

Figure 2.6: Single-cell miRNA measurements. (A) The locations of cells in each chamber along all 6 lanes of a device, as determined by brightfield microscopy, are represented as white circles and overlaid on a heat map of CT values obtained from RT-qPCR measurements of miR27a in K562 cells. Red circles indicate NTC. (B) Fluorescence image of entire device, corresponding to experiment in (A) after 30 PCR cycles. Cell corpses remain after heat lysis and are visible as punctuate fluorescent spots adjacent to reaction chambers.

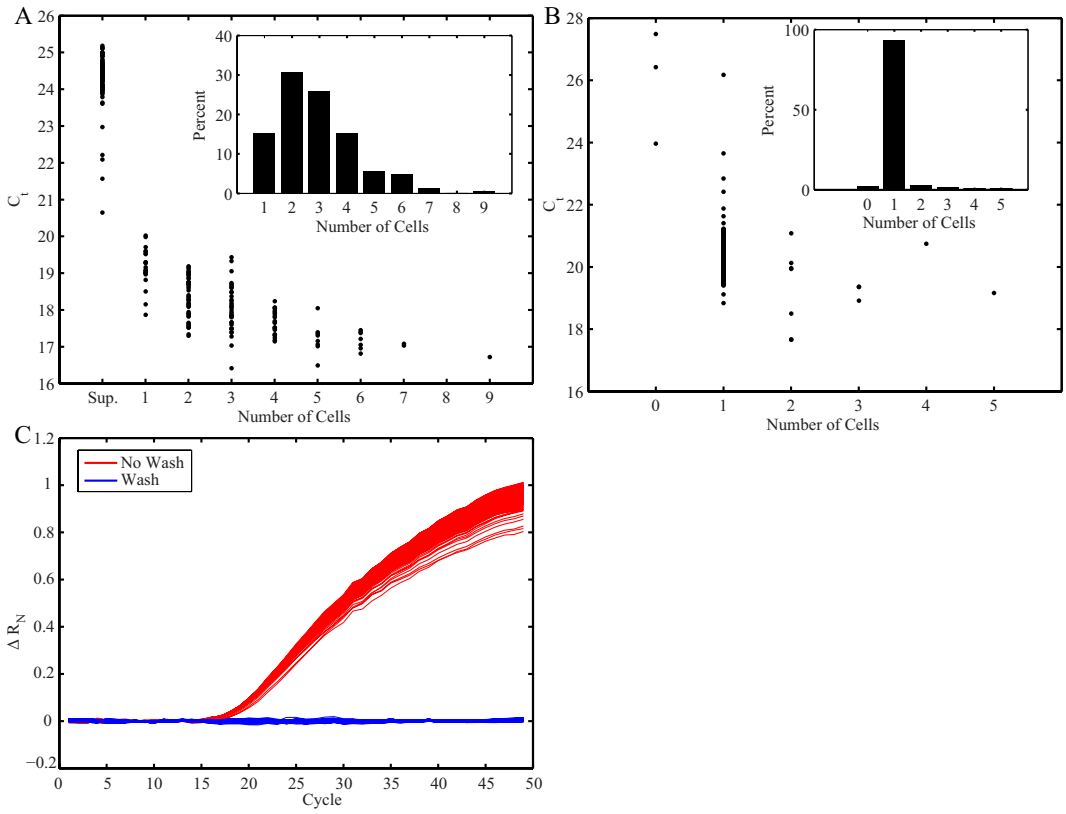

Figure 2.7: On-chip cell washing. (A) Measurements of GAPDH in cells washed in PBS off-chip prior to injection into microfluidic device, without an on-chip wash contain background signal from template in supernatant. Without on-chip washing, untrapped cells remain in the capture chambers, resulting in fewer single cell measurements (histogram inlayed). Detection of residual RNA after washing is dramatically reduced by comparison to off-chip results (Figure 2.6) due to small volume processing. (B) On-chip washing was found to reduce the background signal from free RNA in the supernatant, and dramatically increased the number of single cells analyzed. (C) Comparison of GAPDH measurements from loading purified RNA and washing, or not washing, the cell capture chambers.

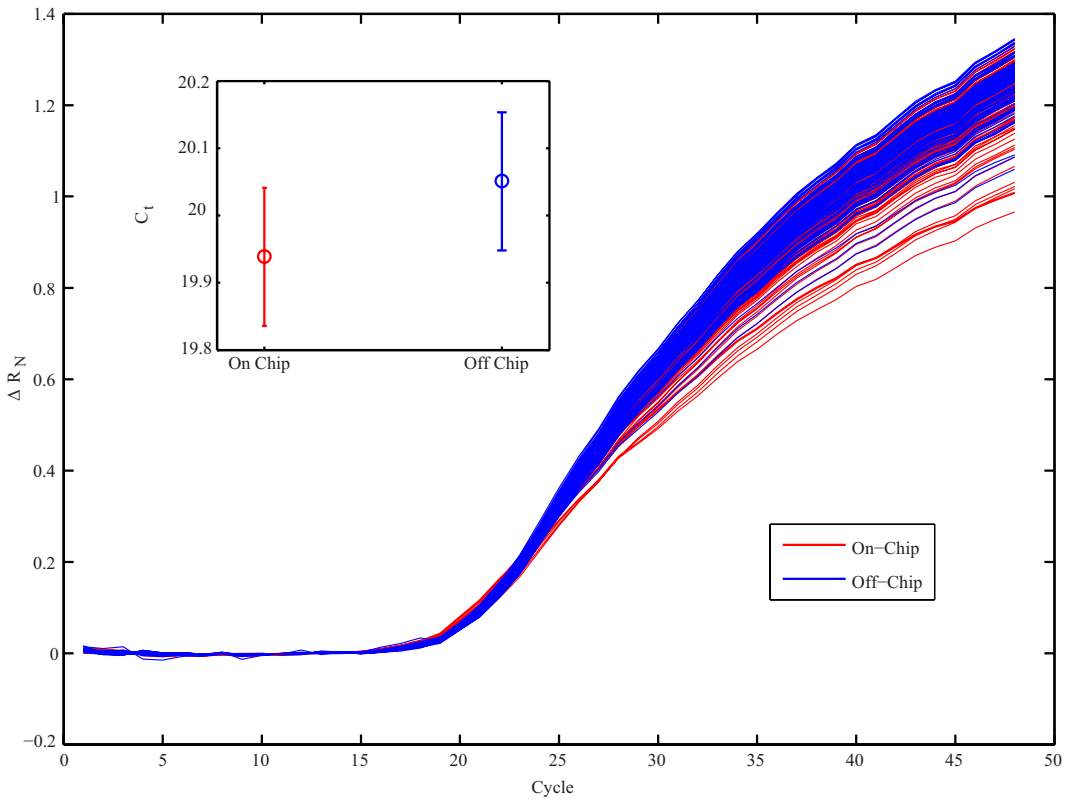

Figure 2.8: Comparison of GAPDH measurements from K562 cell lysate with RT performed in the microfluidic device or RT performed in tubes prior to qPCR in the device. Obtained CT values (inset) show no significant difference in efficiency.

array and technical error of less than 10% in absolute concentration, near the limit of qPCR precision. The highest measurement variability was observed in the 78 fg sample, where shot noise (Poisson sampling noise) is most pronounced and accounts for approximately 50% of the measurement variance. Template amounts below 625 fg resulted in a digital pattern characteristic of single molecule amplification (49/50 for 78 fg, 19/50 for 10 fg) and consistent with the expected occupancy of chambers as determined by a binomial distribution[62]. Based on the frequency of single molecule detection in the 10 fg sample, we measured the average copy number of GAPDH to be 979 ± 240 transcript copies per single cell equivalent (20 pg) (Figure 2.3). This measurement is comparable to previous reports[79] and is in close agreement with an independent estimate based on normalizing the dilution series to CT values obtained for single molecules (copies/20 pg = 0.5×copies/40 pg = 0.5×(1+efficiency)(CT(40 pg) - CT(single molecule)) = 1407 ± 153 copies/20 pg). It should be noted that

these estimates represent a lower bound since they do not account for RT efficiency; the RT efficiency of GAPDH has been previously estimated to be ∼50%[89] but is dependent on transcript secondary structure and assay design. A comparison of CT values obtained from on-chip qPCR from cDNA synthesized off-chip demonstrated that on-chip RT efficiency is equal to that obtained off-chip when working from the same RNA concentrations (Figure 2.8). Finally, comparison of the same dilution series of RNA, assayed for GAPDH both on-chip and in tubes (20 µL volume) (Figure 2.3C), showed that on-chip analysis provides improved sensitivity.

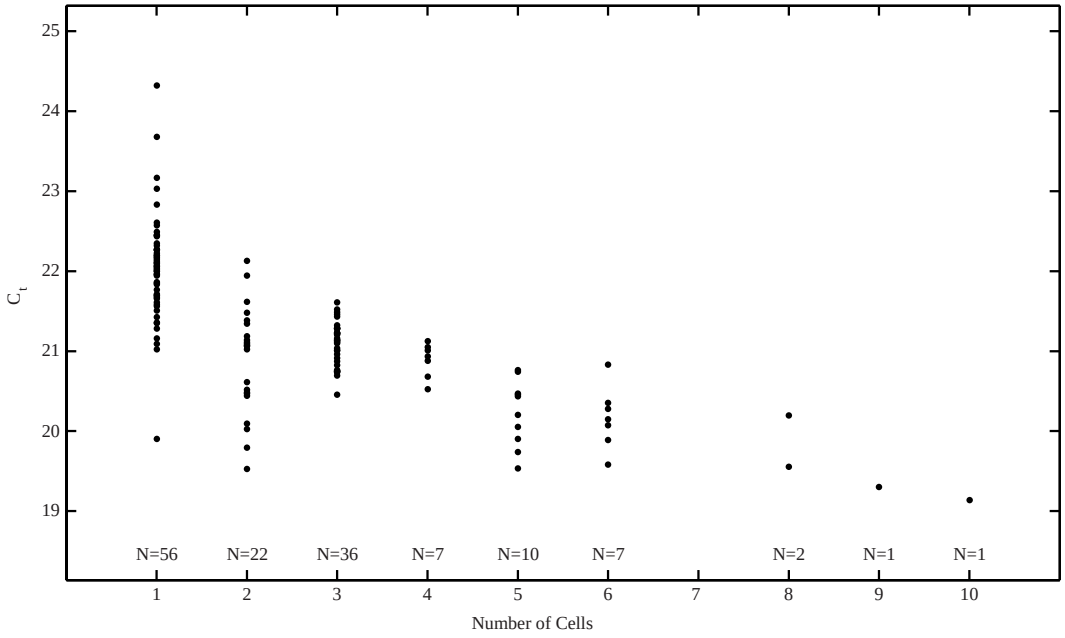

Figure 2.9: Measurement of miR16 in hESC cell aggregates demonstrates that the number of cells is reflected in corresponding cycle threshold (CT) values.

We next evaluated the efficiency and reliability of on-chip cell processing by comparing our GAPDH measurements of purified RNA to measurements performed directly from single K562 cells (Figure 2.3C, Figure 2.4C). K562 cells were loaded directly from culture medium followed by washing and analysis using a chemical lysis and one-step RT-qPCR protocol (Cells Direct™, Invitrogen). Using a CT threshold of 31.5, corresponding to the mean CT of a single molecule of GAPDH (CT = 30.5) plus two standard deviations (s.d. = 0.5), we observed successful amplification in 100% of single cells (N = 233) (Figure 2.4A-B). Adjacent chambers that did not contain a cell were clearly separated from single cell measurements with an average delta CT

value of 5.7 (5 empty chambers, 3 of which amplified) (Figure 2.4A-B). Consistent with previous reports[40], we observed a log-normal distribution of GAPDH in single cells with mean CT values of 20.3 (s.d. = 0.8) and an average of 1761 (s.d. = 648) copies per cell (Figure 2.4C). These expression levels are consistent with previous estimates in single cells[79]. Additionally, the mean CT of 20.3 observed for single cells matches measurements of single cell equivalent lysate (CT = 20.2, Figure 2.3D). Using digital PCR on cDNA prepared from K562 cell lysate, we measured an average of 1229±72 GAPDH molecules per single cell equivalent. We conclude that the relative efficiency of on-chip single cell lysis and mRNA extraction/accessibility is equal to that achieved when working from RNA purified from large numbers of cells. Finally, as expected, RT-qPCR measurements from chambers loaded with more than one cell show reduced variability and lower CT values (Figure 2.7A, Figure 2.9). Taken together, these results establish the precise measurement of mRNA abundance with single molecule sensitivity and the dynamic range needed for single cell analysis.

2.4.3 Application to Measurement of Single Cell miRNA Expression

We next applied our technology to the study of single cell miRNA expression. miRNAs are thought to provide a unique signature of cellular state and are central players in orchestrating development and oncogenesis, making them a promising class of biomarker for single cell analysis[16, 20, 115]. Importantly, the short length of miRNAs (∼22 nucleotides) makes them difficult to detect by hybridization approaches, so that RT-qPCR is the dominant quantification strategy. To demonstrate the robustness and throughput of our technology, we performed a total of 1672 single cell measurements to examine single-cell variability in the expression of 9 miRNAs spanning a wide range of abundance (>16000 copies per cell to <0.2 average copies per cell). K562 cells were again chosen as a heterogeneous population for this study since they are known to exhibit mixed characteristics of erythrocytes, granulocytes, and monocytes[116, 117]. We first measured the expression of miR-16, a highly expressed microRNA that is found in many tissue types[118] and has been suggested as a suitable internal standard for normalization[60]. We found that miR-16 was log-normally distributed across K562 cells, but with slightly lower expression and notably tighter regulation than GAPDH, having an average of 804 (s.d. = 261) copies per cell and

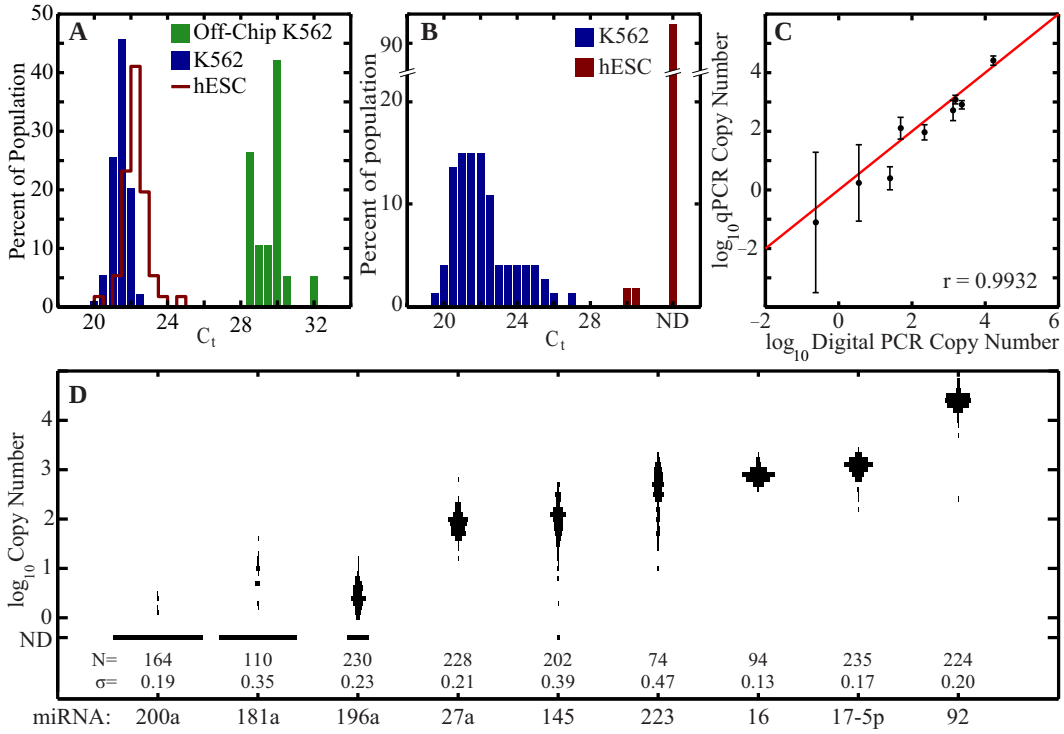

Figure 2.10: Single cell miRNA measurements. (A) Single cell measurements of miR-16 expression in K562 cells and hESCs. Measurements of single K562 cells isolated using a microcapillary and assayed in 20 µL volumes are shown for comparison of technical variability. The observed shift in mean CT values between on and off-chip measurements is due to lower template concentrations, and hence increased required PCR cycles, in the off-chip samples. (B) Differential expression of miR-223 between K562 cells and hESCs. Right-most bar indicates cells for which miR-223 was not detected (ND). (C) Mean single cell miRNA copy numbers measured by RT-qPCR in the microfluidic device compared to digital PCR measurements from bulk cell lysate. Error bars represent standard deviation of single cell measurements for each miRNA. (D) 2072 single cell measurements of the expression of 9 miRNA in K562 cells. Reflected histograms represent the expression distributions for each miRNA.

a standard deviation of 30% (mean CT = 21.4, s.d. = 0.4). This strikingly low variability is within our estimates of cell volume differences (Figure 2.5). Matched experiments on single cells, isolated by micropipette into 20 µL volume tubes displayed an increase in measurement variability to ∼90% (mean CT = 29.5, s.d. = 0.9), demonstrating the improved precision of parallel microfluidic cell processing in nL volumes (Figure 2.10A). Microliter volume experiments also showed a pronounced increase in measured CT values that results from the low concentration of template and the large number of required PCR cycles.

To demonstrate the utility of our device for measuring differential expression in single cells we next measured the expression of miR-223, a miRNA implicated in myeloid differentiation[18, 117]. In contrast to miR-16, K562 cell miR-223 expression was found to be highly variable (mean CT = 22.2, s.d. = 1.6, copy number = 513, s.d. = 406) and was not log-normally distributed (Figure 2.10B), consistent with the known functional heterogeneity of K562 cells. These measurements highlight the utility of single cell miRNA expression analysis for assessing the heterogeneity of cell populations and for identifying miRNAs that are useful biomarkers of cellular state. To further explore this possibility we measured the expression of an additional 7 miRNAs (9 total) and plotted the patterns of single cell expression in K562 populations (Figure 2.10C). Following the procedure described above, we used single molecule CT values, obtained by digital PCR, to translate measured CT values to absolute copy number. Assuming 100% efficient amplification, we observed that the copy number, calculated as 2(CT(single cell) CT(single molecule)), was well correlated (coefficient of 0.9932) with the average copy number obtained by digital PCR of cDNA prepared from bulk lysates (Figure 2.10D). Single cell measurements revealed distinct patterns of miRNA expression, with miR-16, miR-92, and miR-17-5p each exhibiting unimodal and tightly regulated distributions, while miR-223, miR-196a, and miR-145 showed multi-modal distributions and a high level of cellular heterogeneity. Notably, for the lowest abundance miRNA, miR-200a, we detected expression in only a small fraction of cells and at levels below ∼5 copies per cell. The average miR-200a copy number over all cells was within factor of two of that obtained by digital PCR (0.2 copies per cell). In contrast, miR-92 was found to be the most abundant miRNA and was present at approximately 60,000 copies per cell. These measurements established miRNA quantification in single cells with a dynamic range of greater than 10^4 and at single molecule sensitivity.

Finally, to illustrate the utility of single cell measurements in precisely assessing differences in both the average expression and the heterogeneity between two different cell populations, the expression levels of miR-16 and miR-223 in K562 cells were compared to those in CA1S cells[111, 112], a human embryonic stem cell line (hESC). Although miR-16 was found to be expressed in hESC at similar levels to K562 (ΔCT = 0.6), we observed approximately a two-fold greater variability in expression (mean CT = 22.0, s.d. = 0.7) (Figure 2.10A). In contrast, when compared to K562, single CA1S cell measurements of miR-223 showed strong down-regulation, with miR-223 detected in only 3.6% of cells. The absence of significant miR-223 expression in hESC is expected due to the role of miR-223 as a differentiation-specific miRNA[18, 117].

2.4.4 Co-regulation of miR-145 and OCT4 in Single Cells

The measurement of multiple transcripts in individual cells allows for quantitative measurements of gene co-regulation that would otherwise be masked by cellular heterogeneity[90]. To demonstrate this capability we designed an optically multiplexed assay to study the co-regulation of miR-145 and OCT4, a known target of miR-145[119], during the differentiation of hESCs (Figure 2.11A-C). A total of 1094 single cell measurements were performed at 0, 4, 6, and 8 days of differentiation. Cell distributions at each time point were used to map out the evolution of these transcripts and showed that average miR-145 levels increased approximately 20 fold (copy numbers: D0: mean = 18.9, s.d. = 25.5, D8: mean = 380.3, s.d. = 259.4) over 8 days. Increases in miR-145 were accompanied by progressive down-regulation of OCT4, ultimately reaching an average of 30-fold suppression (copy numbers: D0: mean = 755.7, s.d. = 306.4, D8: mean = 27.8, s.d. = 124.5) after 8 days (independently verified by mRNA-FISH) (Figure 2.12). Notably, single cell analysis at day 6 showed a bimodal distribution in both OCT4 and miR-145, revealing a transition of cellular state[119] that likely reflects the spontaneous differentiation of a subpopulation of cells. The observed single cell dynamics of miR-145 and OCT4 co-regulation are not apparent in population measurements, highlighting the use of scalable single cell transcriptional analysis in correlating molecular signatures to cellular decision making[90].

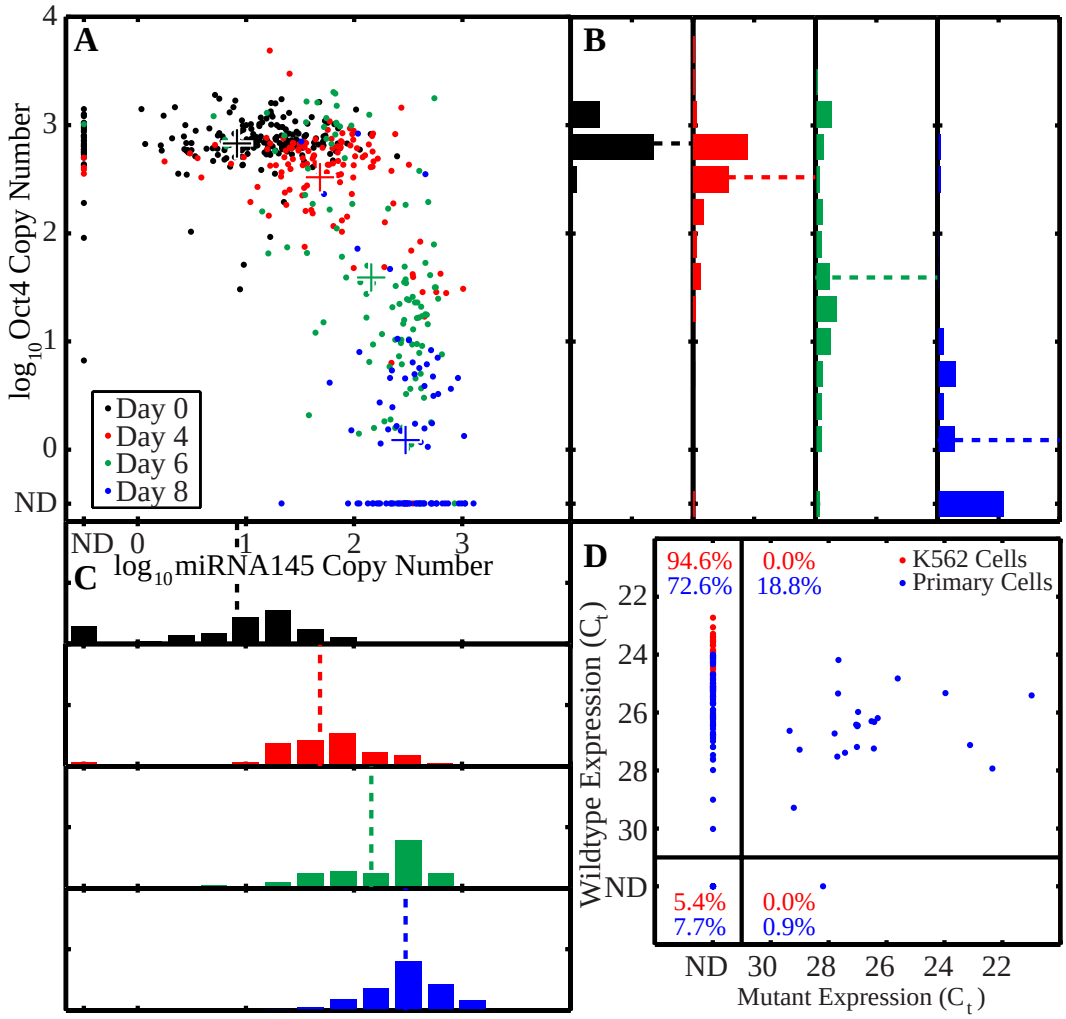

Figure 2.11: Optical multiplexing of single cell RT-qPCR. (A) Multiplexed analysis of the co-expression of OCT4 and miR145 in differentiating hESC. Points are color-coded to represent single cell measurements (N = 547) for each time point. Crosses represent population mean copy number. (B,C) Histograms showing the distribution of each transcript are projected on the axes with the mean copy number indicated by a dashed line. (D) Co-expression measurements of SP1 wild-type and SNV mutant transcripts in primary cells isolated from a lobular breast cancer sample. Mutant SP1 is detected in 23 of 117 primary cells, and undetected in K562 cells (N=37).

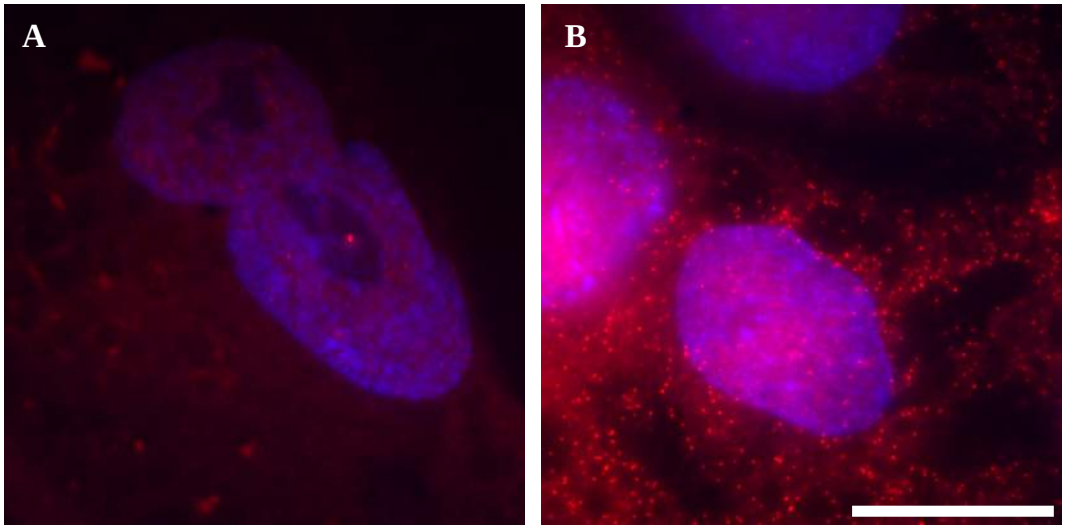

Figure 2.12: mRNA-FISH of OCT4 (red) counterstained with DAPI (Blue) in CA1S cells (A) Representative image of mRNA-FISH of OCT4 in a CA1S cell after 7 days of FBS differentiation. Estimate of average copy number of OCT4 mRNA as determined by manual inspection of image stacks is 42 (s.d. = 41, N=6). (B) Representative image of undifferentiated CA1S cells. Estimate of average copy number as determined by manual inspection of image stacks is 988 (s.d. = 368, N = 6). Scale bar = 10 µm.

2.4.5 SNV Detection in Primary Cells

Finally, to establish the specificity of our method we used multiplexed measurements of mRNA single nucleotide variants (SNV) to assess the genomic heterogeneity within a primary tumor sample. A total of 117 single cells isolated from a plural effusion of a metastatic breast cancer were assayed for the expression of a SNV mutant of the transcription factor SP1, previously identified by deep sequencing[32] (Figure 2.11D). Primers were designed using sequences flanking the SNV location and do not discriminate between the genomic DNA and mRNA transcript. Of the 117 primary cells analyzed, 22 (18.8%) were heterozygous for the mutant and wildtype allele, 85 (72.6%) were homozygous wildtype, 1 (0.9%) was homozygous mutant and the transcripts were undetected in 9 (7.7%). We did not detect the SP1 mutation in 37 control K562 cells and failed to detect the wild-type transcript in only 2 of these cells. In the absence of copy number alterations in the primary sample, these observed frequencies would suggest a mutant to wild-type SP1 ratio of 11.2% ($18.8\times1 + 0.9\times2 = 20.6$ mutant to $18.8\times1 + 72.6\times2 = 164$ wild-type). However, using digital PCR on purified DNA from the primary sample, we found the ratio of mutant to wild-type

SP1 alleles to be 18.7 ± 2.3%, in agreement with the previously reported ratio of 21.9%, obtained by deep sequencing[32]. The lower frequency of cells expressing the mutant SP1 allele may be due to allelic expression bias or an amplification of the SP1 mutant allele, both of which are supported by Shah et al.[32]. Regardless, given that the frequency of tumor cells within the original sample was approximately 89%[32], both DNA molecule counting and single cell RNA expression measurements show that the metastasis of this tumor is derived from multiple cancer cell lineages.

2.5 Conclusion

Here we have demonstrated the first implementation of scalable and quantitative single cell gene expression measurements on an integrated microfluidic system. The presented device performs 300 high-precision single cell RT-qPCR measurements per run, surpassing previous microfluidic systems by a factor of ∼100 in throughput. Further scaling the throughput to over 1000 measurements on a device with an area of one square inch is straightforward as each array element occupies an area of 0.6 mm^2. In terms of performance, we have established a dynamic range of at least 10^4, measurement precision of better than 10%, single molecule sensitivity, and specificity capable of discriminating the relative abundance of alleles differing by a single nucleotide. Compared to tube-based single cell RT-qPCR, microfluidic processing provides improved reproducibility, precision, and sensitivity, all of which may be critical in identifying subtle differences in cell populations. Nanoliter volume also results in a 1000-fold reduction in reagent consumption, thereby enabling cost effective analysis of large numbers of single cells.

In over 3300 single cell experiments, using adherent and suspension cell lines as well as clinical samples, we have shown that microfluidic RT-qPCR is well-suited to the quantitative analysis of miRNA expression and SNV detection, both of which are difficult or inaccessible by alternative hybridization methods. Notably, our device allowed for precise comparison of the distributions of GAPDH and miR-16 expression. miR-16 was found to be exquisitely regulated in K562 cells, a finding that is striking given the known functional heterogeneity of this population and the high observed variability in the expression of other measured miRNAs. We postulate that higher observed variability of GAPDH expression reflects the fundamentally stochastic process of transcriptional bursts followed by mRNA degradation. Incorporation of miRNA

into the RISC complex is known to provide enhanced stability so that miRNA are inherently less subject to temporal fluctuations; miRNA are thus particularly suited as biomarkers for assessing single cell state and population heterogeneity. We anticipate that scalable and precise single cell miRNA analysis will become an invaluable tool in stratifying populations of mixed differentiation state[20].

Here we have established the critical element of combining all single-cell processing steps into an integrated platform. This functionality provides a solid foundation upon which increasingly advanced microfluidic single cell transcription analysis may be built. We anticipate that more complex fluid routing[120], to distribute cell contents across multiple chambers, will allow for the multiplexed measurements of tens of targets across hundreds of cells, and for combining this technology with single molecule detection by digital PCR. Alternatively, the microfluidic system described here could be used for single cell processing and pre-amplification, with recovered reaction products analyzed by high-throughput microfluidic qPCR or sequencing. We contend that the simplicity of device operation will soon allow for the robust and automated implementation of single cell RT-qPCR, leading to its widespread adoption in research applications and opening the prospect of diagnostic tests based on single cell analysis.

Table 2.3: mRNA FISH Probes

Probe Sequence (5' - 3')	Probe Name	Position	GC content (%)
tgaaatgagggcttgcgaag	OCT4_1	2	50
aaatccgaagccaggtgtcc	OCT4_2	61	55
atcacctccaccacctggag	OCT4_3	95	60
aggtccgaggatcaacccag	OCT4_4	138	60
aggagggccttggaagctta	OCT4_5	161	55
aatcccccacacctcagagc	OCT4_6	215	60
atccccccacagaactcata	OCT4_7	253	50
actagccccactccaacctg	OCT4_8	289	60
tcaggctgagaggtctccaa	OCT4_9	322	55
agttgctctccaccccgact	OCT4_10	354	60
ttctccttctccagcttcac	OCT4_11	418	50
ctcctccgggttttgctcca	OCT4_12	440	60
ttctgcagagctttgatgtc	OCT4_13	466	45
cttggcaaattgctcgagtt	OCT4_14	488	45
tgatcctcttctgcttcagg	OCT4_15	510	50
atcggcctgtgtatatccca	OCT4_16	533	50
aaatagaacccccagggtga	OCT4_17	560	50
tcgtttggctgaataccttc	OCT4_18	582	45
taagctgcagagcctcaaag	OCT4_19	612	50
gcagcttacacatgttcttg	OCT4_20	636	45
tccacccacttctgcagcaa	OCT4_21	661	55
gattttcattgttgtcagct	OCT4_22	684	35
tctgctttgcatatctcctg	OCT4_23	706	45
actggttcgctttctctttc	OCT4_24	743	45
ttgcctctcactcggttctc	OCT4_25	766	55
ctgcaggaacaaattctcca	OCT4_26	788	45
atctgctgcagtgtgggttt	OCT4_27	814	50
atccttctcgagcccaagct	OCT4_28	851	55
ttacagaaccacactcggac	OCT4_29	874	50
tagtcgctgcttgatcgctt	OCT4_30	910	50
ctcaaaatcctctcgttgtg	OCT4_31	932	45
ctgagaaaggagacccagca	OCT4_32	954	55
agaggaaaggacactggtcc	OCT4_33	976	55
atagcctggggtaccaaaat	OCT4_34	1010	45
agtacagtgcagtgaagtga	OCT4_35	1038	45
ttccccctcagggaaaggga	OCT4_36	1064	60
tgacggagacaggggaaag	OCT4_37	1086	60
agtttgaatgcatgggagag	OCT4_38	1116	45
attcctagaagggcaggcac	OCT4_39	1139	55

Chapter 3

High-Throughput Microfluidic Single-Cell Digital PCR[1]

3.1 Overview

Here we present an integrated microfluidic device for the high-throughput digital PCR (dPCR) analysis of single cells. This device allows for the parallel processing of single cells and executes all steps of analysis including cell capture, washing, lysis, reverse transcription, and dPCR analysis. The cDNA from each single cell is distributed into a dedicated dPCR array consisting of 1020 chambers, each having a volume of 25 pL, using surface tension-based sample partitioning. The high density of this dPCR format (118,900 chambers per cm^2) allows the analysis of 200 single cells per run, for a total of 204,000 PCR reactions using a device footprint of 10 cm^2. Experiments using RNA dilutions show this device achieves the shot-noise limited performance in quantifying single molecules, and with a dynamic range of 10^4. We performed over 1200 single cell measurements, demonstrating the use of this platform in the absolute quantification of both high and low abundance mRNA transcripts, as well as microRNA that are not easily measured using alternative hybridization methods. We further apply the specificity and sensitivity of single cell dPCR to performing measurements of RNA editing events in single cells. High-throughput dPCR provides a new tool in the arsenal of single cell analysis methods, with a unique combination of speed, precision, sensitivity and specificity. We anticipate this approach will enable new studies where high-performance single cell measurements are essential, including the analysis of transcriptional noise, allelic imbalance, and RNA processing.

[1]A version of this chapter has been published: Adam White, Kevin Heyries, Colin Doolin, Michael VanInsberghe, and Carl L. Hansen, *High-Throughput Microfluidic Single-Cell Digital PCR*, Analytical Chemistry, 2013.

3.2 Introduction

Cells are the fundamental unit of biology. Despite this the vast majority of gene expression measurements have been performed using bulk samples of RNA extracted from large populations of cells having undefined composition and heterogeneity. Underlying the interpretation of such data is the assumption that all cells are similar, and that the ensemble average of many individuals accurately captures the biology. Unfortunately this assumption is often false. Significant cellular heterogeneity exists in most samples and is manifest at multiple levels including epigenetic[121, 122] and transcriptional states[123], protein expression[124] and post-translational modifications, growth characteristics[125], and functional responses[126]. Population measurements generally obscure this heterogeneity and muddy the biological interpretation: existing protocols for the isolation of rare stem cell populations typically provide functional purities between 1% and 50%[10, 127, 128], resulting in significant and often overwhelming contamination from undefined subpopulations; the analysis of gene expression responses can be blurred by cellular asynchrony[129]; and many fundamental biological questions, including the degree to which cells regulate mRNA expression and processing, require measurements at the single cell level.

The development of methods to measure and understand cellular variability has reached the point of mission critical and stands to impact a wide array of fundamental and applied fields ranging from immunology to regenerative medicine to microbiology. In response to this need, an expanding array of single cell genomics methods are being advanced, each appropriate to different levels of inquiry. The coupling of whole transcriptome RNA amplification with high-throughput sequencing is now an established method for global analysis of single cell expression profiles[130]. Although there still remain issues of representational bias, technical noise, and sequencing cost, the continued development of improved instrumentation, bioinformatics approaches, and optimized reagent kits[34] is likely to bring single cell WTA analysis into the mainstream. RT-qPCR, either in conventional[40, 58] or microfluidic[90, 94] formats, is perhaps the most versatile method for single cell gene expression analysis[131]. Although well-suited to identifying and monitoring cellular subpopulations using established panels of genes[20, 60, 132], RT-qPCR does not provide absolute measurements and has limited precision and specificity when working with low abundance templates. These limitations make RT-qPCR suboptimal for applications that require high-performance measurements of a small number of targets, including studies

of transcriptional noise or allelic imbalance, single cell genotyping, and the absolute quantitative analysis of low copy transcripts.

For such demanding applications two single molecule counting methods have emerged: mRNA fluorescence in situ hybridization (mRNA FISH)[23, 26] and digital PCR (dPCR)[62]. mRNA FISH has the important advantage of preserving spatial information regarding the location of cells within a tissue and has been applied to whole organisms. However, this method requires a lengthy sample preparation protocol, complex probe design, and the need for sophisticated image acquisition and analysis steps. In addition, although mRNA FISH can in principal provide absolute transcript numbers, in practice this is often limited by difficulty in resolving closely localized fluorescent spots, interference from background fluorescence, ambiguity in defining cellular boundaries, and a broad distribution of intensities from hybridization events. More fundamentally, the need for multiple hybridization probes makes mRNA FISH poorly suited to measurements of small RNA species or discrimination of transcripts with high sequence homology[26].

The alternative approach, dPCR, uses compartmentalization of single molecules at limiting dilution followed by PCR amplification and end-point detection to enable precise and highly specific quantification of transcripts. Although this approach has been used to make precise measurements of single cell transcription[62], throughput is typically restricted by the labour and cost of cell isolation and processing in conventional microliter volumes, as well as limitations in the throughput of dPCR analysis. Microfluidic systems can address these issues by providing economy of scale, automation and parallelization, as well as increased reproducibility and sensitivity in small volume reactions[68]. We previously developed a microfluidic device that implements integrated RT-qPCR at a throughput of 300 single cells per run[129]. This device performs steps of cell lysis, RT, and PCR by sequentially transferring reagents through three chambers, ending with PCR amplification of each cell product in single 50 nL chambers. A related device, featuring additional cell processing chambers and sample elution capabilities, has recently been released as a commercial product (Fluidigm C1™). In separate work we have also developed a dPCR format that uses surface tension partitioning to achieve planar dPCR densities up to 400,000 chambers/cm^2[133]. Here we combine the advantages of integrated single cell processing[129] and high-density dPCR[133] to enable high-throughput single cell dPCR. Our device is capable of processing 200 single cells per run, each of which is analyzed in an array of 1,020

PCR reactions, each having a volume of 25 pL, for a total of 204,000 PCR reactions per experiment. We establish the technical performance of this system using RNA dilutions and demonstrate its use in making absolute single cell measurements of the expression of high- (GAPDH) and low-abundance (BCR-ABL) transcripts, as well as the abundance of a mature microRNA (miR-16). Finally we apply our system to the measurement and single nucleotide discrimination of RNA editing of EEF2K transcripts in single cells.

3.3 Methods

The microfluidic device presented here consists of 200 identical modules (Figure 3.1A) divided into 4 linear arrays. Each array contains 50 modules (Figure 3.1B) with 3 chambers connected in serial, followed by a dPCR array. This architecture allows for the implementation of a three-step protocol that requires sequential additions of reagents without purification, followed by dPCR analysis of the resulting products. Examples of two such protocols, one for mRNA quantification and one for miRNA quantification, can be performed as shown in Figure 3.1C (see below for protocol details). Cells are first trapped in the cell capture chamber (0.8 nL) using hydrodynamic traps[129] and are then washed with fresh PBS. Reagents are then introduced through the cell capture chamber to fill the subsequent cell lysis chamber (10 nL) and the RT chamber (50 nL). Finally, half of the product from each RT chamber is loaded into an independent dPCR array having 1020 chambers, sufficient to accurately measure the mRNA and miRNA targets ranging from approximately 3 to 5,000 copies per cell. This section describes device fabrication and operation, as well as experimental protocol details.

3.3.1 Device Fabrication

Microfluidic devices were fabricated using multilayer soft lithography[65], following a similar procedure to those previously described[79, 89, 129]. The microfluidic device was designed using in-house developed software to generate a digital drawing of the device in the Caltech Intermediate Form (CIF) file format. Further processing was done with CleWin (Phoenix Software) to array and arrange the device to be suitable for fabrication on 4-inch silicon wafers. Five separate 5-inch photomasks (Microchrome) for flow and control layers were printed at 2 µm resolution using a

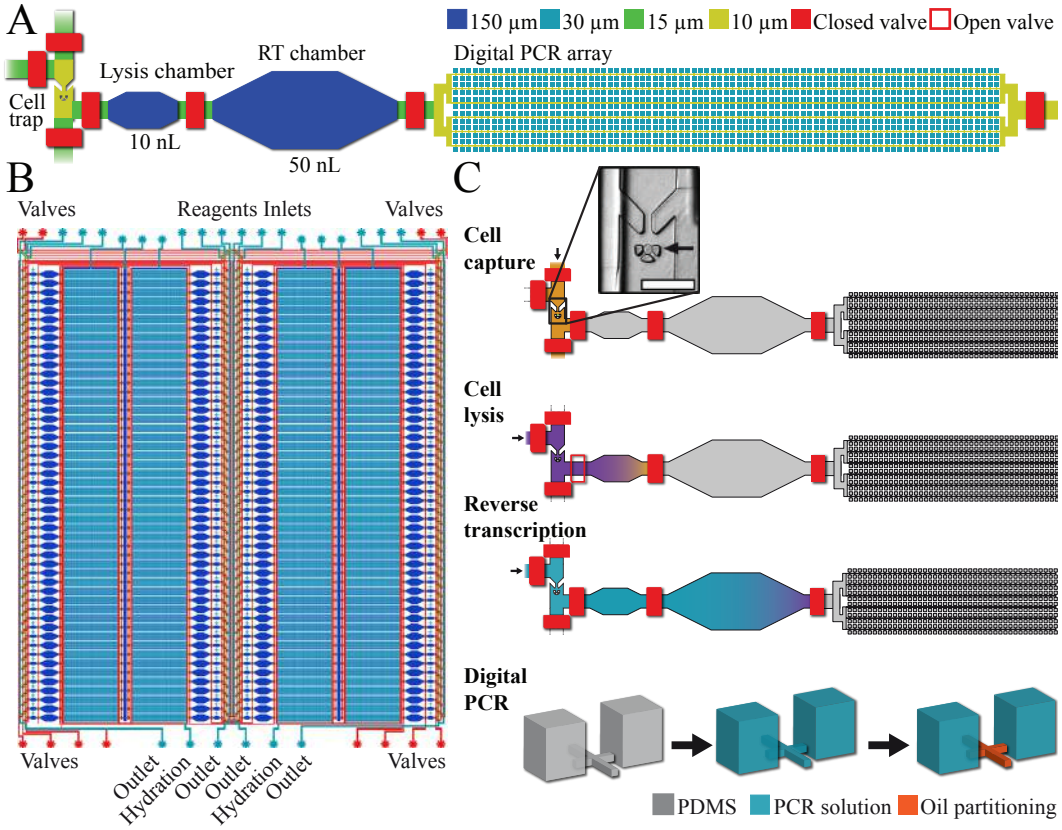

Figure 3.1: Microfluidic device design and operation. (A) Layout of the microfluidic modules for single cell digital PCR analysis. The cells are trapped, lysed and the transcript target is reverse transcribed before being injected into a digital PCR array. The respective height dimensions for the chambers and channels are indicated. (B) Complete microfluidic device. Four main panels contain 50 identical modules capable of parallel processing of up to 200 single cells. The device also contains a network of hydration channels to prevent water loss during thermocycling. (C) Workflow schematic for single cell digital PCR analysis of mRNA. Depending on the protocol used for mRNA or miRNA analysis, cells are either chemically or heat lysed after being trapped (insert, K562 cells trapped; the scale bar is 100 µm). Transcripts are then reverse-transcribed to cDNA by mixing RT reagents using diffusion. PCR reagents are then injected into the device, mixed by diffusion with cDNA products and injected in to the digital PCR array using dead end filling. A fluorinated oil (FC-40) is then used to displace the remaining PCR solution in the channels and compartmentalize individual PCR digital chambers.

LaserWriter (Microtech). The flow layer refers to the layer of channels used to handle samples and reagents, while the control layer refers to the layer of channels below the flow layer which are used to valve flow channels

The flow mold was manufactured by the subsequent layering and lithography of four different photoresists. Fabrication using photoresists was done according to manufacturer's specifications. Blank silicon wafers (5 inches, Silicon Quest) were dehydrated at 190 °C for 1 hour and exposed to hexamethyldisilazane (Sigma) for 5 minutes prior any use. First, 16 µm thick valvable channels were fabricated by spinning SPR220-7 (Rohm and Haas). After exposure and development the entire wafer was baked at 190 °C for one hour. Next, a layer of 12 µm thick SU8-3010 (MicroChem) was used to create the cell traps and channels into the digital array. A 50 µm layer of SU8-3025 (MicroChem) was then used to make the 25 pL reactors of the digital array as well as the microfluidic channels responsible for reagent transfer into and out of the device. Finally 150 µm high SU8-100 (MicroChem) was used to construct the large 10 nL and 50 nL chambers. To fabricate the control mold a single layer of 25 µm high SU8-3025 was used. After fabrication, all the molds were coated with an ∼100 nm layer of poly(paraxylylene) (parylene C) to prevent adhesion by polymerized poly(dimethylsiloxane) (PDMS) and increase mold durability[134].

The microfluidic devices were assembled through the subsequent bonding of three layers of replica molded PDMS on top of a 50×75mm glass slide. Approximately 60 g of 5:1 (part A:part B) PDMS (General Electric, RTV 615) was degassed, poured on to the flow mold and then baked at 80 °C to polymerize for 60 minutes. Meanwhile 20:1 PDMS was spun at 1800 rpm for 60 s on the control molds and was left to cure at 80 °C for 30 minutes. PDMS casted onto the flow mold was then carefully peeled off, trimmed to device size and reagent inlets and outlets were punched using a 20 gauge coring tool (Technical Innovations). The PDMS flow layer was manually aligned on top the PDMS coated control molds and cured for a further 30 minutes at 80 °C. While this is happening 20:1 PDMS was spun at 1800 rpm for 60 s onto cleaned 50 x 75 mm glass slide and baked at 80 °C for 30 minutes. Following bonding, the combined two layer PDMS structure was peeled from the mold and holes were punched to allow fluid input to the control layer. The PDMS slab was then cropped into individual devices and deposited on the PDMS coated glass slides to complete the devices and baked overnight at 80 °C. Finally, the devices were kept in a sealed container with 99% humidity for at least 24 hours prior to any use.

3.3.2 Device Operation

The device was operated through control of 12 pneumatic valves, which apply pressure (30 psi) to the Krytox (DuPont) oil used as fluid in the control lines. The device may be controlled using a manifold of manual valves, however for current study valves were controlled by solenoid actuators (Fluidigm Corp.) in a semi-automated fashion through a digital input-output card (NI-DAQ, DIO-32H, National Instruments) using a LabView program (National Instruments). The solenoids are connected to the microfluidic device by Tygon tubing ending in stainless steel pins (20-gauge, Small Parts Inc.) fitted into the control line ports. Reagents were injected into the device through pipette tips (Xcluda Style G Aerosol Barrier Pipet Tips, BioRad) plugged into device ports and applying pressure though a manifold of manual valves.

The microfluidic device was designed to be compatible with commercially available lysis and RT-qPCR reagents. Following a common procedure for cell loading, the microfluidic device was used to perform either chemical lysis followed by RT and digital PCR, or heat lysis followed by RT and digital PCR. The microfluidic device was designed to implement one-pot chemistries, by which reagents are sequentially added to the reaction without intermediate product purification steps.

3.3.3 Cell Loading

Each cell-loading lane was primed by flowing PBS with 0.5% (m/v) bovine serum albumin through the channel for 30 s. This treatment helped prevent cells from adhering to the PDMS walls of the microfluidic channels. Cells were taken directly from suspension culture and injected into the cell loading lanes. Typically 5 µL to 20 µL of cells in suspension at concentrations between 5×10^5 and 1×10^6 cells/mL were injected into the device with a flow rate of approximately 20 nL/s. Concentrations higher than 2×10^6 cells/mL occasionally caused clogging at the inlet port or in the channel at trap locations. Following loading, 2 µL of the PBS solution was run through each of the four lanes of cell traps in order to displace the culture medium and remove any free nucleic acids that may be present. Finally valves were actuated to isolate each of the cell traps. Manual inspection of each of the 200 cell traps was then performed to confirm and record the number of cells present in each trap.

3.3.4 Detecting mRNA with Chemical Lysis and RT-dPCR

For measurements of mRNA, we used the CellsDirect™ One-Step qRT-PCR kit (Invitrogen) to perform chemical lysis followed by RT and digital PCR. Lysis solution (15 µL) was prepared according to the manufacturer and loaded into the 4 reagent injection lanes. Lysis is performed by opening valves to the cell trap chambers and injecting the lysis reagent through the cell trap chambers and dead-end filling the 10 nL chamber. The lysis reaction is incubated at room temperature for 10 min, followed by heat-inactivation of the lysis reagent at 70°C for for 10 min. Temperature is controlled by placing the device on a flatbed thermocycler.

The one-step RT-qPCR mix [prepared as 1 µL of SuperScript III RT/Platinum Taq Mix, 25 µL of 2× Reaction Mix (with ROX reference dye), 2.5 µL of 20× TaqMan Assay (primers and probes, Life Technologies), 1µL of 50 mM MgSO4, 5.5 µL of water, and 5 µL of 1% Tween-20] was then combined with the cell lysate into the 50 nL reaction chamber, and allowed to mix by diffusion for 30 minutes. Reverse transcription was performed by incubating the device on a flatbed thermocycler at 50 °C for 20 minutes. The RT product and PCR reaction mix was then pushed into the digital PCR array. After completely dead-end filling all of the chambers, fluorinated oil (FC-40, Sigma) was used to partition the array of digital PCR chambers[133]. A continuous flow of this oil was maintained throughout the thermocycling reaction to ensure reaction segregation. Light mineral oil, applied between the glass substrate and the thermocycler, was used to improve the thermal contact during thermoclying (30 second hot-start at 95 °C, followed by 30 cycles of 95 °C for 3 seconds and 60 °C for 30 seconds). Commercially available primers and probes were used to measure GAPDH (Hs_02758991_g1, Life Technologies) and BCR-ABL (Hs_03024784_ft, Life Technologies). The procedure is summarized in the table below.

3.3.5 Detecting miRNA with Heat Lysis and RT-dPCR

The protocol for detecting microRNAs is similar to the protocol used for measuring mRNA transcripts. Cells were trapped, washed, and isolated between valves as describe above. However, in this protocol, heat lysis (85 °C for 7 minutes) was used in the place of chemical lysis and was followed by a 2-step RT and PCR reaction using the High Capacity cDNA Reverse Transcription kit (Applied Biosystems) and the TaqMan® Fast Universal Master Mix. The RT reaction was performed in the

Table 3.1: Chemical Lysis and 1-step RT-dPCR Protocol

Step	Description	Time
1	Prime device with PBS 0.5 mg/mL BSA and 0.5 U/µL RNase Inhibitor	1 min
2	Inject cell suspension (passive cell trapping)	1 min
3	On chip cell washing with PBS containing 0.5 mg/mL BSA and 0.5 U/µL RNase Inhibitor	1 min
4	Close valves partitioning cell loading channel and isolating single cells	30 sec
5	Count cells by visual inspection with microscope	7 mins
6	Inject lysis reagent through the cell capture chamber, dead-end filling the 10 nL chamber	1 min
7	Close reagent injection valve, creating isolated reactors combining the cell capture chamber and lysis reservoir chamber	30 sec
8	Perform lysis at room temperature and heat inactivation of the lysis reagent at 75 °C by placing device on flatbed thermocycler	25 min
9	Flush reagent injection lines with reagent for RT-qPCR	30 sec
10	Inject RT-qPCR reagent through combined cell-capture/lysis chamber into 50 nL RT chamber	5 min
11	Close valve to RT chamber. Allow for mixing by diffusion (30 mins) before RT (20 mins)	50 min
12	Open valves to digital PCR chamber array, and inject RT product (continuing to push with RT-qPCR reagent). Close all valves after dead-end fill	3 min
13	Prime the oil fluidic bus lines, before opening valves to allow the oil to flow through the reactors and to the output port. Place on flatbed thermocycler with light mineral oil and tape down for thermal contact	8 min
14	Run RT-qPCR protocol	(varies)

Table 3.2: Heat Lysis and 2-Step RT-dPCR Protocol

Step	Description	Time
1	Prime device with PBS 0.5 mg/mL BSA and 0.5 U/µL RNase Inhibitor	1 min
2	Inject cell suspension (passive cell trapping)	1 min
3	On chip cell washing with PBS containing 0.5 mg/mL BSA and 0.5 U/µL RNase Inhibitor	1 min
4	Close valves partitioning cell loading channel and isolating single cells	30 sec
5	Count cells by visual inspection with microscope	7 mins
6	Heat lysis by placing device on flatbed thermocycler and heating to 85 °C	7 min
7	Flush reagent injection lines with reagent for RT	2 min
8	Inject RT reagent through the cell capture chamber, dead-end filling the 10 nL RT chamber	1 min
9	Close reagent injection valve, creating isolated reactors combining the cell capture chamber and RT chamber	30 sec
10	Perform reverse transcription (pulsed temperature protocol) by placing device on flatbed thermocycler	2.5 hr
11	Flush reagent injection lines with reagent for PCR	2 min
12	Inject PCR reagent through combined cell-capture/RT chamber into 50 nL mixing chamber	5 min
13	Close valve to mixing chamber. Allow for mixing by diffusion	40 min
14	Push RT product and PCR mix into digital PCR array, and partition array with oil	8 min
15	Run digital PCR protocol	(varies)

10 nL chamber, and the 50 nL chamber was simply used to mix the RT product with the PCR reagent prior to injection into the dPCR array. A pulsed temperature RT protocol was carried out by placing the microfluidic device on a flatbed thermocycler (2 min at 16 °C, followed by 60 cycles of 30 seconds at 20 °C, 30 seconds at 42 °C, and 1 second at 50 °C). Following RT thermocycling the RT enzyme was inactivated at 85 °C (5 min), and then the device was cooled to 4 °C. After injection into the dPCR array, fast PCR thermocycling was performed as described in the protocol for measuring mRNA, but with temperatures according to manufacturer specifications (95 °C for 30 seconds, followed by 30 cycles of 95 °C for 3 seconds and 60 °C for 30 seconds). Commercially available primers and probes were used to measure miR-16 (hsa-miR-16, Applied Biosystems). The procedure is summarized in the table below.

3.3.6 Measurement of RNA Editing

The EEF2K RNA edit location (hg18 chr16:22204361, hg19 chr16:22296860) was initially identified and validated by Shah et al. through RNA-seq on an estrogen-receptor--positive metastatic lobular breast cancer[32]. This editing location was not predicted by Park et al. in their RNA editing analysis of the K562 ENCODE RNA-seq data[135]. However, our inspection of their mapped RNA-seq data (GEO GSM958729) revealed that replicates 1 and 2 had 20/57 and 15/48 mapped reads with A to G variants, respectively, indicating that it may also be a candidate edit in K562 cells as well.

A two-colour MGB TaqMan qPCR assay was designed to distinguish between wildtype (A) and variant (G) (F: CCC TCC TCA AAG TGC TGA GAT TAC, R: TTC AAT GGA ATT CAG CTC TCA CAT, WT: VIC- AGATGCT**A**GGTGCG, Edit: 6FAM- ATGCT**G**GGTGCG). This assay was initially validated against DNA and total RNA purified from K562 cells. After 40 cycles of PCR, the predicted edit was not detected in either the DNA samples or the no-RT controls on the RNA samples, but was present in all reverse-transcribed RNA samples. The cDNA product, gDNA and no-RT RNA additionally all contained only a single amplicon of the expected length (108 bp). Probe specificity for the single nucleotide variant was confirmed by performing microfluidic digital PCR in custom chips consisting of 765 2-nL arrays; the majority of all positive chambers (69 only variant, 406 only wildtype, 93 variant and wildtype) showed amplification in only one colour. The primer specificity in purified total RNA and DNA, probe specificity, and detection of the variant in only reverse-transcribed RNA strongly suggest that we are measuring true RNA editing events.

cDNA was synthesized using the High Capacity cDNA kit (Applied Biosystems). Final reaction brews contained 1× RT buffer, 1× RT Random Primers, 5 mM dNTPs, 0.1 % Tween-20, 3.3 U/µL MultiScribe Reverse Transcriptase and were incubated at 25 °C for 10 min, 37 °C for 1 hour, 85 °C for 5 minutes and held at 10 °C until PCR cycling. PCR reaction brews contained 1× CellsDirect Buffer (Invitrogen), 0.1 % Tween-20, 900 nM each forward and reverse primer, 250 nM each probe and 0.04 U/µL Platinum Taq (Invitrogen) and were cycled for 2 min at 95 °C, followed by 40 cycles of 95 °C for 15 s, 61 °C for 1 minute. All conditions for single-cell RT-qPCR were the same, except the PCR cycling times were reduced (30 second hot-start at 95 °C, followed by 30 cycles of 95 °C for 3 seconds and 60 °C for 45 seconds).

3.3.7 Cell Culture and RNA Purification

K562 cells were obtained from ATCC (CCL243) and were cultured in DMEM (Gibco) supplemented with 10% FBS (Gibco). Purified RNA was extracted from K562 cells using the mirVana RNA isolation kit (Ambion) according to manufacturer directions.

3.3.8 Device Analysis

Microfluidic devices were scanned at 2 µm resolution using a custom built confocal scanner (Huron Technologies International Inc.). Automated analysis of the digital images was performed with in-house software written in C. 50 rows of 1020 chambers of the digital PCR array (51,000 total) were analyzed simultaneously by specifying manually control points (top left, top right and bottom left) of the region to be analyzed. The chambers were automatically located by detecting a pre-mixed passive dye (ROX) using a previously described algorithm6. A fluorescence intensity measurement was then calculated for each chamber by summing the pixel values the fluorophore of interest in a 21×21 pixels square region centered at each chamber and normalized to the overall fluorescence of the ROX. The fluorescence intensity values of every chamber in each of the 50 sample lanes were then plotted on a single histogram, which was repeatedly smoothened using a gaussian kernel until only one point on the histogram remained with both neighbouring points larger than it. This minimum point was then used as the thresholding value to distinguish positive chambers from negative chambers and the number of positive chambers in each of the sample lanes was written to a data file.

This data file was then further processed using SigmaPlot® software to determine the number of transcripts present in each cell. Figures and plots were generated using the same software. Log normal distribution curve fitting used log normal, 3 parameters with default settings.

3.3.9 Transfer Efficiency Measurements

Fluorescence images were used to measure the sequential transfer of oligonucleotides from the cell capture chamber into the 10 nL and 50 nL chambers. The cell capture chamber was loaded with a solution of 10 µM FAM-labeled 40-mer poly-A oligonucleotides (IDT), 0.1% Tween-20, and ROX passive reference dye (from CellsDirect kit, Invitrogen, P/N 54880) diluted 100×, and was pushed into the subsequent chambers

with water containing 0.1% Tween 20 and diluted ROX reference dye. The transfer efficiency for each chamber was calculated as (Initial Signal Final Signal)(Initial Signal), where Signal = (FAM Intensity FAM Background) (ROX Intensity ROX Background).

3.3.10 Ripleys K-Function

Ripleys K-function with the rectangular edge correction conditions described by Goreaud et al.[136] was used to assess the spatial distribution of the hits in the array. Variance-stabilized K-function estimates for each array were given a z-score for each distance s based on the mean and standard deviation derived from 500 randomly generated arrays with the same fill factor.

3.4 Results

3.4.1 Device Performance

We first characterized the efficiency, and uniformity of mixing and sample transfer in our microfluidic device using FAM labelled 40 bp oligonucleotides. Sample transfer between the lysis chamber and RT chamber, as measured by fluorescence quantification, was found to be better than 99%; the amount of oligonucleotide remaining in the 10 nL chamber was below 1%, which is determined as the limit of detection for this measurement based on 2 standard deviations from measured background fluorescence (Figure 3.2A). We next assessed the mixing of reagents in the 50 nL chamber by taking time lapse images of fluorescence and calculating the variability in oligonucleotide concentration across the chambers. Regression of the resulting data to an exponential decay curve yielded a mixing time constant of approximately 11 minutes (Figure 3.2D). Based on this analysis we implemented a 30 minute wait time in our protocol to allow for sufficient reaction mixing. Finally, we measured the reproducibility of transfer from the RT chamber to the digital PCR array. Fluorescence measurements of the 50 nL chamber before and after injection into the dPCR array showed that the fraction of solution that was injected into the digital PCR array was 50.38% (s.d. =1.31%) (Figure 3.2E).

We next performed a series of experiments to assess the signal to noise and measurement sensitivity of our system using total RNA template purified from K562

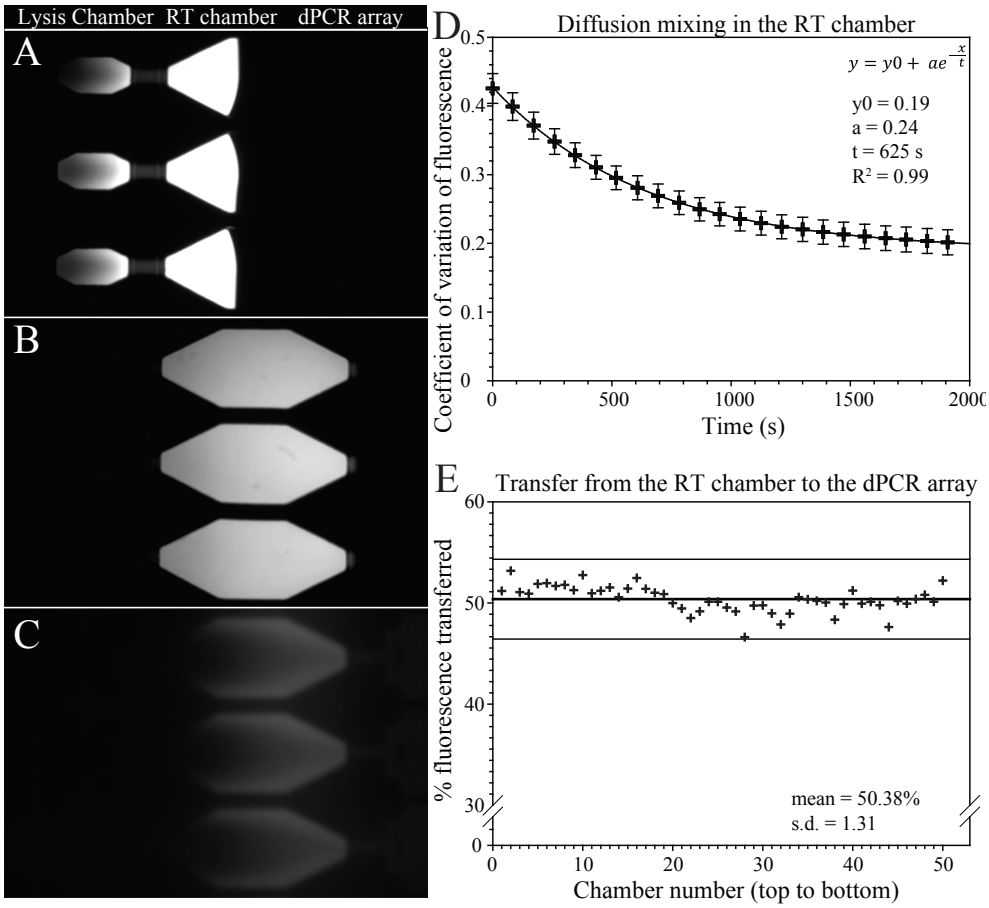

Figure 3.2: Characterization of the microfluidic device. (A) A solution containing 40 base oligonucleotides labelled with FAM was injected in the lysis chamber following the normal procedure. A second solution (not fluorescent) was then used to sequentially push the first solution into the RT chamber (B), and then the dPCR array (C). (D) Mixing by diffusion in the RT chamber (B) was monitored by measuring the standard deviation of the fluorescent signal over time. As expected, the signal follows an exponential decay with an averaged time constant (t) of 625 seconds (R^2=0.9999). (N=50) (E) To measure the amount of the cell sampled by the dPCR array, the fluorescent solution in the RT chamber was pushed into the digital PCR array using a non-fluorescent solution (C). The transfer efficiency was evaluated for 50 chambers and found to be 50.38% (s.d.=1.31). $\pm 3\sigma$ from the mean lines are also displayed.

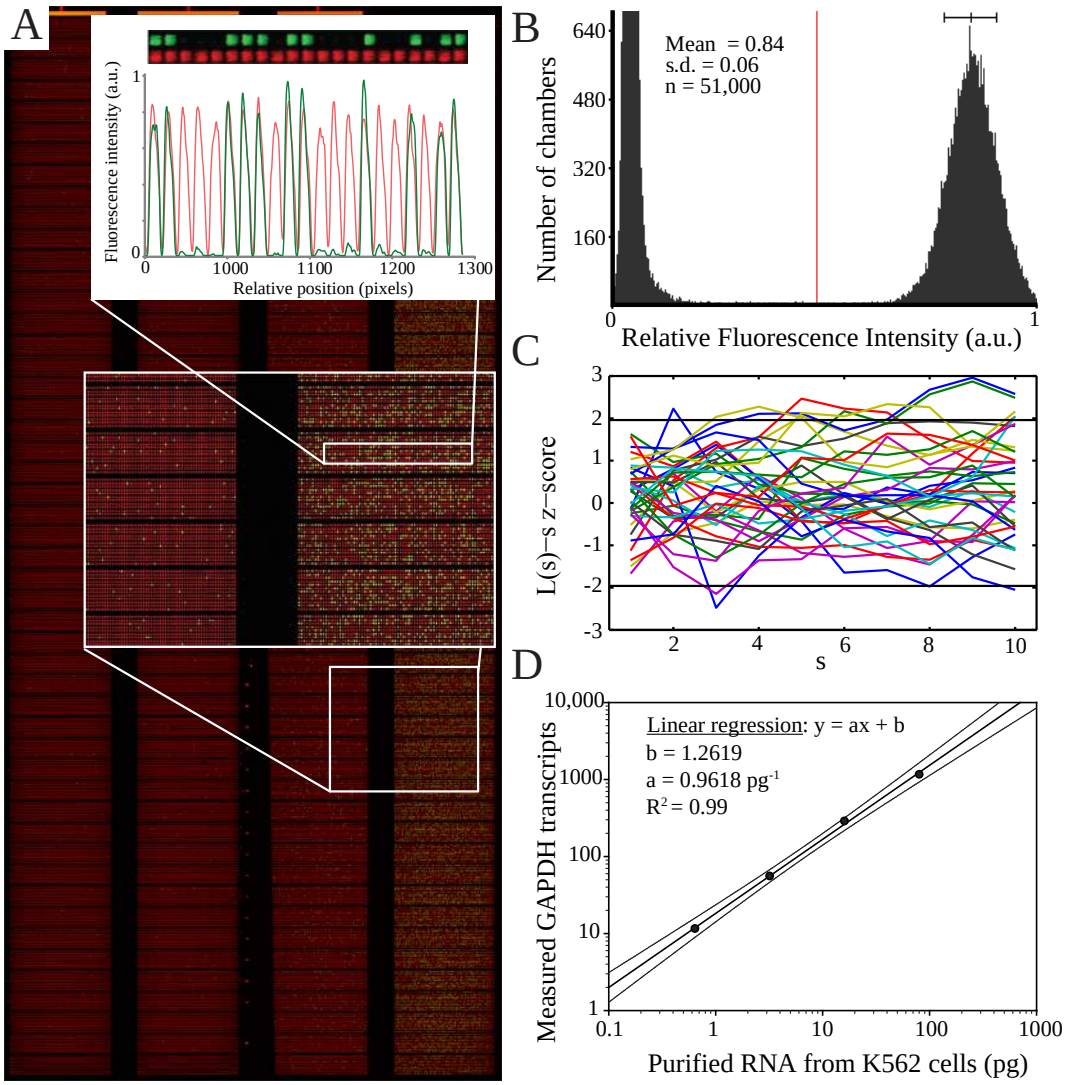

Figure 3.3: (A) End point fluorescence signal from the entire microfluidic device after dPCR targeting GAPDH. RNA dilutions have been loaded into 4 different visible panels and reverse-transcribed on chip. The resulting cDNA is quantified by digital PCR where digital PCR positive hits (green) in 30 pL chambers have a high signal to noise ratio (>30). A passive dye (red) is visible in all the chambers. (B) Histogram of the distribution fluorescence intensity for 51,000 digital PCR chambers with 20 pg RNA as starting material. Normalized mean and standard deviation of the bright, or positive, chambers are indicated. (C) Randomness of the distribution of detected transcripts within a distance s in the dPCR array assessed by using z-scores of a variance stabilized Ripley K-function (L-function) within a 95% confidence interval. (D) Dynamic range of the digital PCR arrays using 5-fold serial dilutions of total RNA purified from K562 cells, looking at GAPDH mRNA. Linear regression analysis using the experimental data was performed (parameters displayed with 95% confidence boundaries).

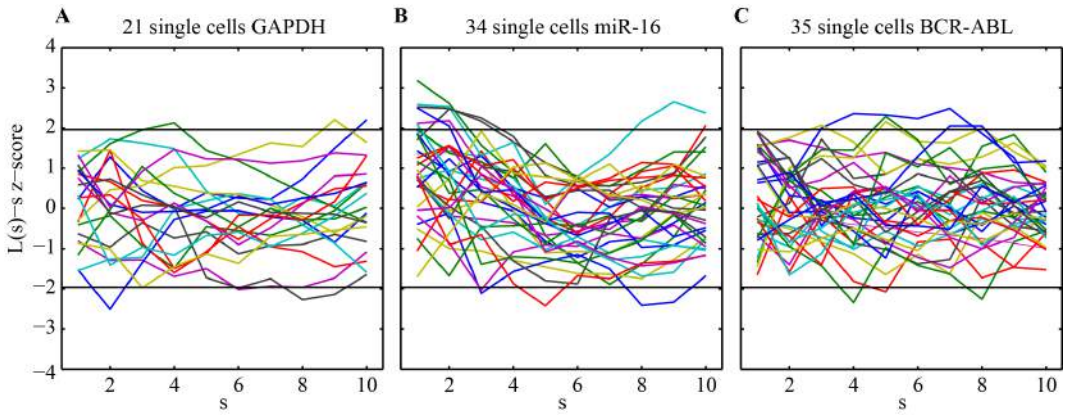

Figure 3.4: Z-scores of variance stabilized Ripleys K-function estimates for the spatial distribution of digital counts at distance s from single cells in high (A, GAPDH, average 60% full), medium (B, miR-16, average 30% full) and low (C, BCR-ABL, average 2.3% full) fill factors. The 95% confidence intervals (1.96 standard deviations) are shown in black.

cells. Using hydrolysis probes (TaqMan®), the signal to noise ratio obtained using the 4 different assays allowed a clear and unambiguous discrimination between the positive and negative chambers (Figure 3A). Figure 3B shows a histogram of fluorescent intensities, with a signal to noise ratio in excess of 30, obtained across 51,000 fluorescent chambers in one lane of the device measuring GAPDH transcripts (Figure 3.3A insert and Figure 3.3B).

Digital PCR requires template molecules to be randomly distributed among reaction chambers in order to accurately infer the number of molecules in the array from the number of reaction chambers with PCR amplification. Our integrated single-cell dPCR device mixes PCR solution with template by diffusion in 50 nL chambers prior to injection into the array of 1020 $\times$ 25 pL dPCR chambers, having an aggregate array volume of approximately 25 nL. We assessed the randomness of the resulting distribution of cDNA molecules across the dPCR array by plotting the z-score of the variance stabilized Ripleys k-function[133, 137] for 50 sub-arrays in a single lane of the device loaded with purified RNA at a concentration of $\sim$18 pg per array (single cell equivalent) (Figure 3.3C), with the RNA loaded through the cell processing chambers, and subsequent processing performed in the same sequence as during single cell analysis. This analysis shows that the distributions are not significantly different from random and lie within a 95% confidence interval constructed around

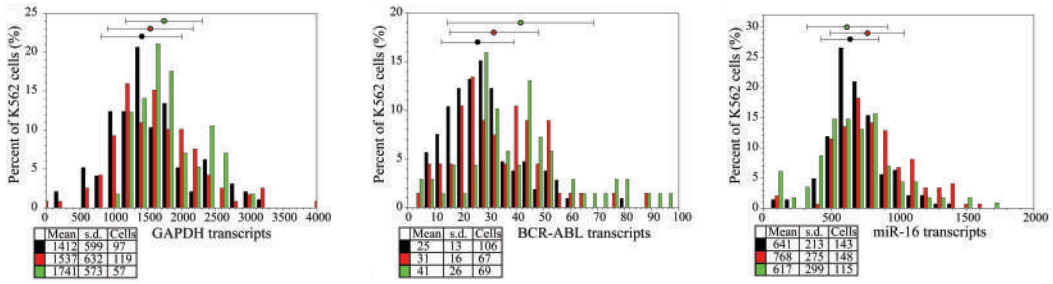

Figure 3.5: Digital PCR measurements on K562 single cells. From left to right: (A) GAPDH mRNA transcripts abundance measurements over 3 independent experiments. The transcript abundance frequency displayed on the x-axis is binned every 200 transcripts. (B) BCR-ABL fusion gene mRNA transcript measurement over 3 independent experiments. The transcript abundance frequency displayed on the x-axis is binned every 4 transcripts. (C) MicroRNA miR-16 measurements over 3 independent experiments. The transcript abundance frequency displayed on the x-axis is binned every 100 transcripts.

the mean of 500 simulated data sets, based on a Poisson distribution of template molecules in each chamber[137, 138]. This statistical analysis was also repeated for single cell measurements and demonstrates that mRNA distributions are also within 95% confidence intervals under this scenario (Figure 3.4).

Finally, to verify the response and precision of the device, we measured the abundance of GAPDH mRNA from serial dilutions of total RNA purified from K562 cells (Figure 3.3D). Measured concentrations from 5-fold RNA dilutions were in excellent agreement with the expected template abundance and dilution factor (R^2=0.9989), with tested values spanning a chamber occupancy rate between 0.02% and 48% (Figure 3.3A), corresponding to a range of 80 to 0.64 pg total RNA template per reaction.

3.4.2 Single Cell Transcript Measurements

We then conducted a series of single cell experiments to establish the combined capabilities of high-throughput cell processing and dPCR analysis. As a first test we performed measurements of GAPDH transcripts from single K562 cells (Figure 3.5A). GAPDH encodes for glyceraldehyde 3-phosphate dehydrogenase and is a commonly used high-copy number endogenous control for RT-qPCR experiments[62, 129, 139]. Over a total of 3 device runs we observed successful amplification for 100% of isolated single cells (N = 288). We note that the total number of cells analyzed was lower

than the theoretical device capacity due to the use of some device lanes for controls and sub-optimal cell trapping efficiency; these experiments were performed with an un-optimized cell trap geometry that resulted in approximately 60% single cell occupancy. Further trap optimization has resulted in 96% single cell occupancy. However, reaction chambers that did not capture a cell provide stringent no-cell-controls from which to evaluate background signal in analysis. In these no-cell controls, we observed a very low frequency of mRNA detection events, with an average of 1.6 hits per no cell (N = 106 chamber), corresponding to background mRNA contamination levels below 0.1%. No correlation was observed between background signal and the copy-number measured on single cells in adjacent wells.

The measured number of transcripts in single cells revealed a log-normal distribution ($0.94 < R^2 < 0.98$) of GAPDH with an average copy number of 1,563 transcripts per single cell. In three replicate measurements, performed on separate devices and different cultures, the mean GAPDH expression was very reproducible, ranging from 1,412 to 1,741 copies per cell. These values are in good agreement with estimates of 1,761 (SD = 648) copies we have previously made by normalizing single cell microfluidic RT-qPCR measurements to a standard curve calibrated by dPCR[129]. All replicates revealed a large variability in GAPDH expression between cells, with measured values spanning approximately ten-fold in absolute copy number ($\sim$400 to 4000 copies). This variability in GAPDH levels was also consistent between runs with an average standard deviation of 601 ± 24 copies per cell.

To demonstrate the use of high-throughput digital PCR in accurate quantification of low abundance transcripts, we next measured the expression of BCR-ABL transcripts, a fusion gene resulting from a reciprocal translocation of chromosomes 9 and 22 that is associated with chronic myelogenous leukemia (CML) and is also present in K562 cells. Over 3 runs we reliably detected the BCR-ABL fusion transcript in every cell analyzed (N = 242), with a mean expression of 33 copies per cell, a range spanning 25 fold in relative expression (4 to 100 copies per cell), and a standard deviation of 18.9 copies per cell (Figure 3.5B). These measurements were consistent with an independent study based on RT-qPCR[140] which measured BCR-ABL mRNA in single K562 cells ranging from 2 to 262 copies per cell with the majority of cells containing approximately 40 copies per cell.

Using an alternative two-step RT-PCR protocol we next demonstrated the use of our technology for absolute measurements of microRNA (miRNA) levels in single

WT EEF2K mRNA (copies) \ Edited EEF2K mRNA (copies)	0	1	2	3	
0	35 (16%)	10	2	0	12 (5%)
1	42	16	7	0	
2	20	12	4	0	
3	21	7	3	0	
4	10	8	3	1	
5	7	1	0	0	
6	0	7	0	0	
7+	3	0	2	0	
	103 (47%)				71 (32%)

Figure 3.6: Measurement of single nucleotide RNA editing of EEF2K in single K562 cells. Single cells are binned according to abundance of wildtype (WT) or edited EEF2K transcript. Quadrants containing homozygous wildtype, homozygous edit, heterozygous, and not-detected EEF2K expression are indicated in colour.

cells. miRNAs are a large family of conserved short (∼22 base pairs) non-coding RNAs that associate into the RNA induced silencing complex (RISC) and function as post-transcriptional regulators via targeted degradation of complementary transcripts or by repressing translation[141]. miRNA are important regulators in many biological processes, including development, oncogenesis[142], and immunity, making them of high interest as biomarkers of disease[143]. Due their short length miRNA are not easily amenable to single molecule analysis by RNA FISH[144] and although hybridization techniques have been used to visualize miRNAs[145, 146], single molecule quantification of miRNA copy numbers and variability in single cells by FISH has not been achieved. Using a commercially available RT-qPCR detection strategy, based on miRNA-specific stem-loop reverse transcription primers[60], we measured the expression and variability of miR-16, a microRNA expressed at medium levels across a broad range of tissues, in K562 cells. Over 3 replicates, K562 cells were found to have a mean copy number of 675 per cell which is in close agreement with dPCR measurements performed on bulk samples[129]. The distribution of miR-16 expression was consistent across runs, with a standard deviation of 262±44 (Figure 3.5C).

Finally, we applied our single cell dPCR device to measure the extent of single nucleotide RNA editing. Editing of RNA molecules by nucleoside deaminases has recently gained attention as a mechanism by which transcripts can be modified away

from the genomic code, with potential implications for transcript stability, alternative splicing, translation efficiency, and protein sequence. Next generation sequencing techniques have provided strong evidence for large numbers of RNA editing events across different tissues. These events are typically incomplete, representing a fraction of total RNA. However, little is known regarding the variability of editing between individual cells. Is there a subset of cells that edit all transcripts? Is the frequency of editing similar across different cells? To investigate these questions we used the specificity of dPCR to measure adenosine to inosine editing of position chr16:22296860 (hg19) in the mRNA coding for EEF2K in single cells. This edit was initially identified in a lobular breast cancer[32] and found to be edited at a frequency of ∼0.33 in RNA-seq data from ENCODE[147]. Wildtype and edited versions of EEF2K, differing by a single nucleotide substitution, were simultaneously measured on single cells using a two-color TaqMan SNV assay based on minor grove binding probes (Life Technologies). We measured EEF2K in 221 single K562 cells and found 71/221 (32%) cells expressed both wildtype and edited EEF2K transcripts, 12/221 (5%) cells expressed only edited transcripts, 103/221 (47%) cells expressed only wildtype transcripts, and 35/221 (16%) cells in which neither form of EEF2K transcript was detected (Figure 3.6). The population-averaged editing frequency was found to be ∼0.19 from single cell measurements which is consistent with our measurements on dilutions of purified RNA, producing an edit frequency of ∼0.18. We observed no non-specific amplification in any no-cell reactions. A control experiment omitting the RT enzyme detected genomic wildtype EEF2K in 10 out of 228 single cell reactions (∼4.4%) and no observed positives for the edited transcript.

3.5 Discussion & Conclusion

Single cell dPCR is particularly well suited to measurements that require high precision and sensitivity. We note that the half-sampling approach implemented here (where we inject half of the single-cell RT product, i.e. cDNA, into the digital PCR array) introduces additional stochastic variation in measured cDNA copy number that is particularly important for low abundance transcripts. A theoretical analysis of the measurement precision of digital PCR has previously been presented[148]. Following this treatment we calculated the expectation value, confidence intervals, and coefficient of variance for our 1020 chamber dPCR array as a function of the total

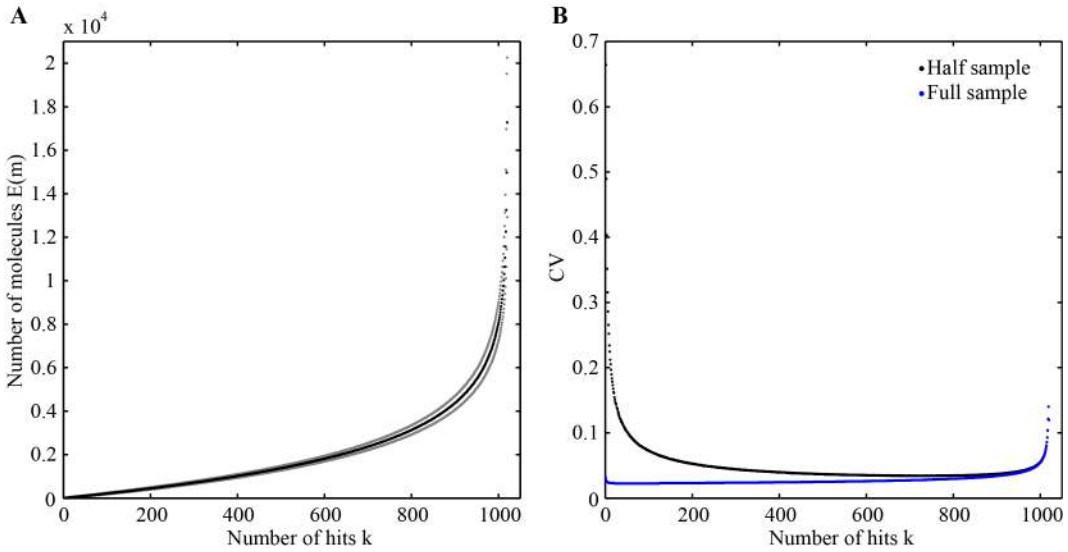

Figure 3.7: The digital array response curve. (A) Average values of the starting molecule number m (black) are shown for the combined half-sampling and digital quantification bounded by 95% confidence interval in grey. Values were derived using a Monte Carlo method to simulate both half sampling and digital PCR array quantification. (B) Coefficient of variance for the quantification with (black) and without (blue) half-sampling.

number of molecules that are loaded into the array (assuming no losses for sampling). In order to generate confidence intervals that also include the effect of half-sampling we implemented a Monte Carlo method. Briefly, a starting population of m molecules were uniformly and randomly assigned to two groups, n (sampled in the array) and o (not sampled in the array). Each n molecules were then uniformly and randomly assigned a detection chamber, allowing for the possibility of multiple molecules assigned to the same chamber. The number of chambers containing at least one molecule (k), was then counted and stored in association with the starting m. This process was repeated for $1 \leq m \leq 20400$ a total of 10000 times each. These results were then searched for each value of k ($1 \leq k \leq 1020$) to generate distributions for the number of starting m molecules which led to k hits. Sample average, standard deviation and 95% confidence intervals were then calculated from these distributions. Based on the results, summarized in Figure 3.7, half sampling is the dominant source of measurement error over the entire dynamic range of measurement (approximately 5 logs). Nevertheless, the aggregate precision is still excellent with 93 % of the potential 5-log dynamic range of the device has a coefficient of variance (CV) less than 0.1, and 75 % has a CV less than 0.05. We further note that incomplete sampling of single cell products is also a feature of previously reported single cell dPCR[62, 149]. This sampling variability could be reduced through improvements in device architecture and/or modified protocols including pre-amplification prior to loading the dPCR array, pushing the sample into the array with an immiscible fluid to avoid dilution, or using sequential load and mix steps to assay dilutions of a single cell product in multiple arrays. Finally, we note that dPCR experiments should be interpreted as measurements of absolute cDNA molecule copy number, with the direct correlation to mRNA abundance dependent on RT efficiency which may vary between different assays.

Here we have demonstrated the application of our system in making absolute measurements of cDNA derived from mRNA and miRNA across hundreds of single cells. Measurements of GAPDH transcript levels, commonly used as an endogenous control in qPCR analysis, show that population-averaged expression measurements are consistent across different cultures, but are widely variable (CV $\sim$ 40%) at the single cell level. This highlights how the common practice of normalizing single cell RT-qPCR expression measurements to a control gene is not advisable and is likely to introduce additional noise. Our measurements also show that miR-16, widely used

as an endogenous reference for miRNA analysis[60], exhibits a similar coefficient of variation (CV $\sim$ 40%) at the single cell level, although at approximately 2 fold lower expression. As a measure of variability we calculate the Fanno factor, defined as F = σ^2/μ, for GAPDH and miR-16 to be 231 and 102 respectively, showing that miR-16 is more tightly regulated in these cells. K562 cells are an inherently heterogeneous sample and much of the measured variability in both GAPDH and miR-16 may represent differences in differentiation state, cell cycle stage, and cell volume differences.

In addition to the quantification of short transcripts such as miRNA, dPCR is uniquely suited to the detection and quantification of transcripts having high sequence homology. Here we have demonstrated this capability in studying the single cell distribution of RNA editing events that give rise to a single nucleotide variant in EEF2K. Given the low copy number of this transcript it is difficult to conclude that the noise in EEF2K measurements represents a significant difference in editing between cells; we note that EEF2K was chosen as it was also found to be edited in other tissues (see methods), but it is not the most abundant edited transcript in K562 cells. Further testing of differences in editing activity between cells may benefit from overexpression of editing substrates. In an analogous application, dPCR may also be used to accurately measure the abundance of transcripts derived from different alleles having heterozygous SNPs, thereby allowing for the assessment of differential allelic imbalance and/or epigenetic silencing across many single cells. Alternatively, analysis of genomic DNA for SNVs or copy number variants may be achieved through improved lysis and nuclei digestion, coupled with pre-amplification.

Our measurements of the BCR-ABL fusion transcript also demonstrate the reliable detection and quantification of rare targets across large numbers of single cells with no false-positives observed in no-cell chambers. This sensitivity and specificity may allow for expanding the range of useful single cell biomarkers, including low-copy transcription factors, and enables the identification and discrimination of minority sub-populations in complex tissues, or the detection of rare cells harbouring mutations for early detection in the monitoring of minimum residual disease[150]. Although increased dPCR density may be used to extend the current throughput of this device from 200 to approximately 1000 cells per run, practical limitations in fabrication are likely to make further scaling difficult. However we believe the throughput presented here is well-suited for the analysis and quantification of ultra-rare cells, such as circulating tumour cells, following enrichment by FACS or immunocapture.

Integrated single cell dPCR provides unique capabilities in terms of combined throughput, precision, sensitivity, and specificity[129, 151]. These capabilities are complementary to the expanding array of single cell analysis tools being developed and applied. Here we have demonstrated how these capabilities may be used to measure a variety of transcriptional features including mRNA expression, miRNA expression, low copy fusion transcripts and SNV discrimination. Moving forward, we anticipate that this single cell platform may be adapted to an expanding range of digital single cell analyses, including analysis of single cell copy number variations or aneuploidy, SNV genotyping, and digital protein quantification[152].

Chapter 4

Single-Cell Analysis of Lipid Nanoparticle RNA Delivery[1]

4.1 Overview

Techniques to manipulate gene expression are fundamental to probing the function of proteins in cellular processes, and hold tremendous potential to enable gene therapies for a wide variety of disorders. Here we use single cell analysis to investigate a method using lipid nanoparticles (LNPs) to deliver small interfering RNA (siRNA) and messenger RNA (mRNA) to efficiently knock down, or knock in, gene expression in cell lines including human embryonic stem cells, fibroblasts, and erythroleukemia-type K562. LNPs were prepared using the NanoAssemblr™ microfluidic-based nanoparticle manufacturing platform, and mimic the neutral cholesterol containing structure of low-density-lipoproteins (LDL). Uptake of siRNA-LNP in embryonic stem cells was enhanced by the presence of apolipoprotein E4 (ApoE4), resulting in efficient uptake after 24 hours with little apparent toxicity. We characterized the siRNA-LNP by measuring the dependence of particle uptake as a function of ApoE, siRNA concentration and incubation time. A microfluidic device for performing high-throughput single-cell digital PCR was used to precisely quantify knockdown of gene expression in hundreds of individual cells. Flow cytometry measurements of LNP uptake and eGFP translation were compared to single-cell digital PCR measurements of mRNA delivery to characterize transfection performance. By examining the cell-to-cell variability, kinetics, and efficiency of using this lipid nanoparticle technology for nucleic acid delivery, we provide quantitative measurements on both expression levels and distributions which should be useful to direct the use of this technology in a variety of applications.

[1]The work in this chapter is in collaboration with Precision Nanosystems Inc.

4.2 Introduction

In this chapter we sought to apply our newly developed single-cell transcription analysis technologies in characterizing the use of nanoparticles for manipulation of gene expression. Lipid nanoparticles (LNPs) are currently one of the leading delivery systems for conveyance of RNA (e.g. mRNA, siRNA) to cell cytoplasm. However, as most studies of LNP performance have relied on bulk measurements of RNA, the cell-to-cell variability in delivered RNA abundance and efficacy remains unknown. By using single-cell digital PCR, we were able to address this knowledge gap by precisely measuring the abundance and distribution of mRNA delivered to cells. Similarly, were able to assess the efficacy of siRNA delivery to perform targeted knockdown of specific genes by measuring the amount of the targeted mRNA in single cells. These single-cell digital PCR measurements provide important transcript information that complements measurements of translated fluorescent proteins or delivered dye by flow cytometry or microscopy. In this study, we combine the single-cell measurement techniques of microfluidic digital PCR and flow cytometry to characterize the performance of a novel LNP reagent for mediating gene expression with single cell resolution in order to inform the development and use of nanoparticles for scientific, and potentially clinical applications.

Delivery of nucleic acids, such as mRNA and small interfering RNA (siRNA), to cells is an important tool for altering gene expression with applications in research and therapeutics[153, 154]. In research settings, RNA interference (RNAi) is now widely used for inhibition of gene expression in dominant hereditary diseases (e.g. Huntington's)[155], cancer[156], and infectious diseases, as well as fundamental studies of the effect of suppressing expression of target genes[157]. Delivery of mRNA is less established than siRNA, however has found utility in the generation of vaccines[158–160], and the reprogramming of cells (e.g. to pluripotency, or directed differentiation)[161, 162]. The major obstacle to RNA-based gene therapy is efficient cytosolic delivery. Recent developments in delivery vehicles, such as the use of lipid nanoparticles (LNPs) to encapsulate siRNA, show promise in addressing this issue, and have now advanced to clinical trials. The past decade has seen intense commercial interest in the development of RNA-LNPs to mediate gene expression. In 2014, improvements in Tekmira's small nucleic acid LNPs enabled Alnylam to achieve 100- to 1000-fold improvements in therapeutic index with siRNA[163]. The same year, Tekmira's siRNA-LNPs were tested in the treatment of Ebola in non-

human primates[164]. Pharmaceutical companies such as Merk and AstraZeneca have invested hundreds of millions of dollars into Moderna Therapeutics, a company that is developing mRNA-based therapies. Delivery of mRNA enables the cell to make a wide variety of proteins itself, bypassing much of the expense and difficulty of manufacturing protein drugs. Some of the most successful drugs today are proteins such as Genentech's Herceptin for breast cancer, and the therapeutic expectation of mRNA has helped Moderna raise over $1 billion from investors and partners in the past five years[165]. Development and application of LNPs for research and gene therapy would greatly benefit from understanding the amount of mRNA delivered in individual cells, and the cell-to-cell variability in delivery (or efficiency of siRNA knockdown of targeted mRNA). Given this commercial and therapeutic interest, the single-cell measurements reported here are useful and timely information for the development of RNA delivery technology.

Messenger RNA (mRNA) delivery has several advantages over DNA for mediating gene expression, including the lack of any requirement for nuclear localization or transcription and the low likelihood of genomic integration[161]. Delivery of mRNA for cell reprogramming has the advantage that the timing and dose is transient and can be controlled. However, the labile nature of mRNA and its capacity to elicit innate immune responses are important limitations to its application. Double- and single-stranded RNAs interact with certain pattern-recognition receptors (PRRs), including Toll-like receptors (TLRs)[166], which detect pathogen-associated molecular patterns as a first-line defense against microbial invasion, and activate cellular and inflammatory reactions as part of an antiviral response. Endogenous RNA molecules are distinguished from those of invading microbes by nucleotide modifications that affect PRR engagement[167]. Recent studies have shown that by incorporating these modifications into delivered mRNA, the immune response was substantially reduced[159, 160], and almost negligible for small doses[161]. In particular, nucleotide analogs of pseudouridine (or 2-thiouridine) and 5-methylcytidine triphosphates have been substituted during in vitro transcription[161, 168].

These advancements have assuaged a major obstacle in RNA therapeutics, however the major barrier to widespread adoption of RNA delivery in therapeutics and research remains the need for safe and effective drug delivery vehicles[153, 169, 170]. While 'naked', or chemically modified mRNA has shown efficacy in certain physiological settings such as in vitro cell reprogramming[161], and in vivo delivery to liver[168],

there are many tissues that require an additional delivery system to facilitate transfection. This is because naked mRNA is subject to degradation by endogenous enzymes, and is too large and too negatively charged to cross cellular membranes[160, 161]. Strategies to improve mRNA delivery include chemical modifications such as conjugation of polymers or viral elements[171–174], or encapsulation within lipid nanoparticles (LNPs)[153, 175]. LNPs are made from a variety of lipid compositions and different methods to yield different sizes and structures[170, 176, 177]. Formulation of RNA encapsulated LNPs is one of the most widely used strategies for in vivo delivery of siRNA, and has been successfully used to silence therapeutically relevant genes in primates[175, 178, 179] and are being evaluated in clinical trials. This chapter describes single cell measurements aimed a characterizing a new class of LNPs that are fabricated using a microfluidic process that was developed in a collaboration between Dr. Carl Hansen's laboratory and Dr. Pieter Cullis' laboratory. This process has since been commercialized by Precision Nanosystems Inc., a University of British Columbia startup company. The NanoAssemblr™ from Precision Nanosystems uses a microfluidic herringbone structure[180] to enable rapid mixing of lipids in ethanol with an aqueous phase containing RNA as described elsewhere[177, 181, 182]. This results in the precipitation of lipid nanoparticles ∼50-60 nm in diameter. These LNPs may be formulated at 'limit size' defined by the lipid composition, and exhibit low polydispersity[177, 181].

Quantitative measurement techniques are fundamental to evaluating the efficacy of RNA delivery and altered gene expression. To date, studies quantifying RNA delivery tend to use PCR or molecular imaging strategies. Quantitative PCR measurements have been useful in measuring dose-response and temporal relationships in bulk samples[183, 184], but would benefit from measurements of individual cells in order to assess potential heterogeneity in either mRNA delivery or altered gene expression. For example, if RT-qPCR from a bulk-sample (e.g. from hundreds to thousands of cells) shows ∼50% knockdown of a target gene, it remains unknown whether all cells exhibit 50% knockdown, or whether half the cells have complete (100%) knockdown and the other half have no (0%) knockdown (resulting in the same 50% knockdown upon averaging). Single-cell analysis can answer this question and elucidate cell heterogeneity in terms of delivery or response. Imaging techniques have the advantage of analyzing single cells and preserving spatial information, however are generally limited in throughput of cells due to field of view and laborious proto-

cols. Furthermore, measurement of fluorescently labeled oligonucleotides by imaging generally lacks the precision of qPCR or especially dPCR. This is particularly true for measurement of siRNAs, as the short length makes labeling with multiple fluorescent probes challenging[185]. However, microscopy has been useful to examine LNP uptake and intracellular transport[186, 187]. Considering the potential utility of using LNPs to deliver RNA to cells and manipulate gene expression, evaluation of the efficiency of delivery would benefit from precise quantification of RNA within single cells.

The goal of this project is to characterize the delivery of mRNAs by LNPs through precisely measuring the distribution of mRNA within single cells. We combine flow cytometry with microfluidic single-cell digital PCR to perform high-throughput single-cell measurements. In addition to measuring the abundance and distribution of delivered mRNA, this study also looks at conditions affecting LNP uptake, kinetics of transfection and protein abundance, siRNA knockdown of gene expression, and cell viability. These parameters are explored in suspension and adherent cell cultures, with cell lines including human eurythroleukemic cells, hESCs, and fibroblasts. This project is motivated by the potential applications of manipulating gene expression with exogenous RNA, and in particular by the potential advantages that mRNA dosing may provide to reprogramming somatic cells (i.e. fibroblasts) into induced pluripotent stem cells. By characterizing the performance of LNP transfection, this study aims to provide an informed basis for their use in a broad range of applications requiring the manipulation of gene expression.

4.3 Methods

4.3.1 Microfluidic Single-Cell Digital PCR

Microfluidic single-cell dPCR was performed using the CellsDirect kit protocol for mRNA developed and described in detail in Chapter 3. A TaqMan Gene Expression Assay (primers and probe) for eGFP (Mr04329676_mr, FAM, MGB) was ordered from Life Technologies (Cat # 4351372). The GAPDH assay (Hs02758991_g1) was also from Life Technologies (Cat # 4331182).

4.3.2 Cell Culture

The human embryonic stem cell line, CA1S, was used for LNP uptake and siRNA knockdown experiments. CA1S were normally cultured in mTESR (STEMCELL Technologies, Cat # 05850), a feeder-free maintenance medium. Wells were coated with Matrigel (Corning, Product #354277). Medium was exchanged daily. Cells were passaged with TrypLE (Life Technologies, Cat # 12604013).

The human newborn foreskin fibroblast cell line, BJ (ATCC CRL-2522) was used for mRNA transfection experiments. BJ cells were cultured in EMEM (Gibco) supplemented with 10% FBS. Cells were passaged with TrypLE (Life Technologies, Cat # 12604013).

The human erythroleukemia cell line, K562 (ATCC CCL-243) was used as a model cell line for suspension cultures. K562 cells were cultured in DMEM (Gibco), with 10% FBS. All cell cultures were incubated at 37°C and 5% CO2. Cell counts and viability staining were performed by the Cedex cell counter.

4.3.3 Lipid Nanoparticle Formulation

LNP were prepared using the NanoAssemblr microfluidic-based nanoparticle manufacturing platform[177]. LNPs prepared using the NanoAssemblr™ instrument mimic the neutral, cholesterol containing structure of low-density-lipoproteins (LDL), which are taken up by cells though the LDL-receptor (LDLR) in presence of Apolipoprotein E4 (ApoE4). LNPs were labeled with a red lipophilic dye (Ex/Em = 549/565 nm) to enable fluorescence imaging of particle uptake in cells. eGFP mRNA was purchased from TriLink Biotechnologies (996 nucleotides, 5-methylcytidine, pseudouridine, L-6101). The siRNA duplex targeting GAPDH was purchased from IDT with the sequence 5'-UGG CCA AGG UCA UCC AUG AdTdT-3' (sense), and 3'-dTdTA CCG GUU CCA GUA GGU ACU-5' (antisense), where the dT represents a DNA base for thymine (the rest are RNA).

4.3.4 Transfection

To measure the ApoE dependence of LNP uptake, CA1S cells were plated at 400,000 cells/well (6-well plates). Twenty-four hours after plating, siRNA-LNPs and ApoE was added to the cultures (24 hours before flow cytometry). Four hours before analysis by flow cytometry, siRNA-LNPs and were added to the 4-hour cohort. Each

experiment condition was performed in duplicate.

In the siRNA knockdown of HPRT in CA1S, cells were seeded at 150,000 cells/well (6-well plate) in 3 mL mTESR. Twenty-four hours later, media was exchanged, and ApoE was added to the media for a final concentration of 1.0 µg/mL. siRNA was added to give final concentrations for a 'low' dose of 0.1 µg/mL siHPRT, and a 'high' dose of 1.0 µg/mL siHPRT. Medium was exchanged again 24 hours later, with mTESR supplemented with the same amount of ApoE and siRNA as previously. 48 hours after transfection, cells were collected for analysis by single-cell digital PCR (final cell number was $\sim 2\times10^6$ per well).

For siRNA knockdown of GAPDH, CA1S cells were plated at 350,000 cells/well (6-well plates). Twenty-four hours later, ApoE (1.0 µg/mL final concentration) and siRNA (1.0 µg/mL and 0.1 µg/mL final siRNA concentrations) were added during media change, and incubated for 24 hours before collection for analysis. Cells were cultured in 3 mL mTESR medium. Non-Targeting siRNA was included as a parallel control to show that GAPDH knockdown was specific to siGAPDH.

K562 cells were transfected with siGAPDH in 96-well plates, seeded at $\sim 5\times10^5$ cells/mL (200 µL culture volume). ApoE was added to a final concentration of 1.0 µg/mL, and siGAPDH was added to different wells for each concentration tested. Cells were incubated for 24 hours before measurement.

In mRNA transfections of BJ and K562 cells, cells were seeded at 400,000 cells/well (6-well format), and transfected for 24 hours with 100 ng/mL and 500 ng/mL eGFP mRNA. ApoE was added to the media at a final concentration of 1.0 µg/mL.

For the proof-of-concept imaging of eGFP and mCherry in BJ cells, 500 ng/mL for each eGFP and mCherry mRNA was added to 6-well plates containing $\sim 4\times10^5$ cells/well (3 mL total media), and incubated for 24 hours.

To test repeated high-dosing, a transfection protocol was adapted from a commercial iPS reprogramming kit (Stemgent), and a modification to this protocol from Warren et al.[188]. BJ cells were seeded on day 0 at low-density (50,000 cells/well; 6-well plate). Medium (EMEM) with 10% FBS was supplemented with 1.0 µg/mL ApoE. Cells were transfected by adding LNPs to the culture after each daily media change for two weeks. Cells were split 1/6th during passage on day 7 before becoming confluent. Over the first four days, the dosage was increasingly ramped up from 25%, 50%, 75%, to 100% of the final dose of RNA (400 ng/mL, 2 mL) by increasing the volume of LNP-media added. This same protocol was performed in parallel on

cells cultured with Pluriton medium (Stemgent) supplemented with B19R interferon inhibitor (200 ng/mL), in wells coated with Matrigel (Corning).

4.3.5 Flow Cytometry

Flow cytometry was performed on a BD FACSCalibur (BD Biosciences), collecting 50,000 events, and analyzed using FlowJo (FlowJo Data Analysis Software, LLC). Only 15,000 events were collected during the reprogramming time-course experiment.

4.3.6 Microscopy

Fluorescence microscopy was used to visually inspect transfection (LNP delivered fluorescent dye) and eGFP in BJ cells. Cells were imaged at different locations in the 6-well plate, in 90 minute intervals for 90 hours. The 6-well plate was on an automated stage inside a custom build environmental enclosure for the microscope, with the temperature at 37°C, 5% CO_2, 70% humidity. ImageJ was used to combine brightfield, eGFP and DiI fluorescence images. Due to background fluorescence and signal-to-noise issues, these images were only used for qualitative observations of cell morphology, fluorescence signal location within cells, and time duration to see eGFP.

4.4 Results

4.4.1 ApoE-Dependent LNP Uptake

We sought to measure the uptake of lipid nanoparticles in a variety of cell tissues (e.g. blood, hESC), and types (e.g. primary, suspension or adherent). In particular, human embryonic stem cells are traditionally hard to transfect, and we wanted to test the transfection performance of our LNPs in this system. In order to explore the potential of using these LNPs in embryonic stem cell applications, we used flow cytometry to measure the uptake of LNPs in human embryonic stem cells adapted to in vitro culture (CA1S)[189]. The uptake of lipid nanoparticles is inferred by measuring the intensity of a fluorescent reporter dye (DiI), which is encapsulated in the LNPs, and can be used to trace the LNP cargo delivery in cells (Figure 4.1). This flow cytometry measurement facilitates high-throughput single-cell analysis, however it is poorly suited to properly assessing LNP uptake and release as cells may appear

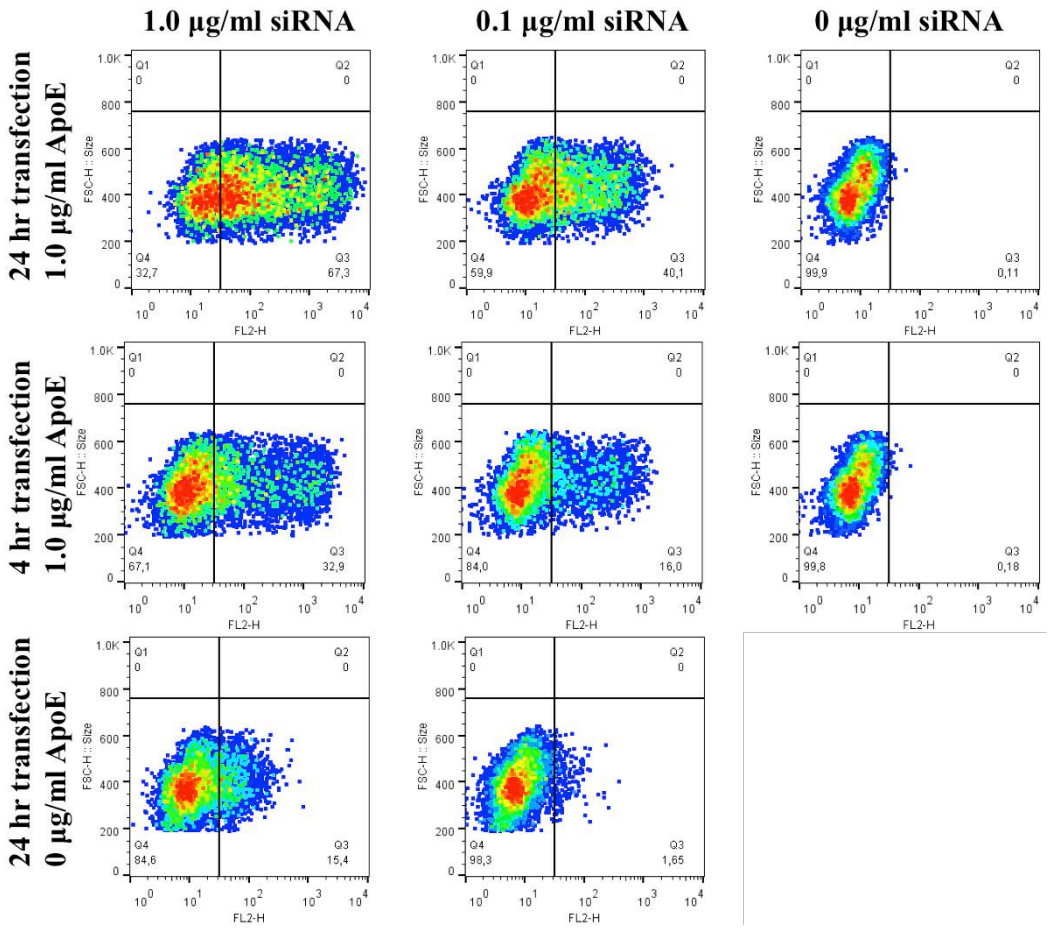

Figure 4.1: ApoE-dependent LNP in hESC. Flow cytometry measurements of forward-scatter (FSC) vs. DiI (FL2), where DiI fluorescence was used as a reporter for cellular uptake of LNPs. From left to right: siRNA-LNP dose was 1.0 µg/mL; siRNA-LNP dose was 0.1 µg/mL; untreated control. From top to bottom: 24 hour transfection with 1.0 µg/mL ApoE; 4 hour transfection with 1.0 µg/mL ApoE; 24 hour transfection without ApoE. Transfection for 4 hours without ApoE showed negligible uptake and is not shown. Experimental replicates yielded similar results (Figure 4.2).

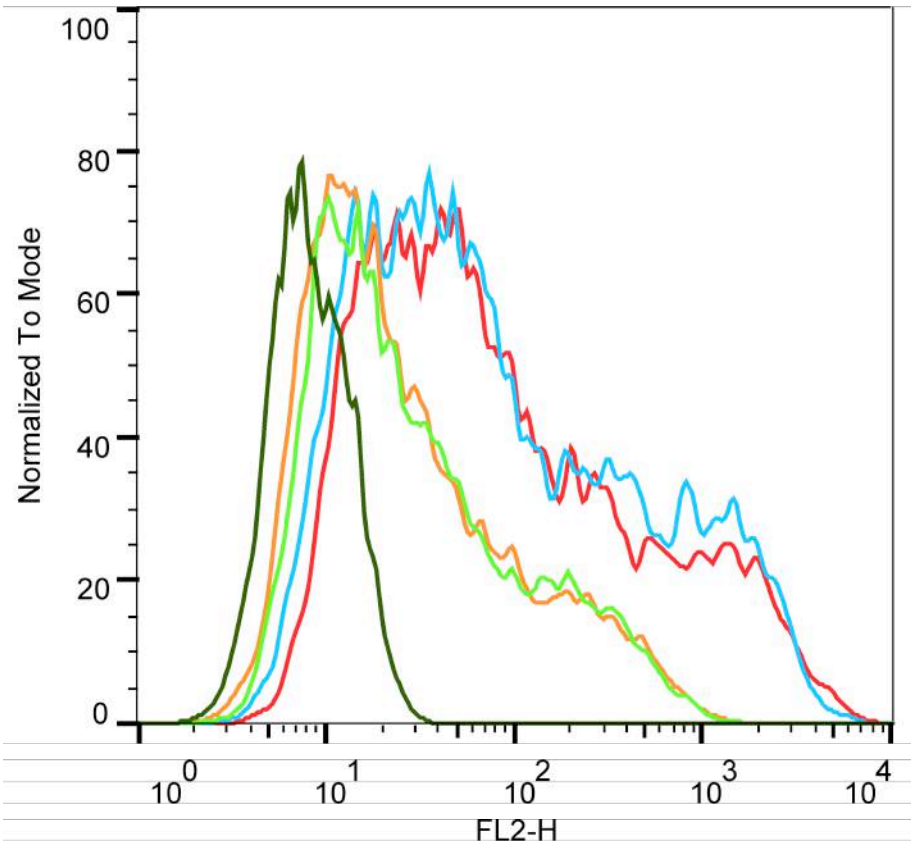

Figure 4.2: Replicates for ApoE-dependent LNP uptake experiment in hESC. Histogram displays flow cytometry measurements of DiI (FL2), where DiI fluorescence was used as a surrogate for cellular uptake of LNPs (same experiment as Figure 4.1). Untreated cells are shown in dark green; cells receiving a siRNA-LNP dose of 0.1 µg/mL shown in orange and light green; cells receiving a siRNA-LNP dose of 1.0 µg/mL shown in blue and red.

fluorescent if LNPs are bound to the cell membrane, or if contained within endosomes. The flow cytometry detection of this dye should therefore be seen as a metric of LNP association with the cell, and may overrepresent the number of transfected cells.

Previous studies in the brain[190] and liver[175] have shown that LNP uptake is facilitated by adsorption of endogenously produced apolipoprotein E (ApoE) to the LNPs, which can then be recognized by scavenging receptors and low-density lipoprotein receptors. This takes advantage of the property that these LNPs mimic natural cholesterol. We hypothesized that adding exogenous ApoE to hESC cultures would similarly increase the transfection efficiency. We measured the uptake of LNPs after 4 hours and 24 hours of transfection, measuring approximately 15% of hESCs containing the delivered dye after a dose of 1.0 µg/mL for 24 hours (Figure 4.1). This measurement represents a lower bound on positive uptake, as the threshold for calling a cell positive is set to exclude all of the untransfected negative control cell population. Furthermore, sufficient dye must be delivered to be detected by flow cytometry. The addition of 1.0 µg/mL ApoE increased the transfection efficiency, to 67.3%, a ∼4.4X increase (Figure 4.1). In the presence of ApoE, cells positive for DiI continued to increase from 32.9% at 4 hours of transfection to 67.3% at 24 hours. However, it is notable that almost half of the transfection occurs within the first 4 hours. This experiment delivered non-targeting siRNA (siNT) (i.e. not complementary to any mRNA), and viability for all treated conditions matched the untreated control. These transfection results encourage future testing of LNP transfection in primary hESC.

4.4.2 siRNA Knockdown

We next assessed our ability to knock down gene expression by LNP delivery of siRNA. Using the previously developed microfluidic device for performing single-cell digital PCR measurements[191] (from Chapter 3), we measured levels of the targeted transcript within single-cells undergoing a treatment of siRNA-LNP. We treated hESC cultures for 48 hours with a low dose (0.1 µg/mL), and high dose (1.0 µg/mL) of siRNA targeting HPRT. For a low-abundance transcript, HPRT, we observed a distribution of transcript abundance (Figure 4.3) ranging from 0 to 25 per individual cell, with a mean of 8.8 copies per cell (s.d. 5.6 copies, N=35). Upon treatment, we witnessed the HPRT distribution shift towards lower copy number, with less than 10% of cells containing more than 10 transcripts, and a small percentage containing no detected HPRT copies (mean 6.6 copies per cell, s.d. 5.0 copies, N=48). Increasing

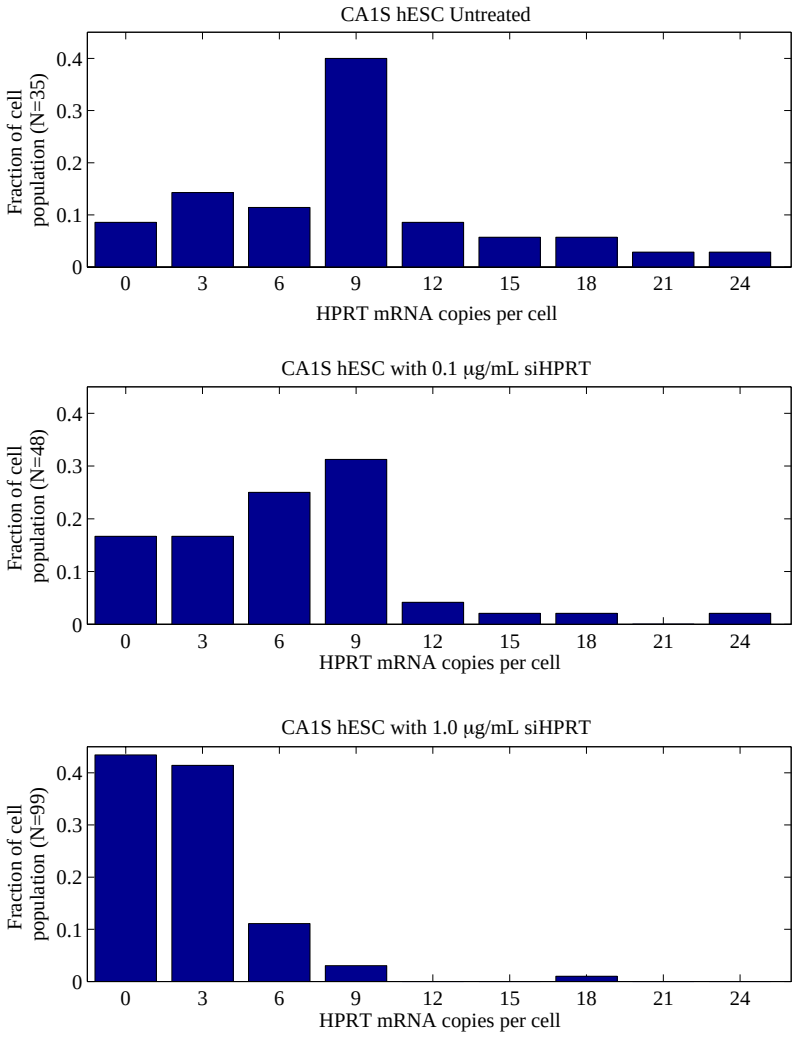

Figure 4.3: siNRA knockdown of HPRT in human embryonic stem cells. Histograms showing the distribution of measured HPRT transcripts measured in single CA1S hESC undergoing 48 hours of transfection at dose of 1.0 µg/mL (bottom), 0.1 µg/mL (middle), and an untreated control (top).

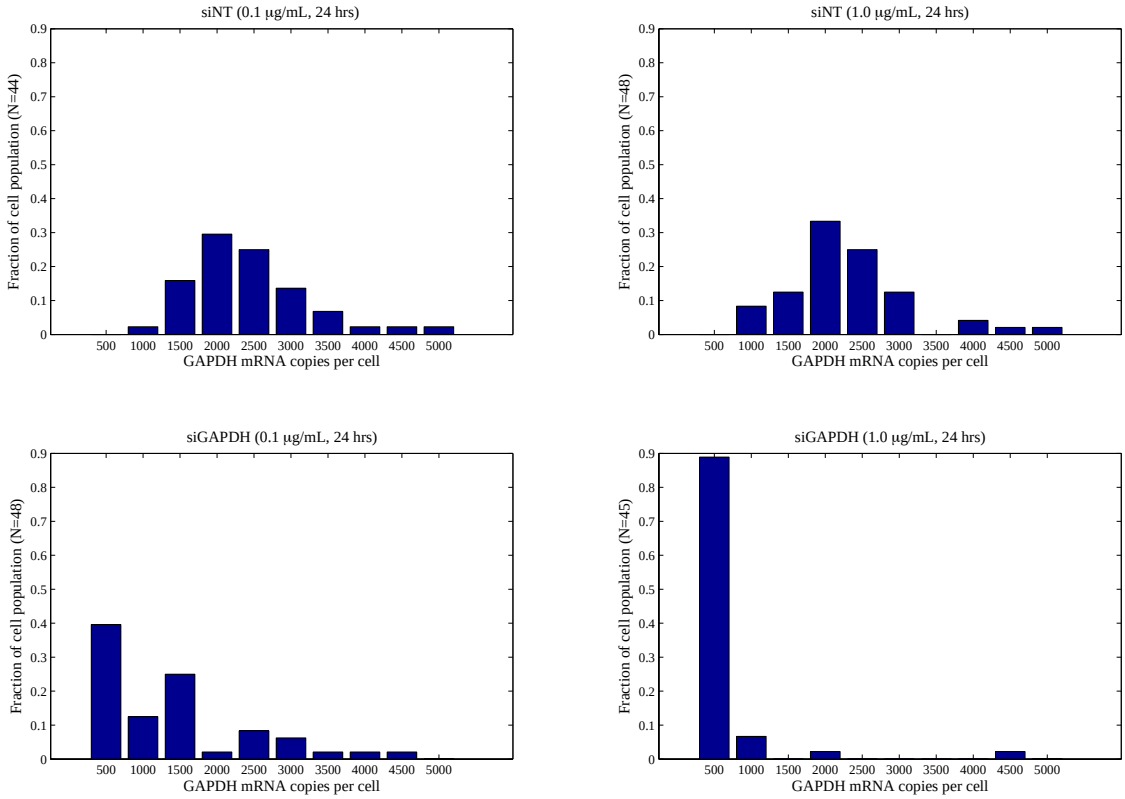

Figure 4.4: siNRA knockdown of GAPDH in human embryonic stem cells. Histograms showing the distribution of measured GAPDH transcripts measured in single CA1S hESC undergoing 24 hours of transfection at dose of 1.0 µg/mL, 0.1 µg/mL, and non-targeting siRNA (siNT) control.

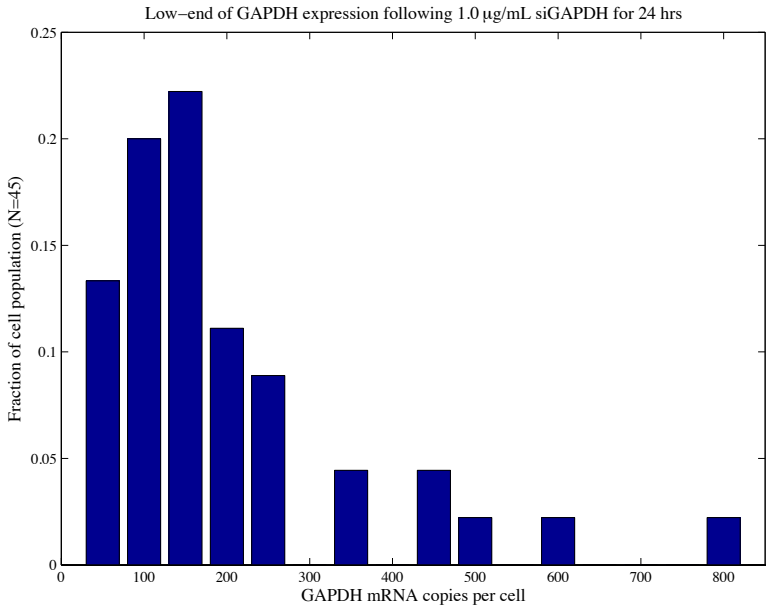

Figure 4.5: Low-end of GAPDH expression following 1.0 µg/mL siGAPDH for 24 hrs. This is a detailed view of the histogram information from Figure 4.4.

the siRNA dose to 1.0 µg/mL further shifted the transcript abundance to a distribution between 0 and 10 copies per single cell, with over 80% of the cells containing 0 to 4 copies (mean 2.3 copies per cell, s.d. 2.6 copies, N=99). Trypan blue staining showed similar viability between untreated and treated cultures (∼97%). Following a similar dosing treatment, but only transfecting over 24 hours, we measured knockdown of a highly expressed gene, GAPDH (Figure 4.4). Here we observed GAPDH constitutively expressed in all cells (mean 2,430 copies per cell, s.d. 781 copes) . Similar to knockdown of HPRT, GAPDH expression exhibited partial knockdown at 0.1 µg/mL siGAPDH. With a 24-hour dose of 1.0 µg/mL siGAPDH, we measured significant knockdown of GAPDH (mean 362 copies per cell, s.d. 693 copies), with ∼89% (40/45) of cells containing less than 750 copies (see Figure 4.5 for detailed histogram information). Remarkably, the same dose that is unable to completely eliminate the tens of HPRT transcripts is able to knock down hundreds to thousands of GAPDH transcripts in each cell (but still not completely eliminate it, with the lowest measure of 8 copies per cell). The difficulty in completely eliminating such 'housekeeping' genes may reflect the speed at which such genes are transcribed com-

pared to interacting with siRNA. Furthermore, nascent mRNA residing in the nucleus is inaccessible to siRNA, and it is possible that fragments of the degraded transcripts are still detectable RT-qPCR. Treated cultures remained viable, however significantly higher doses targeting GAPDH will lead to toxicity, as GAPDH is needed in glycolysis. Increasing a dose of non-targeting siRNA from 0.1 µg/mL to 1.0 µg/mL did not significantly alter the abundance of GAPDH, indicating the reduction of GAPDH under targeted siRNA was the result of RNA interference and not due to the particles by themselves. The abundance of GAPDH in cells treated with non-targeting siRNA fit a log-normal distribution similar to untreated cells.

In addition to the adherent CA1S hESCs, we measured the dose-response relationship in a suspension cell line, K562 (Figure 4.6A). K562 cells are a human erythroleukemia cell line we have previously characterized GAPDH with single cell RT-qPCR and dPCR. Using single-cell dPCR, we measured a mean of 1,453 (s.d. 519) GAPDH transcripts 20 hours after a dose of 6 ng/mL (see Methods section for details). Increasing the dose to 60 ng/mL did not change expression significantly (mean 1,511 copies, s.d. 509 copies), but dramatic reduction in transcript levels (mean 582 copies, s.d. 421 copies) occurs with a dose of 600 ng/mL, suggesting a possible threshold of LNP delivery (i.e. siRNA abundance) before knockdown occurs (Figure 4.6A). With a siRNA dose of 1.2 µg/mL, GAPDH levels were reduced to a mean of 153 copies (s.d. 132 copies), a ∼90% knockdown of constitutive levels. Notably however, GAPDH was still detected in all cells, with the minimum detected being 1 copy. In a separate experiment repeating some of these doses, and looking at a higher dose of 2.5 µg/mL siRNA, results showed a greater knockdown effect (Figure 4.6B). For this transfection, cells were incubated with siRNA-LNPs for 24 hours. This extra time may have contributed to the greater knockdown, but we previously observed the majority of uptake occurs within 4 hours. It should also be noted that this difference may arise from using a different manufacturing batch of siRNA-LNPs, or from a different thawed vial (and passage number) of K562 cells. In this experiment, knockdown of GAPDH was observed with a siRNA dose of 60 ng/mL, yielding a mean of 1,063 copies of GAPDH per cell (s.d. 504, N=48). Increasing the siRNA dose to 600 ng/mL resulted in significant knockdown, with a mean average of 132 GAPDH transcripts measured per single cell (s.d. 206, N=46). The minimum number of GAPDH transcripts detected was 5. With a treatment of 1.2 µg/mL siRNA, GAPDH levels dropped to an average of 61 copies per cell (s.d. 64), with 1/47 cells

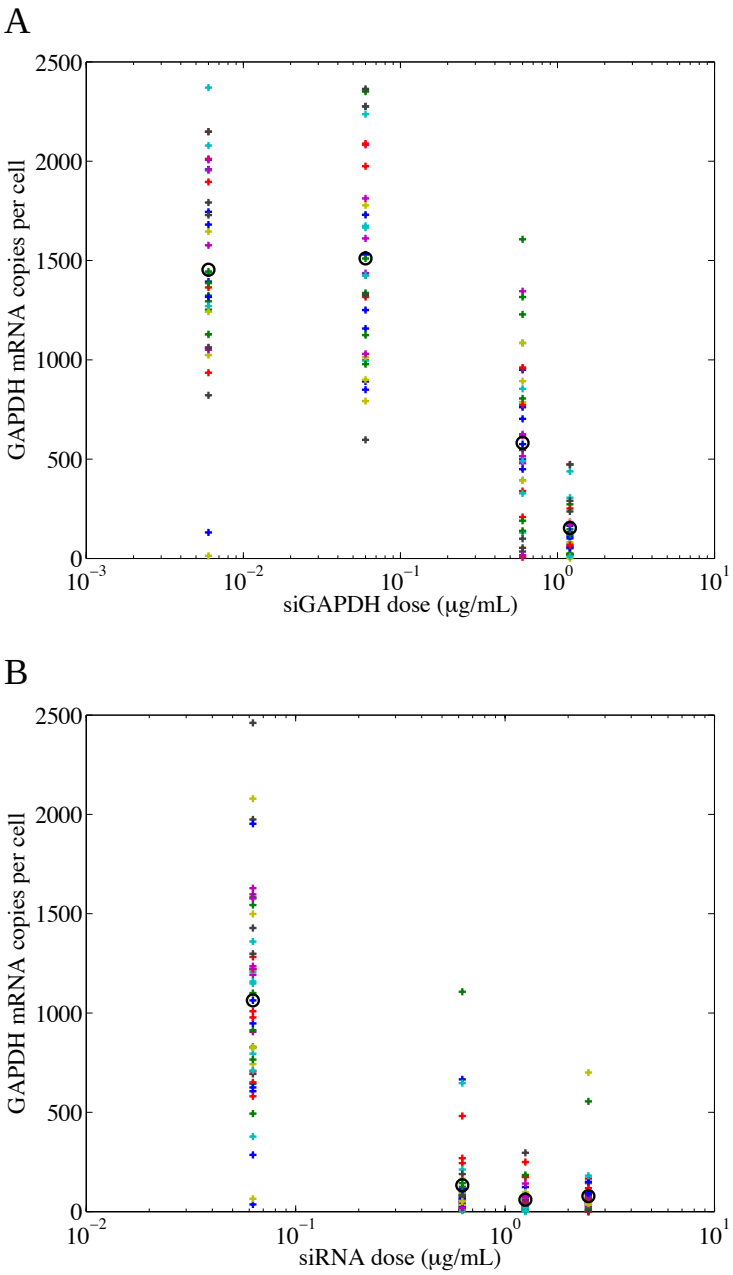

Figure 4.6: Single-cell dose-response curve for siGAPDH treatment in K562 cells. Coloured marks represent single-cell digital PCR measurements of GAPDH mRNA copies. Black circles indicate mean. Experiments in A and B show variability in response to siRNA treatment over biological replicates (and different LNP batches).

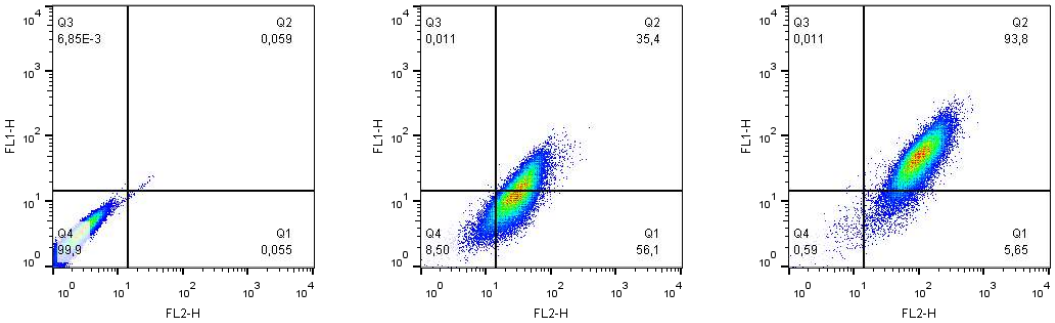

Figure 4.7: Single-cell flow cytometry measurement of LNP delivery and eGFP expression in K562. Flow cytometry profiles show eGFP signal vs. DiI, where eGFP fluorescence was used as a reporter for translation from delivered mRNA, and DiI was a reporter of LNP uptake. From left to right: untreated control sample; 24 hour transfection of 100 ng/mL eGFP mRNA-LNP; 24 hour transfection of 500 ng/mL eGFP mRNA-LNP. The fluorescence signal threshold to call positive eGFP and DiI detection was set such that it excluded signal from untreated cells.

without detected GAPDH. Increasing this dose to 2.5 µg/mL siRNA resulted in 3/49 cells without detected GAPDH. For this final dose, the mean (78 copies/cell) and standard deviation (124 copies/cell) are increased due to the presence of seeming outliers (Figure 4.6B). By measuring gene expression knockdown in individual cells, these results reveal the variability in expression knockdown, and show that there is a distribution of knockdown levels rather than a binary response with some cells exhibiting complete knockdown while others are unaffected.

4.4.3 mRNA Delivery

Having demonstrated the ability to knock down gene expression with siRNA delivery, we sought to expand our capabilities of manipulating gene expression to include mediating, or knocking-in, gene expression. We chose to test our transfection system in suspension and adherent cell culture conditions, using K562 as our suspension condition. As proof-of-concept, we delivered mRNA encoding for green fluorescent protein (eGFP), the detection of which was useful for reporting successful translation of delivered mRNA. Using flow cytometry, we were able to measure LNP transfection (or at least cellular localization) by detection of delivered dye fluorescence (Figure 4.7). We were then able to compare the single-cell flow cytometry measurements of transfection and protein abundance, to the delivered mRNA levels in single cells as

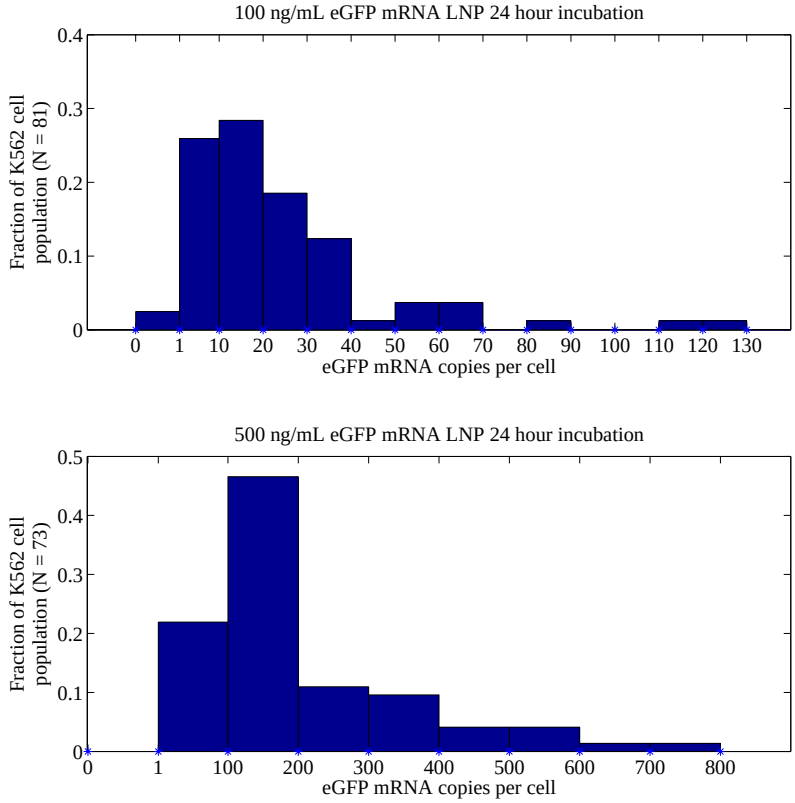

Figure 4.8: Single-cell measurement of mRNA delivered by LNP in suspension culture (K562). (Top) Histogram showing the distribution of eGFP mRNA measured by single-cell digital PCR in K562 cells administered 100 ng/mL for 24 hours. (Bottom) Histogram showing the distribution of eGFP mRNA measured by single-cell digital PCR in K562 cells administered 500 ng/mL for 24 hours.

measured by microfluidic digital PCR (Figure 4.8). In K562, a dose of 500 ng/mL eGFP mRNA-LNP for 24 hours resulted in ∼94% of cells reporting eGFP positive, and over 99% of cells were positive for the particle dye (Figure 4.7). A dose of 100 ng/mL for 24 hours showed reduced penetrance, with ∼91% of cells transfected but only 35% of cells positive for eGFP. Using microfluidic single-cell dPCR, we confirmed the presence of eGFP mRNA in 100% (N=73) of the K562 cells transfected with the 500 ng/mL dose (Figure 4.8), with a mean abundance of 201 copies (s.d. 150 copies) per cell. Interestingly, reducing the mRNA-LNP dose 5X, to 100 ng/mL, resulted in more than a 5X reduction in eGFP transcripts measured in single-cells (mean 23 copies, s.d. 23 copies). This supra-linear relationship between dose and measured mRNA levels may be due the speed at which eGFP mRNA is degraded in the cell. Inspection with microscopy revealed that LNP uptake is rapid within the first 4 hours, and the low-dose culture condition may rapidly become LNP-depleted compared to the high-dose condition. Compared to the flow cytometry measurement of 91% cells transfected at the dose of 100 ng/mL, we detected eGFP mRNA in 98% (79/81) of cells, albeit at low levels. Measurement after 24 hours was chosen as such 'overnight' treatments are common in cell culture experiments, and also to give time for eGFP translation. The doubling time for K562 cells is approximately 24 hours, which may result in dilution of eGFP mRNA or protein. Analysis of flow cytometry measurements using different cell population gates revealed no significant correlation between cell size and LNP dye or eGFP expression (Figure 4.9).

For adherent culture conditions, we transfected a human neonatal foreskin fi-

Figure 4.9 *(following page)*: Effect of different population gates on flow cytometry measurement of LNP delivery and eGFP expression in K562 cells. (A) A generous gate is displayed in the flow cytometry profile of K562 cells showing granularity (side scatter, SSC) and size (forward scatter, FSC). (B,C) The corresponding measurements of eGFP (FL1) vs. LNP dye (FL2) for 100 ng/mL and 500 ng/mL RNA dosages, as in Figure 4.7. (D) A relatively small gate at the densest region of the K562 cell population and the measured eGFP and LNP dye for 100 ng/mL (E) and 500 ng/mL (F) eGFP mRNA doses. (G) The smallest and largest cells are gated and resultant eGFP vs. dye profiles are shown in H and I respectively (500 ng/mL RNA dose). (J) Reverse-gating of cells with the highest intensity of eGFP and dye yields a subpopulation (K) with size and granularity similar to the generous gate in A. (L) Plot of eGFP (FL1) vs. size (FSC) shows that eGFP intensity is not proportional cell size.

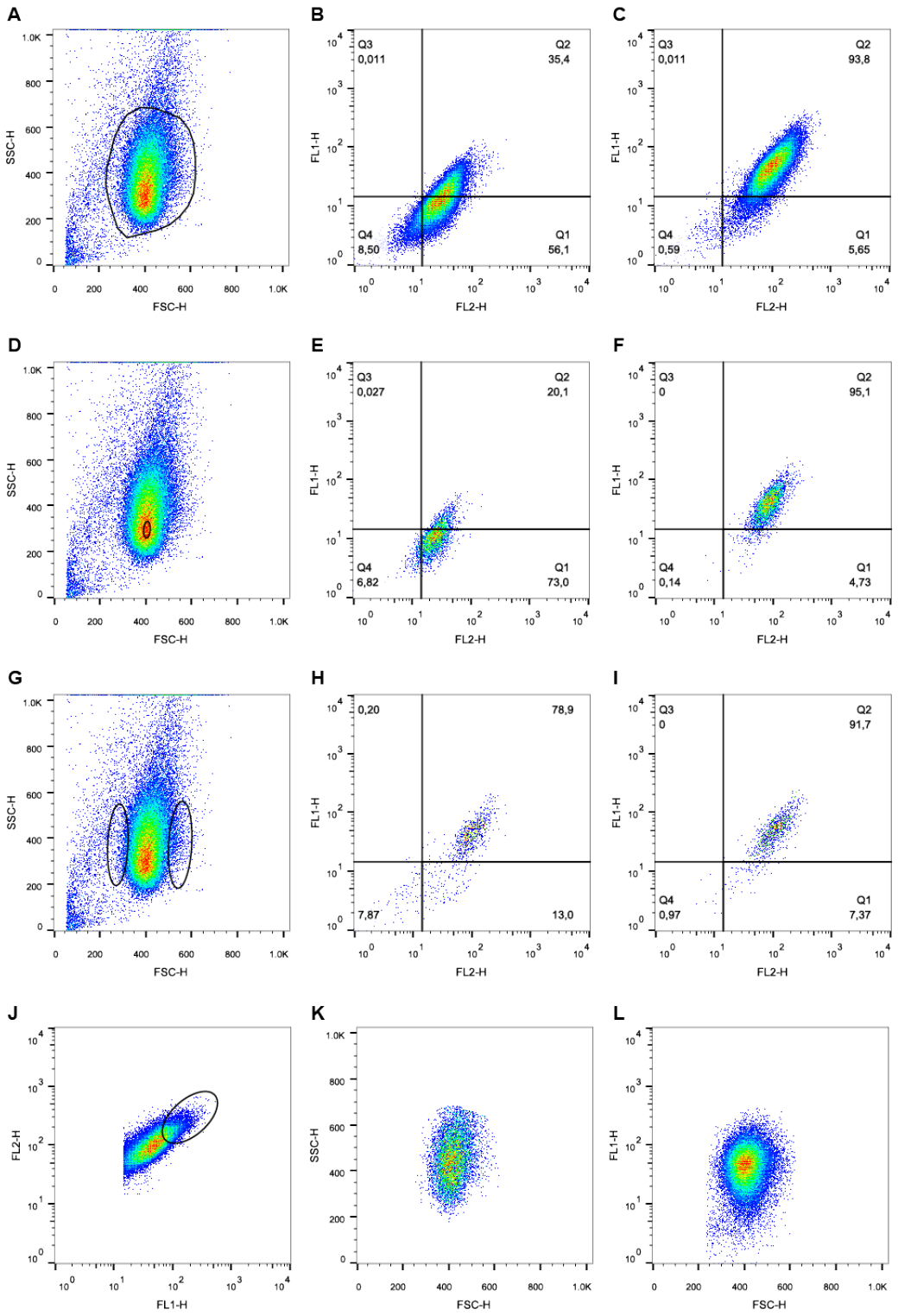
A
SSC-H
FSC-H
B
Q3 0,011
Q2 35,4
Q4 8,50
Q1 56,1
FL1-H
FL2-H
C
Q3 0,011
Q2 93,8
Q4 0,59
Q1 5,65
D
E
Q3 0,027
Q2 20,1
Q4 6,82
Q1 73,0
F
Q3 0
Q2 95,1
Q4 0,14
Q1 4,73
G
H
0,20
78,9
7,87
13,0
I
Q3 0
Q2 91,7
Q4 0,97
Q1 7,37
J
K
L

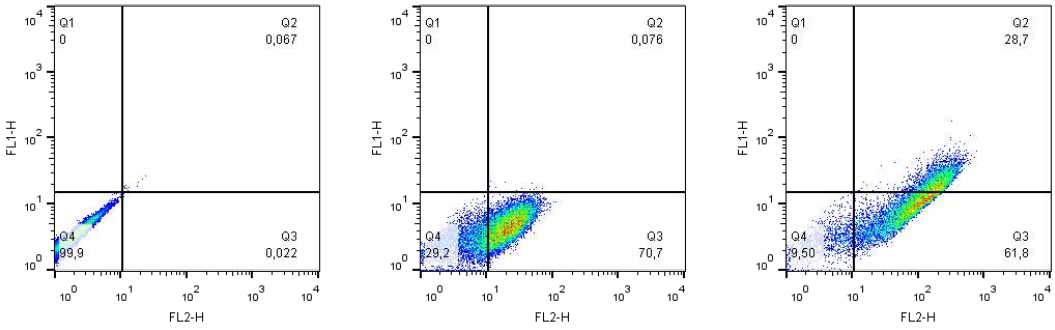

Figure 4.10: Single-cell flow cytometry measurement of LNP delivery and eGFP expression in BJ. Flow cytometry profiles show eGFP signal vs. DiI, where eGFP fluorescence was used as a reporter for translation from delivered mRNA, and DiI was a reporter of LNP uptake. From left to right: untreated control sample; 24 hour transfection of 100 ng/mL eGFP mRNA-LNP; 24h hour transfection of 500 ng/mL eGFP mRNA-LNP. The fluorescence signal threshold to call positive eGFP and DiI detection was set such that it excluded signal from untreated cells.

broblast cell line, BJ. BJ cells were selected as they have been extensively used in transfection studies to produce iPS cells, and could provide a basis for comparison with our LNP transfection technique. In contrast to K562 cultures, BJ cells transfected with the same dose showed markedly less transfection and eGFP. Cells dosed at 100 ng/mL were ∼71% positive for delivered dye, but no eGFP was detected (Figure 4.10). This corresponded to 76% (42/55) of cells containing eGFP mRNA (Figure 4.11), but RNA levels were low, with most cells containing between 1 and 20 copies (mean 6 copies, s.d. 7.5 copies). Increasing the dose to 500 ng/mL resulted in 90% of cells positive for fluorescent dye, but only 29% positive for eGFP (Figure 4.10). Single-cell RT-dPCR revealed this population to contain eGFP mRNA in all cells (N=86), with abundance ranging from tens to hundreds of transcripts (mean 213 copies, s.d. 220 copies). Uptake and transcript abundance is somewhat higher in K562 cells, and this may simply be due to geometric constraints in adherent cell culture, where only some of the cell surface is exposed to LNPs, as compared to cells in suspension. The differences in protein abundance suggest a physiological difference between K562 and BJ cells, and further experiments are needed to elucidate if this difference is due to mRNA accessibility (e.g. endosome trafficking of LNP cargo), or differences in translation kinetics. Taken together, these results could be interpreted as suggesting a minimum of ∼20 eGFP transcripts per cell are required to detect

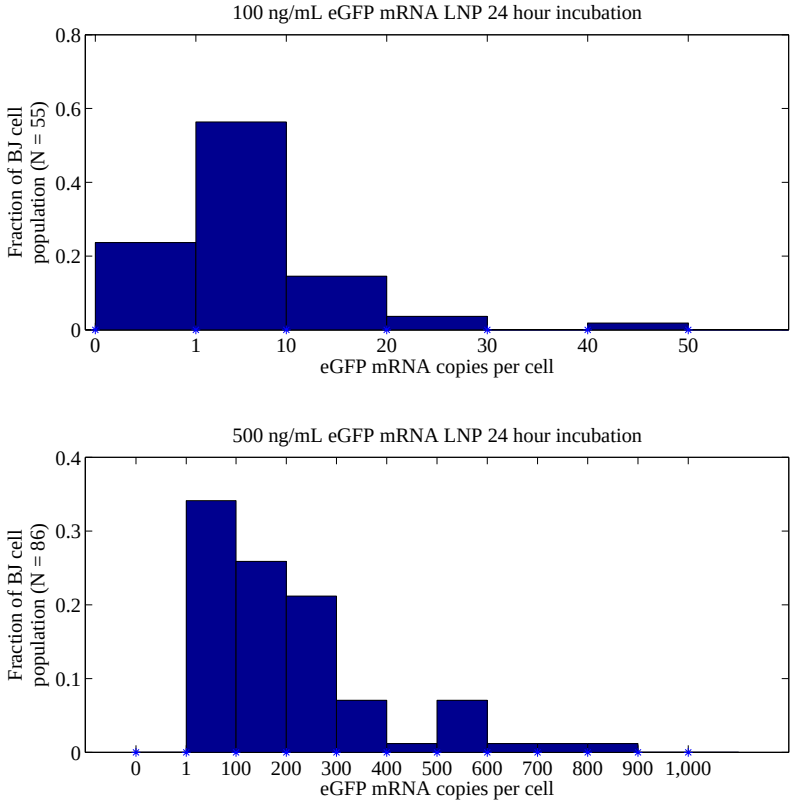

Figure 4.11: Single-cell measurement of mRNA delivered by LNP in adherent culture (BJ). (Top) Histogram showing the distribution of eGFP mRNA measured by single-cell digital PCR in BJ cells administered 100 ng/mL eGFP mRNA-LNP for 24 hours. (Bottom) Histogram showing the distribution of eGFP mRNA measured by single-cell digital PCR in BJ cells administered 500 ng/mL mRNA-LNP for 24 hours.

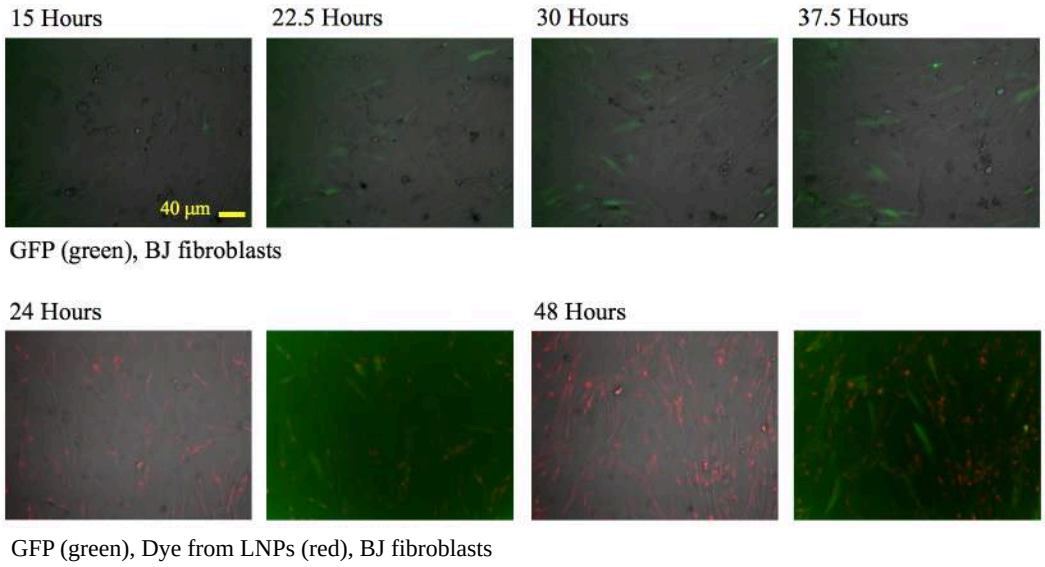

Figure 4.12: Inducing gene expression with mRNA delivery. Time-lapse microscopy imaging of DiI (red) and eGFP (green) fluorescence in BJ cells dosed with 500 ng/mL eGFP mRNA (at 0 hours). Images suffered from high background fluorescence and low signal-to-noise, and were used gauge the onset of eGFP signal, while flow cytometry was used to quantify eGFP and DiI in cells.

eGFP at this time point. One concern with adapting this LNP system to mRNA delivery is that the long mRNA strands (relative to the short siRNA duplexes, ∼22 bp) may be more susceptible loss of function due to a number of factors including fragmentation from shear stress during formulation, secondary structure, or endosomal trafficking. Also, we do not know what fraction of synthesized RNA is full length. The result showing 94% of K562 cells positive for eGFP indicates functional transcripts, however further verification of the state of delivered mRNA is needed.

Visual inspection of cells undergoing transfection (Figure 4.12) showed rapid and widespread uptake of LNPs during the first 4 hours, as reported by DiI fluorescence localized within cells. eGFP was visible after ∼10 hours, and remained in cells for over 72 hours. In contrast to the diffuse eGFP signal throughout the cytoplasm, DiI signal was often punctuate, suggesting the dye was contained within intracellular membranes such as endosomes. Notably, DiI particularly accumulated in two opposite points on either side of the nucleus. Cells exhibiting DiI uptake in endosomes, but without eGFP expression, may reflect endosomal recycling or sequestering of mRNA as a major factor limiting functional transfection efficiencies[186].

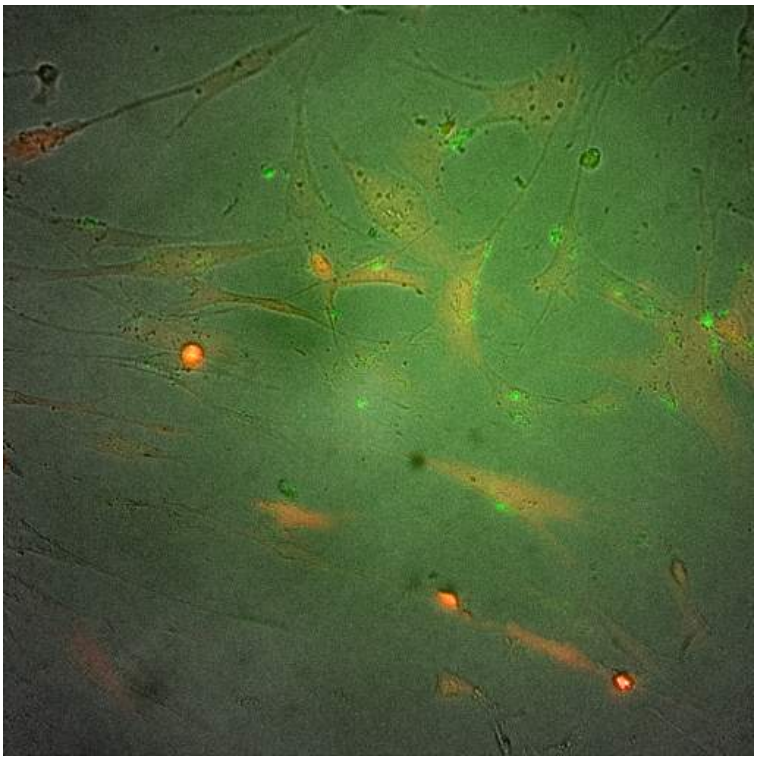

Figure 4.13: Inducing gene expression with delivery two different mRNAs. Proof-of-concept demonstration of delivering multiple RNAs, showing false-colour overlay of fluorscence from eGFP (green) and mCherry (red), resulting in diffuse orange signal in cytoplasm.

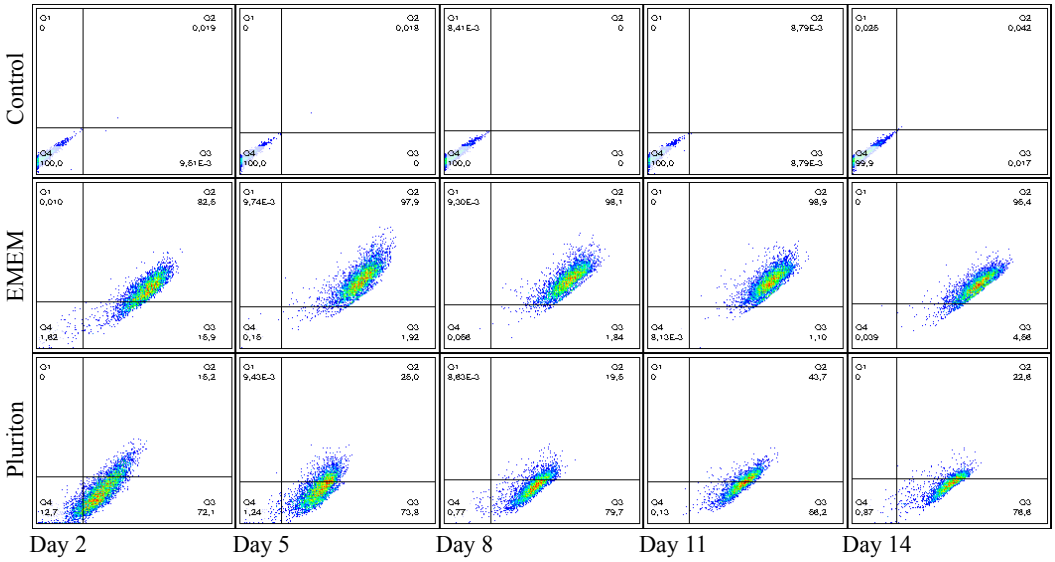

Figure 4.14: Time-course measurement of mRNA-LNP performance in BJ cells with daily doses for two weeks. Flow cytometry plots showing eGFP signal vs. DiI as a measure of protein abundance and particle uptake (respectively). The 'Control' series refers to untreated (i.e. not dosed with mRNA-LNP) BJ cells in EMEM (10% FBS). The 'EMEM' series refers to BJ cells treated daily with mRNA-LNP, in normal culture conditions of EMEM with 10% FBS (and ApoE). The 'Pluriton' series refers to BJ cells treated daily with mRNA-LNP in reprogramming culture conditions of Pluriton medium and matrigel (no serum, but with ApoE).

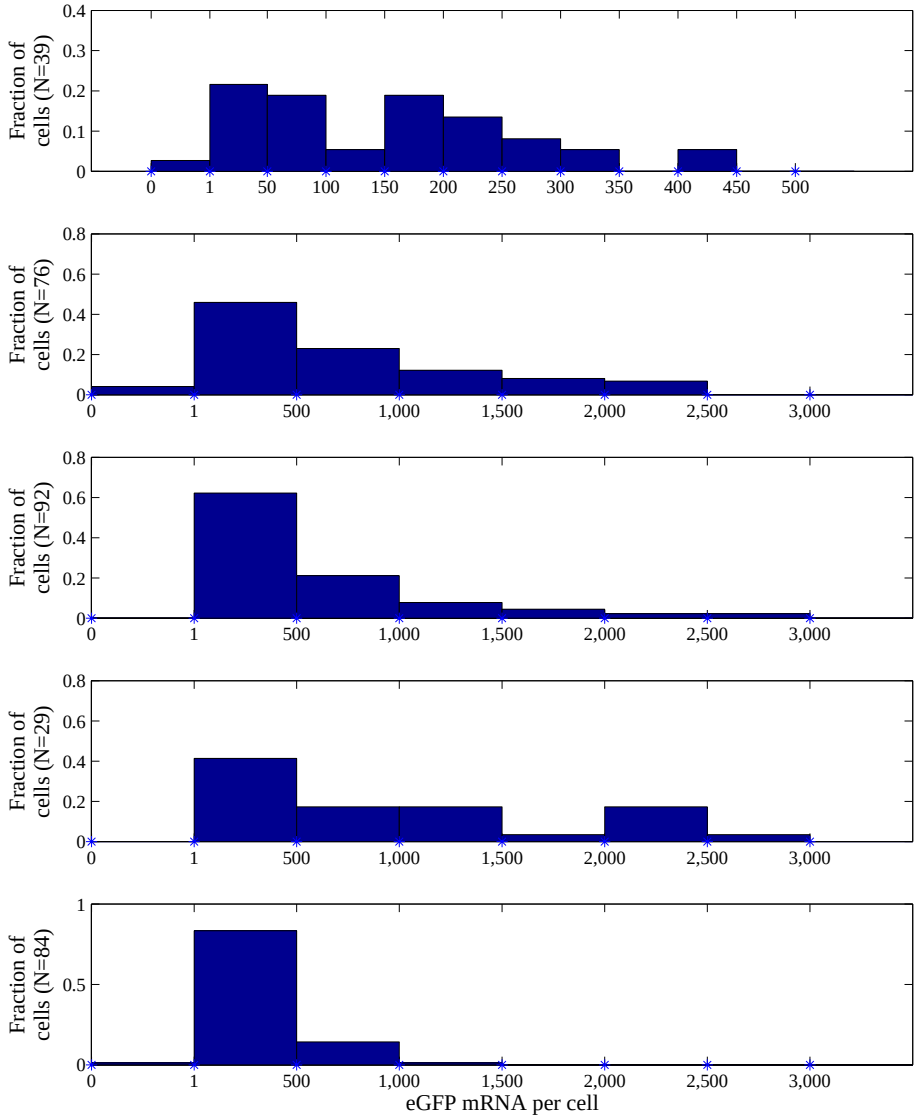

Figure 4.15: Distribution of delivered mRNA in BJ cells with daily doses for two weeks. Histograms display results from single-cell digital PCR measurement of eGFP transcripts from cells undergoing daily transfections in EMEM with 10% FBS. The time-course is represented from top-to-bottom: day 2, day 5, day 8, day 11, day 14, and corresponds to measurements on cells from the 'EMEM' series in Figure 4.14.

One of the applications of mRNA delivery of keen interest is the reprogramming of cells, in particular the creation of iPS cells that can then be directed in differentiation to desired tissue types (e.g. neurons). Reprogramming fibroblasts to pluripotency was recently demonstrated with the transfection synthetic mRNA encoding the transcription factors Klf4, c-Myc, Oct4, and Sox2 (originally achieved by Yamanaka and colleagues by enforced expression)[188]. As demonstration of delivering more than one mRNA at the same time, we simultaneously delivered two different mRNAs, encoding for eGFP and mCherry, and observed fluorescence from both proteins after a dose of 500 ng/mL each (Figure 4.13). Reprogramming protocols with RNA transfections typically involve repeated high doses over multiple weeks, and we sought to evaluate the use of LNPs for repeated mRNA delivery as required for reprogramming. For this experiment, a transfection protocol was adapted from a commercial iPS reprogramming kit (Stemgent). Further modifications by Warren et al.[188] to perform reprogramming in xeno-free conditions, and without feeder-cells, were also incorporated. BJ cells were transfected by adding LNPs to the culture after each daily media change for two weeks (details in Methods section). Cells were seeded in 6-well plates at low-density, 50,000 cells per well, and were passaged on day 6 at ∼80% confluence. Over the first four days, the dosage was increasingly ramped up from 25%, 50%, 75%, to 100% of the final RNA dose (400 ng/mL, 2 mL), so as not to overdose the low cell concentration[188]. Cells were analyzed on day 2, 5, 8, 11, and 14 by measuring LNP uptake (dye) and eGFP with flow cytometry (Figure 4.14), and mRNA abundance with microfluidic single-cell RT-dPCR (Figure 4.15). Trypan blue staining showed all culture conditions supported over 95% viable cells. Although we previously showed incomplete penetrance of eGFP in BJ cells after 24 hours of transfection, this experiment demonstrated that nearly complete penetrance was possible after longer time with repeated doses. Figure 4.14 shows ∼98% of cells positive for LNP dye by day 2, and over 99% from day 5 to 14. The fraction of cells reporting eGFP increased from 82.5% of cells on day 2, to ∼98% by day 5. The fraction of eGFP-positive BJ cells was maintained above 95% from day 5 to day 14. Single-cell RT-dPCR measurements in Figure 4.15 show mean abundance of delivered eGFP mRNA to be 196 copies (s.d. 212) on day 2, rising to upwards of thousands of copies per cell for days 5 through 11 (day 11 mean 1,002 copies, s.d. 803). Day 14 shows reduced mRNA levels compared to previous measurements, perhaps due to increased cell numbers. This result demonstrated the performance of these LNPs in

a long-term, high-dose, transfection protocol.

Interestingly, substitution of our normal BJ medium (EMEM, 10% FBS) for medium designed for mRNA reprogramming (Pluriton, Stemgent) resulted in dramatically less transfection and translation. This reprogramming condition is xeno-free, absent of any serum additions, and replaces the feeder-cells normally used in Stemgents protocol with matrigel to provide a substrate and extracellular matrix. Both media conditions were supplemented with 1 µg/mL apoE to facilitate uptake, although the FBS also contains lipoproteins. The reprogramming culture conditions resulted in ∼87% of cells containing DiI on day 2, increasing to ∼99% for day 5 through 14. Despite a high-percentage of cells reporting positive particle uptake, only ∼20% of cells were eGFP-positive (with day 11 being an outlier at 43%). In stark contrast to the hundreds or even thousands of mRNA found by day 5 in the normal culture, cells in the reprogramming conditions continued to have only tens to low hundreds of mRNA present throughout the experiment. Notably, the growth rate of cells in the reprogramming condition matched normal culture conditions (with and without transfection) for the first 7 days (Figure 4.17), but showed dramatically reduced proliferation after cell passage (while viability remained over 95%). It is possible the difference in plating or growth after cell passage may be ameliorated by the addition of ROCK inhibitor (e.g. Y27632, Stemgent), but it is interesting to note that cells in EMEM/FBS conditions did not require this. The difference in transfection and translation efficiencies between these two conditions underscores the need to characterize (and optimize) LNP performance in application-specific conditions. Further experiments are needed to determine whether the differences are due to the media, lack of serum, or the matrigel.

4.5 Discussion

The study of gene expression requires the ability to both *measure* gene expression, and *perturb* the system. LNPs, particularly the recently developed particles used in this study, represent an effective means for manipulating gene expression through the delivery of RNA to the cytoplasm. Combining this ability to perturb gene expression with precise transcript measurements by high-throughput single-cell digital PCR provides an opportunity to study gene expression at the single cell level. To apply this technology properly, LNP transfection behaviour must first be characterized in order

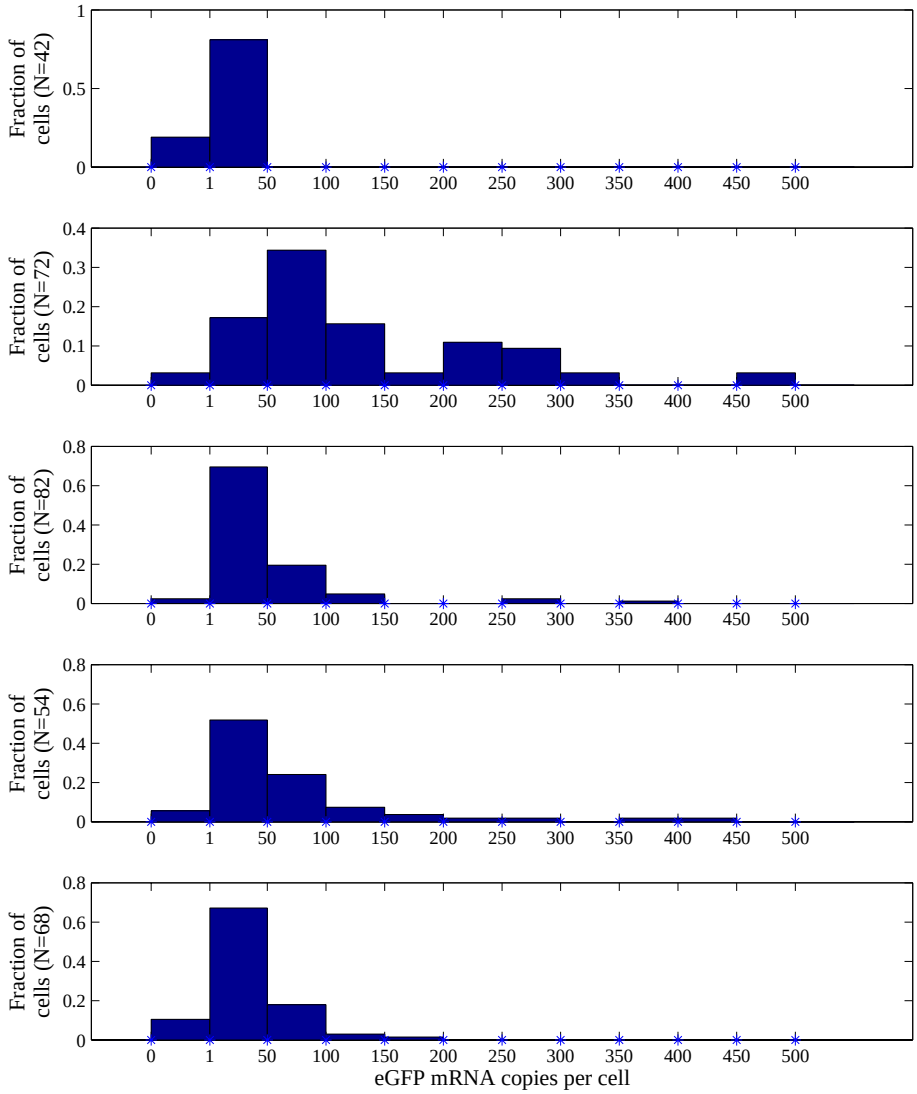

Figure 4.16: Distribution of delivered mRNA in cells under mock reprogramming conditions. Histograms display results from single-cell digital PCR measurement of eGFP transcripts from cells undergoing daily transfections in Pluriton medium with a substrate coated with matrigel (no serum). The time-course is represented from top-to-bottom: day 2, day 5, day 8, day 11, day 14, and corresponds to measurements on cells from the 'Pluriton' series in Figure 4.14.

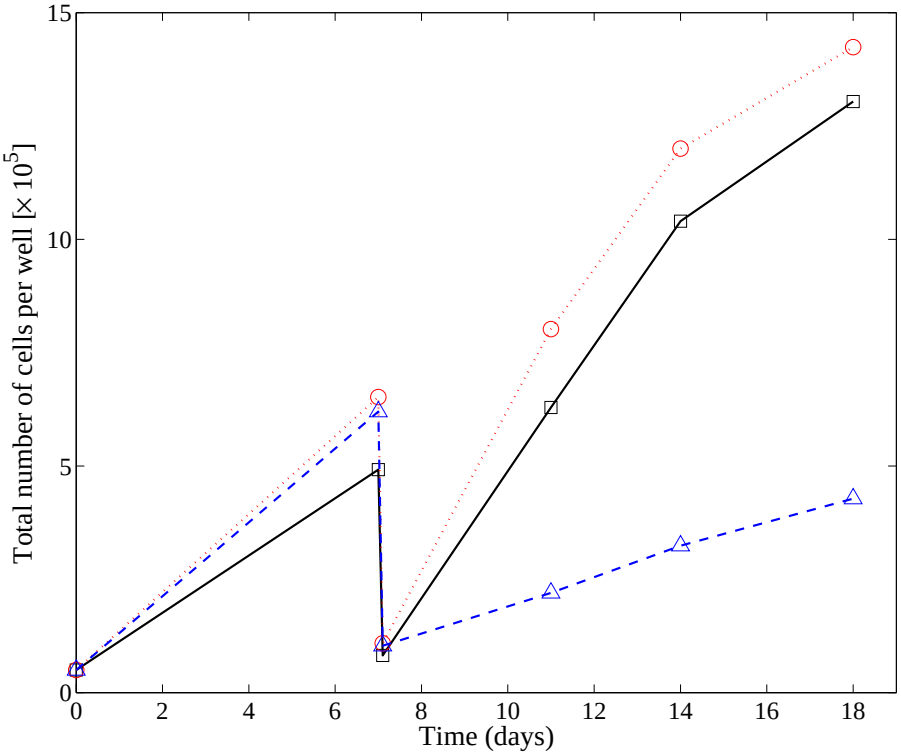

Figure 4.17: Comparison of BJ cell numbers in different media conditions undergoing daily transfections. Cells were passaged by splitting 1/6, on day 7. Red circles represent cells undergoing daily transfections in EMEM with 10% FBS; Blue triangles represent cells undergoing daily transfections in Pluriton with matrigel; Black squares represent untreated cells in EMEM with 10% FBS.

to provide an informed basis for protocol development and optimization. In this study we have begun the important work of characterizing the use of LNP RNA delivery to manipulate gene expression. Through the use of single-cell analysis techniques such as microfluidic digital PCR and flow cytometry, we investigated the kinetics, precision, variability and single cell distribution of LNP transfection performance.

Our results indicate that transfection begins rapidly after addition of LNPs to culture media, with uptake efficiency greatly enhanced in the presence of ApoE. The high transfection efficiency seen through DiI measurements and siRNA knockdown effects show that 1.0 µg/mL ApoE supplement is sufficient to boost LNP uptake, resulting in a 4X increase in our serum-free hESC conditions. Further optimization may be possible by increasing ApoE concentrations, as seen in neuronal cultures[190]. ApoE facilitation is convenient as ApoE is endogenously synthesized by astrocytes in the brain or neuronal *in vitro* cutlure conditions, and lipoproteins are also highly abundant in common culture conditions with medium containing fetal bovine serum. Furthermore, the results presented in this study show that siRNA-LNPs efficiently knockdown expression of targeted genes, and mRNA-LNPs effectively give rise to functional proteins, at dosage levels that do not lead to any observed toxicity.

One of the questions motivating single cell analysis of RNA delivery was when bulk PCR shows partial knockdown, say 50%, does that reflect all cells with partial knockdown, or some of the cells with 100% knockdown and some with 0%? The siRNA knockdown experiments presented here showed a shifting distribution of target mRNA with increasing siRNA dose, rather than an all-or-nothing change of expression. This study demonstrated the potency of siRNA-LNPs, showing that a dose of 1.0 µg/mL siRNA was sufficient to reduce GAPDH mRNA levels by ∼10-fold, eliminating over one thousand transcripts per cell when measured 24 hours after administration. Complete elimination of such an actively expressed gene is challenging as newly transcribed mRNA is inaccessible in the nucleus, and RT-PCR may detect RNA fragments that no longer give rise to functional protein.

Single-cell analysis is particularly well suited to elucidating the relationship of co-occurrences that would otherwise be masked in the averaging of bulk analysis. In this study we use flow cytometry to measure the relationship between LNP uptake (by DiI) and eGFP protein abundance. We compare this to single-cell digital PCR measurements of the delivered RNA, using cells from the same sample. This transcript information revealed that different cell types (K562 compared to BJ) with

similar amounts of mRNA, gave rise to different amounts of translated protein. This underscores the fact that although LNPs effectively deliver mRNA to cells, physiological differences in translation activity between different cell types can still result in different protein levels.

LNPs are an attractive transfection technology for using RNA to reprogram cells into induced pluripotent stem cells. As opposed to conventional techniques which rely on viruses and genomic inserts, RNA reprogramming is non-integrative and 'footprint free', requiring no clean-up phase compared to DNA vectors or RNA viruses. Furthermore, RNA delivery allows for direct control of the timing and abundance of gene expression. Here we show that LNPs provide efficient delivery to a variety of cell types, and that LNPs potentially offer a convenient, self-contained approach to reprogramming somatic cells to pluripotency. Previous studies have delivered mRNA encoding for the Yamanaka factors (Oct3/4, Sox2, Klf4, c-Myc) and shown conversion efficiencies of 1-4%[188]. Single-cell digital RT-PCR measurements of delivered RNA can provide insight into this low efficiency by revealing the abundance and stochiometry of the different mRNAs at different points during transfection for reprogramming. Our results showing repeated delivery of mRNA to sustain eGFP in over 95% of cells for 2 weeks with no apparent toxicity open many possibilites for maintaining high levels of ectopic proteins in cells, with scientific and therapeutic applications.

4.6 Conclusion

Here we have shown the utility of single-cell analysis in characterizing the performance of LNP RNA delivery in a variety of *in vitro* conditions. LNP uptake was facilitated by the presence of ApoE, and transfection was particularly efficient in situations where culture medium contains lipoprotein-rich serum. LNPs demonstrated potent siRNA knockdown of a highly expressed gene, and mediated functional protein expression by mRNA delivery. We have shown the efficacy of these particles in the context of adherent and suspension cell cultures, and under different transfection protocols. Single-cell digital PCR measurement of RNA abundance complements microscopy and flow cytometry techniques, and provides insight into the RNA levels required to see functional effects. Importantly, measuring the variability in the number of transcripts delivered to each cell elucidates the heterogeneity and extent to which one can control transfection. By examining the cell-to-cell variability, kinetics, and

efficiency of using this lipid nanoparticle technology for nucleic acid delivery, we provide an informed basis for optimizing the *in vitro* manipulation of gene expression in cells. This single-cell approach may be extended to wide variety of delivery systems, contributing to the development of research tools and therapeutic strategies.

Chapter 5

Conclusion

In this thesis I set out to address the need for techniques enabling high-throughput single-cell gene expression analysis. Through developing scalable microfluidic technology integrating components to perform cell isolation, lysis, reverse-transcription, and final measurement by real-time or digital PCR, this research has contributed to the tools available for precisely measuring transcripts in single cells. The utility of this technology is demonstrated in measuring the cell-to-cell variability of a variety of transcripts, and miRNAs, in tissues ranging from cell lines to stem cells and primary breast cancer samples. Additionally, this measurement tool is used to assess another tool - a transfection reagent - in order to help understand and improve its use and development.

5.1 Contribution to Knowledge

This research has made an impact in three main areas: engineering technology, technology transfer, and biological findings.

Although microfluidic technology is a relatively young field, a long-sought goal in microfluidics research has been the development of integrated technology for scalable analysis of transcription in single cells. This project achieved this goal through development of the first integrated system for cell isolation and RNA analysis in a scalable fashion. The core functionality established here provides the foundation from which a variety of on-chip single-cell analyses can be developed. In particular, this stands to impact the burgeoning field of single-cell DNA and RNA sequencing. Through combining scalable cell processing with high-density digital PCR, this project further advanced the state-of-the-art in terms of combined throughput and precision for single-cell transcript analysis. It was also interesting to see that this device was well suited to characterizing the performance of other technologies, informing the development and use of lipid nanoparticles for RNA delivery.

In addition to dissemination of this research through publications and conference

presentations, aspects of the technology presented in this thesis will be commercialized to facilitate its widespread adoption in research (and potentially clinical) settings. The microfluidic systems for single-cell trapping followed by RT-qPCR or dPCR are the subject of a patent filing (PCT/CA2011/000612) which has been licensed to Fluidigm Corporation. Fluidigm has since released a commercial product related to this technology for single-cell trapping, lysis, reverse-transcription, and recovery for downstream analysis. This product represents the first major commercial foray into integrated microfluidic single-cell devices, and has enabled single-cell studies for users without microfluidic experience.

Finally, although this project is focused on technology development, significant biological insights have been made through single-cell transcription measurements. At the time of their publication, the measurements reported in this thesis were some of the first large number (hundreds) of single-cell transcript measurements explicitly reported in copy number (as opposed to relative vales such as ΔCt). In addition to observing how tightly regulated certain miRNAs are, or revealing a bi-stable switch-like behaviour in the co-regulation of a miRNA and its target mRNA during differentiation, we precisely quantify and characterize the variability that exists even in 'housekeeping' genes (i.e. GAPDH). These measurements of GAPDH provide an excellent point of comparison for other quantification technologies (e.g. sequencing). The demonstration of single-cell measurement of SNVs in a primary breast cancer sample serves as an example of the sort of assay that may reveal important heterogeneity within clinical cell populations (e.g. the distribution and co-occurrence of mutations). The quantification of the oncogenic fusion transcript BCR-ABL demonstrates the potential utility of using digital PCR in the monitoring of minimum residual disease. Finally, the evaluation of mRNA and siRNA delivery efficacy may lead to new reagents or methods for research, potentially contributing to improved therapeutic strategies.

5.2 Future Recommendations

5.2.1 Extending Microfluidic Single-Cell Analysis

As stated before, the core functionality established here provides the foundation from which a variety of on-chip single-cell and molecular biology protocols can be devel-

oped.

Colleagues in Dr. Carl Hansen's lab are currently pursuing such applications as DNA and RNA sequencing from libraries prepared on integrated single-cell microfluidic devices. Fluidic architecture for recovery of single-cell reaction products is readily incorporable, and represents the logical extension of our microfluidic systems to enable further down-stream analysis. Such functionality has been demonstrated in the C1 device from Fluidigm, which is increasingly being used for single-cell analysis by DNA and RNA sequencing, as well as epigenetic analysis. In the context of this thesis, single-cell whole-transcriptome analysis would be useful to look at global expression changes (e.g. off-target effects) in consequence to siRNA treatment. Performing whole genome amplification or whole transcriptome amplification in limiting dilution 'digital' arrays has also been shown to reduce bias and contributions from contaminating nucleic acids[192].

Although the microfluidic devices presented in this thesis (and the C1) make strides in addressing the bottle-neck between cell isolation and nucleic acid processing, issues with cell isolation remain one of the greatest limitations with this technology. More routine still are studies coupling FACS with RT-qPCR arrays (e.g. Fluidigm Biomark). The challenge in microfluidic isolation of single-cells with physical cell traps is that many cell-types of interest do not readily form single-cell suspensions. This can result in clumping and clogging. Primary cells, thawed samples, or tissues requiring aggressive dissociation protocols, often suffer from viability and clumping issues. Damaged cell membranes may lead to RNA contents leaking and altering detectable abundance. Treating cell suspensions with DNase (to digest DNA clumping), or suspending them in different solutions (e.g in presence of EDTA, or Ficoll) may ameliorate clumping of cells. Physical cell traps may be tailored to capture cells of different size ranges, if a universal cell trap is difficult to engineer. A possible approach could be to encapsulate single cells in uniform-sized droplets or gels before isolating with uniform traps. Upstream manipulation of cells could also include nucleus or cytoplasm isolation (or fixing cells). Ultimately, for many tissues, researchers and clinicians would like to able to perform single-cell analysis while preserving spatial information and molecular imaging or techniques such as laser-capture microdisection[193] or Tomo-Seq[194] remain advantageous over our microfluidic approach to single-cell isolation[195]. Having a linear array of cell traps also increases the risk of a cell clog as the number of traps is scaled from tens to hundreds and po-

tentially thousands, suggesting the need for improved cell bypass lanes or a parallel loading strategy.

The device designs presented for single cell RT-qPCR or digital PCR are limited in the number of different transcripts that can be simultaneously measured to the number of fluorescent probes that can be spectrally distinguished. This optical multiplexing is generally limited to 3 or 4 colours (and a passive reference dye) when using commercially available hydrolysis probes (e.g. TaqMan) and common filters. This limitation can be overcome by splitting the template reaction into separated assay chambers (that can be of the same probe colour), thereby spatially multiplexing the reaction. Pre-amplification of the pooled cDNA may be required to preserve representation when partitioning into multiple assay chambers.

There are a number of further types of analyses the microfluidic single-cell digital PCR device could be adapted to accomodate. Future work could look at the ability to measure genomic copy number alterations, potentially with a pre-amplification step. In the course of this work I explored the potential use of microfluidic digital PCR for protein counting, by using a proximity ligation assay[196]. In the proximity ligation assay, two different antibodies bind to a target protein of interest. Each antibody is attached to a short DNA strand, and when the two antibodies are in close proximity (as in when bound to the same protein) the DNA strands can be ligated together. This newly combined DNA strand then forms the starting template for PCR amplification, and could be quantified with digital PCR. Performing the proximity ligation assay in a microfluidic single-cell digital PCR device may be a direct way to combine and correlate mRNA measurements with protein abundance[152]. The current microfluidic device for single-cell digital PCR could be easily modified with additional chambers to perform antibody binding and ligation prior to dPCR. One of the limitations of the proximity ligation assay is the likelyhood of false-positive PCR reactions due to ligation of DNA from antibodies in close proximity but not bound to the same protein. This probability is reduced by diluting the bound antibodies prior to ligation, but false-positives remain. Although single-cell digital PCR does not eliminate this issue, it does offer a chance to quantify the base level false-positives, which can then be subtracted from single cell measurements. Ultimately, this microfluidic approach to single-cell protein quantification lacks the throughput and multiplexing capabilities of recently developed single-cell mass cytometry techniques[197].

Beyond genetic and transcript measurements, enzymatic assays (e.g. measuring

telomerase activity) could be incorporated into a similar microfluidic architecture. Cell trapping upstream of analysis could be further utilized to briefly expose the cells to stimuli, before measuring responses in the transcriptome. A more thorough image analysis of isolated cells prior to lysis could also be used to compare morphologies with intracellular contents. The trap and assay architecture of the devices could be used to expose cells to chemical stimuli (e.g. drugs, siRNA, antibodies) prior to rapidly lysing and measuring gene expression (or other molecules of interest). The microfluidic architecture for single-cell molecular biology protocols could also be integrated downstream of cell culture arrays, enabling automated genomic or transcript analysis after testing different culture conditions and treatments.

5.2.2 Further Experiments and Applications for Lipid Nanoparticle Delivery

The use of LNPs to mediate gene expression should be studied further. The ApoE facilitation of LNP transfection warrants further investigation into the mechanism of receptor mediated transport. What is the receptor density of different cells? Can cells be cholesterol starved to stimulate production of more LDL receptors, and does this increase LNP uptake? Future experiments could investigate the effect of incubating the LNPs with ApoE prior to transfection. One potential concern is the addition of ApoE may cause unwanted environmental stimuli in cases where cells are delicately sensitive to culture conditions (e.g. ESC, iPS conversion). In such situations it may be worth exploring alternative protocols such as transfection during cell passaging (adherent cells could be temporarily incubated in suspension with a shake-flask), or pre-mixing LNPs with the plate coating substrate (e.g. Matrigel). The microfluidic single-cell digital PCR device is well suited to investigate the time-scales involved in lipid nanoparticle uptake. For example, single-cells may be isolated in cell traps within the microfluidic device prior to briefly washing them with a solution of mRNA-containing lipid nanoparticles. Cells can then be processed within minutes (or hours) to examine the kinetics of transfection. Using fluorescence microscopy, future experiments could also measure DiI and eGFP in cells trapped in the microfluidic device and directly correlate dye and protein abundance with measured transcript abundance within each cell. Protein abundance could be further quantified with single-cell proximity ligation assay[152].

It would be useful to measure both the delivered siRNA as well as the targeted mRNA in each cell to properly assess the dose-response relationship. This can be measured in the microfluidic single-cell digital PCR device by designing a stem-loop RT primer and TaqMan qPCR assay[59] allowing optical multiplexing[129, 191]. Further experiments testing increased doses and/or transfection times should investigate the feasibility of completely suppressing a highly expressed gene such as GAPDH by siRNA, as RNAi machinery may not be able to keep up with constitutively active transcription. This also raises the question of at what point does siRNA potency become RISC abundance-limited. siRNA is already known to cause off-target down-regulation, and by overwhelming the RNAi machinery exogenous siRNA may further disrupt gene expression regulation by out-competing natural microRNAs for incorporation in RISC[198]. Single-cell RNA sequencing would be useful to asses the genome-wide effect of siRNA transfection. RISC-incorporated RNA could be assessed following antibody pull-down of RISC, and compared with free miRNAs and siRNAs.

In characterizing the performance of LNPs, we sought to understand how well we could control transfection efficiency and how precisely we could control the abundance of delivered RNA to each cell. We have started to explore this with different doses of RNA, and different transfection protocols. However future pulse-chase type experiments are needed to explore the effect of different dosing regimes, for example, the affect of short vs. long transfection times (pulse-width), and high- compared to low-dose (pulse amplitude) on the precision of delivered RNA. Pulse-chase experiments will also be useful in measuring the time between transfection and translation (e.g. eGFP), and the duration of sustained effect. For example, is it possible to sustain low levels of transcripts delivered to the entire cell population?

In investigating how well delivered RNA abundance can be controlled, it would be useful to test delivery of two different mRNAs at different ratios of abundance, and see if this ratio is preserved in delivery. While different RNAs could be combined and encapsulated at different relative abundance during LNP formulation, keeping them individually packaged allows for more control in how they are combined and used. By transfecting with equal amounts of mRNA encoding for two different colours, but with a similar length and sequence (e.g. eGFP and YFP), one could look at the variation in delivery compared to variation in functionality (i.e. translation to protein). It may also be possible to attenuate the noise, or long tails of low-abundance (or high-abundance) proteins by co-delivering microRNA or siRNA targeting the delivered

mRNA.

Chapter 4 focused on the PCR measurement of RNA however a similar analysis could be extended to characterize the delivery or affect of other cargo, such as DNA, proteins, or small molecules. In particular, LNPs could be harnessed to deliver guide DNA strands for CRISPR gene editing. This can be used for applications ranging from editing mutations in genes related to cancer, to antiviral treatments. For example, the CRISPR/Cas9 system can be adapted for antiviral treatment in human cells by specifically targeting the genomes of viral infections[199, 200]. Measurement of delivered DNA is not subject to reverse transcription efficiencies, and could provide a useful surrogate measurement of RNA (or other species) delivery as it could be continually used without re-designing new primers each time the LNP cargo is changed. This study focused on characterizing the performance of a particular LNP reagent, however the single-cell analysis methodologies employed here, namely flow cytometry and single-cell digital PCR, could be used to asses the performance of other transfection methods. Ultimately, the LNP system used in this study should be compared to alternative transfection reagents such as the commonly used Lipofectamine (Life Technologies).

5.3 Final Remarks

Recent years have seen rapid development of single-cell and fluidic technologies, and the work in this thesis may ultimately be integrated into larger work-flows and devices. In particular, micro-wells, integrated electronic components and sensors in microfluidic devices, droplet dispensers for printing arrays of reagents and cells are all exciting technologies pushing the capabilities for single-cell analysis. Advances in 3D printing may be used to construct microfluidic devices (either directly, or as moulds), potentially democratizing microfluidic prototyping.

The development and demonstration of microfluidic single-cell analysis reported here, and in other applications ranging from human haplotyping and drug discovery, to stem cell development and cancer progression, should lead to widespread adoption of this technology.

Bibliography

[1] Y. Sasai and E. M. De Robertis. Ectodermal patterning in vertebrate embryos. *Dev Biol*, 182(1):5–20, 1997.

[2] M. B. Elowitz, A. J. Levine, E. D. Siggia, and P. S. Swain. Stochastic gene expression in a single cell. *Science*, 297(5584):1183–6, 2002.

[3] A. Raj, C. S. Peskin, D. Tranchina, D. Y. Vargas, and S. Tyagi. Stochastic mrna synthesis in mammalian cells. *PLoS Biol*, 4(10):e309, 2006.

[4] M. J. Ravitz and C. E. Wenner. Cyclin-dependent kinase regulation during g1 phase and cell cycle regulation by tgf-beta. *Adv Cancer Res*, 71:165–207, 1997.

[5] M. Anger, W. A. Kues, J. Klima, M. Mielenz, M. Kubelka, J. Motlik, M. Esner, P. Dvorak, J. W. Carnwath, and H. Niemann. Cell cycle dependent expression of plk1 in synchronized porcine fetal fibroblasts. *Mol Reprod Dev*, 65(3):245–53, 2003.

[6] J. Lukas, C. Lukas, and J. Bartek. Mammalian cell cycle checkpoints: signalling pathways and their organization in space and time. *DNA Repair (Amst)*, 3(8-9):997–1007, 2004.

[7] J. A. Smith and L. Martin. Do cells cycle? *Proc Natl Acad Sci U S A*, 70(4):1263–7, 1973.

[8] W. A. Kues, M. Anger, J. W. Carnwath, D. Paul, J. Motlik, and H. Niemann. Cell cycle synchronization of porcine fetal fibroblasts: effects of serum deprivation and reversible cell cycle inhibitors. *Biol Reprod*, 62(2):412–9, 2000.

[9] M. S. Rhyu, L. Y. Jan, and Y. N. Jan. Asymmetric distribution of numb protein during division of the sensory organ precursor cell confers distinct fates to daughter cells. *Cell*, 76(3):477–91, 1994.

[10] O. H. Yilmaz, M. J. Kiel, and S. J. Morrison. Slam family markers are conserved among hematopoietic stem cells from old and reconstituted mice and markedly increase their purity. *Blood*, 107(3):924–30, 2006.

[11] D. Douer, A. M. Levin, R. S. Sparkes, I. Fabian, M. Sparkes, M. J. Cline, and H. P. Koeffler. Chronic myelocytic leukaemia: a pluripotent haemopoietic cell is involved in the malignant clone. *Br J Haematol*, 49(4):615–9, 1981.

[12] M. R. Stratton, P. J. Campbell, and P. A. Futreal. The cancer genome. *Nature*, 458(7239):719–24, 2009.

[13] L. Fink, G. Kwapiszewska, J. Wilhelm, and R. M. Bohle. Laser-microdissection for cell type- and compartment-specific analyses on genomic and proteomic level. *Exp Toxicol Pathol*, 57 Suppl 2:25–9, 2006.

[14] L. Zhang, W. Zhou, V. E. Velculescu, S. E. Kern, R. H. Hruban, S. R. Hamilton, B. Vogelstein, and K. W. Kinzler. Gene expression profiles in normal and cancer cells. *Science*, 276(5316):1268–72, 1997.

[15] K. Ruan, X. Fang, and G. Ouyang. Microrna: novel regulators in the hallmarks of human cancer. *Cancer Lett*, 285(2):116–26, 2009.

[16] D. P. Bartel. Micrornas: genomics, biogenesis, mechanism, and function. *Cell*, 116(2):281–97, 2004.

[17] B. Zhang, X. Pan, G. P. Cobb, and T. A. Anderson. microrna as oncogenes and tumor suppressors. *Dev Biol*, 302(1):1–12, 2007.

[18] C. Z. Chen, L. Li, H. F. Lodish, and D. P. Bartel. Micrornas modulate hematopoietic lineage differentiation. *Science*, 303(5654):83–6, 2004.

[19] G. A. Calin, C. G. Liu, C. Sevignani, M. Ferracin, N. Felli, C. D. Dumitru, M. Shimizu, A. Cimmino, S. Zupo, M. Dono, M. L. Dell'Aquila, H. Alder, L. Rassenti, T. J. Kipps, F. Bullrich, M. Negrini, and C. M. Croce. Microrna profiling reveals distinct signatures in b cell chronic lymphocytic leukemias. *Proc Natl Acad Sci U S A*, 101(32):11755–60, 2004.

[20] O. I. Petriv, F. Kuchenbauer, A. D. Delaney, V. Lecault, A. White, D. Kent, L. Marmolejo, M. Heuser, T. Berg, M. Copley, J. Ruschmann, S. Sekulovic,

C. Benz, E. Kuroda, V. Ho, F. Antignano, T. Halim, V. Giambra, G. Krystal, C. J. Takei, A. P. Weng, J. Piret, C. Eaves, M. A. Marra, R. K. Humphries, and C. L. Hansen. Comprehensive microrna expression profiling of the hematopoietic hierarchy. *Proc Natl Acad Sci U S A*, 107(35):15443–8, 2010.

[21] A. M. Femino, F. S. Fay, K. Fogarty, and R. H. Singer. Visualization of single rna transcripts in situ. *Science*, 280(5363):585–90, 1998.

[22] J. M. Levsky, S. M. Shenoy, R. C. Pezo, and R. H. Singer. Single-cell gene expression profiling. *Science*, 297(5582):836–40, 2002.

[23] A. Raj, P. van den Bogaard, S. A. Rifkin, A. van Oudenaarden, and S. Tyagi. Imaging individual mrna molecules using multiple singly labeled probes. *Nat Methods*, 5(10):877–9, 2008.

[24] H. Maamar, A. Raj, and D. Dubnau. Noise in gene expression determines cell fate in bacillus subtilis. *Science*, 317(5837):526–9, 2007.

[25] A. Raj, S. A. Rifkin, E. Andersen, and A. van Oudenaarden. Variability in gene expression underlies incomplete penetrance. *Nature*, 463(7283):913–8, 2010.

[26] C. Larsson, I. Grundberg, O. Soderberg, and M. Nilsson. In situ detection and genotyping of individual mrna molecules. *Nat Methods*, 7(5):395–7, 2010.

[27] C. Larsson, J. Koch, A. Nygren, G. Janssen, A. K. Raap, U. Landegren, and M. Nilsson. In situ genotyping individual dna molecules by target-primed rolling-circle amplification of padlock probes. *Nat Methods*, 1(3):227–32, 2004.

[28] A. Lagunavicius, E. Merkiene, Z. Kiveryte, A. Savaneviciute, V. Zimbaite-Ruskuliene, T. Radzvilavicius, and A. Janulaitis. Novel application of phi29 dna polymerase: Rna detection and analysis in vitro and in situ by target rna-primed rca. *RNA*, 15(5):765–71, 2009.

[29] Brian Munsky, Gregor Neuert, and Alexander van Oudenaarden. Using gene expression noise to understand gene regulation. *Science*, 336:183–7, 2012.

[30] F. Tang, C. Barbacioru, Y. Wang, E. Nordman, C. Lee, N. Xu, X. Wang, J. Bodeau, B. B. Tuch, A. Siddiqui, K. Lao, and M. A. Surani. mrna-seq whole-transcriptome analysis of a single cell. *Nat Methods*, 6(5):377–82, 2009.

[31] R. Morin, M. Bainbridge, A. Fejes, M. Hirst, M. Krzywinski, T. Pugh, H. McDonald, R. Varhol, S. Jones, and M. Marra. Profiling the hela s3 transcriptome using randomly primed cdna and massively parallel short-read sequencing. *Biotechniques*, 45(1):81–94, 2008.

[32] S. P. Shah, R. D. Morin, J. Khattra, L. Prentice, T. Pugh, A. Burleigh, A. Delaney, K. Gelmon, R. Guliany, J. Senz, C. Steidl, R. A. Holt, S. Jones, M. Sun, G. Leung, R. Moore, T. Severson, G. A. Taylor, A. E. Teschendorff, K. Tse, G. Turashvili, R. Varhol, R. L. Warren, P. Watson, Y. Zhao, C. Caldas, D. Huntsman, M. Hirst, M. A. Marra, and S. Aparicio. Mutational evolution in a lobular breast tumour profiled at single nucleotide resolution. *Nature*, 461(7265):809–13, 2009.

[33] F. Tang, C. Barbacioru, S. Bao, C. Lee, E. Nordman, X. Wang, K. Lao, and M. A. Surani. Tracing the derivation of embryonic stem cells from the inner cell mass by single-cell rna-seq analysis. *Cell Stem Cell*, 6(5):468–78, 2010.

[34] D. Ramskold, S. Luo, Y. C. Wang, R. Li, Q. Deng, O. R. Faridani, G. A. Daniels, I. Khrebtukova, J. F. Loring, L. C. Laurent, G. P. Schroth, and R. Sandberg. Full-length mrna-seq from single-cell levels of rna and individual circulating tumor cells. *Nat Biotechnol*, 30(8):777–82, 2012.

[35] S. Islam, U. Kjallquist, A. Moliner, P. Zajac, J. B. Fan, P. Lonnerberg, and S. Linnarsson. Highly multiplexed and strand-specific single-cell rna 5' end sequencing. *Nat Protoc*, 7(5):813–28, 2012.

[36] S. Islam, U. Kjallquist, A. Moliner, P. Zajac, J. B. Fan, P. Lonnerberg, and S. Linnarsson. Characterization of the single-cell transcriptional landscape by highly multiplex rna-seq. *Genome Res*, 21(7):1160–7, 2011.

[37] X. Adiconis, D. Borges-Rivera, R. Satija, D. S. DeLuca, M. A. Busby, A. M. Berlin, A. Sivachenko, D. A. Thompson, A. Wysoker, T. Fennell, A. Gnirke, N. Pochet, A. Regev, and J. Z. Levin. Comparative analysis of rna sequencing methods for degraded or low-input samples. *Nat Methods*, 10(7):623–9, 2013.

[38] A. R. Wu, N. F. Neff, T. Kalisky, P. Dalerba, B. Treutlein, M. E. Rothenberg, F. M. Mburu, G. L. Mantalas, S. Sim, M. F. Clarke, and S. R. Quake.

Quantitative assessment of single-cell rna-sequencing methods. *Nat Methods*, 11(1):41–6, 2014.

[39] D. Hebenstreit. Methods, challenges and potentials of single cell rna-seq. *Biology (Basel)*, 1(3):658–67, 2012.

[40] M. Bengtsson, A. Stahlberg, P. Rorsman, and M. Kubista. Gene expression profiling in single cells from the pancreatic islets of langerhans reveals lognormal distribution of mrna levels. *Genome Res*, 15(10):1388–92, 2005.

[41] M. K. Chiang and D. A. Melton. Single-cell transcript analysis of pancreas development. *Dev Cell*, 4(3):383–93, 2003.

[42] N. Faumont, T. Al Saati, P. Brousset, C. Offer, G. Delsol, and F. Meggetto. Demonstration by single-cell pcr that reed–sternberg cells and bystander b lymphocytes are infected by different epstein–barr virus strains in hodgkin's disease. *J Gen Virol*, 82(Pt 5):1169–74, 2001.

[43] S. Hahn, X. Y. Zhong, C. Troeger, R. Burgemeister, K. Gloning, and W. Holzgreve. Current applications of single-cell pcr. *Cell Mol Life Sci*, 57(1):96–105, 2000.

[44] K. M. Keays, G. P. Owens, A. M. Ritchie, D. H. Gilden, and M. P. Burgoon. Laser capture microdissection and single-cell rt-pcr without rna purification. *J Immunol Methods*, 302(1-2):90–8, 2005.

[45] A. Stahlberg and M. Bengtsson. Single-cell gene expression profiling using reverse transcription quantitative real-time pcr. *Methods*, 2010.

[46] K. Taniguchi, T. Kajiyama, and H. Kambara. Quantitative analysis of gene expression in a single cell by qpcr. *Nat Methods*, 6(7):503–6, 2009.

[47] I. Tietjen, J. M. Rihel, Y. Cao, G. Koentges, L. Zakhary, and C. Dulac. Single-cell transcriptional analysis of neuronal progenitors. *Neuron*, 38(2):161–75, 2003.

[48] R. K. Saiki, D. H. Gelfand, S. Stoffel, S. J. Scharf, R. Higuchi, G. T. Horn, K. B. Mullis, and H. A. Erlich. Primer-directed enzymatic amplification of dna with a thermostable dna polymerase. *Science*, 239(4839):487–91, 1988.

[49] T. B. Morrison, J. J. Weis, and C. T. Wittwer. Quantification of low-copy transcripts by continuous sybr green i monitoring during amplification. *Biotechniques*, 24(6):954–8, 960, 962, 1998.

[50] S. Tyagi and F. R. Kramer. Molecular beacons: probes that fluoresce upon hybridization. *Nat Biotechnol*, 14(3):303–8, 1996.

[51] D. Whitcombe, J. Theaker, S. P. Guy, T. Brown, and S. Little. Detection of pcr products using self-probing amplicons and fluorescence. *Nat Biotechnol*, 17(8):804–7, 1999.

[52] M. C. Vicens, A. Sen, A. Vanderlaan, T. J. Drake, and W. Tan. Investigation of molecular beacon aptamer-based bioassay for platelet-derived growth factor detection. *Chembiochem*, 6(5):900–7, 2005.

[53] C. A. Heid, J. Stevens, K. J. Livak, and P. M. Williams. Real time quantitative pcr. *Genome Res*, 6(10):986–94, 1996.

[54] K J Livak, S J Flood, J Marmaro, W Giusti, and K Deetz. Oligonucleotides with fluorescent dyes at opposite ends provide a quenched probe system useful for detecting pcr product and nucleic acid hybridization. *PCR Methods Appl*, 4:357–362, 1995.

[55] S. A. Bustin. Quantification of mrna using real-time reverse transcription pcr (rt-pcr): trends and problems. *J Mol Endocrinol*, 29(1):23–39, 2002.

[56] M. W. Pfaffl. A new mathematical model for relative quantification in real-time rt-pcr. *Nucleic Acids Res*, 29(9):e45, 2001.

[57] H. D. VanGuilder, K. E. Vrana, and W. M. Freeman. Twenty-five years of quantitative pcr for gene expression analysis. *Biotechniques*, 44(5):619–26, 2008.

[58] M. Bengtsson, M. Hemberg, P. Rorsman, and A. Stahlberg. Quantification of mrna in single cells and modelling of rt-qpcr induced noise. *BMC Mol Biol*, 9:63, 2008.

[59] C. Chen, D. A. Ridzon, A. J. Broomer, Z. Zhou, D. H. Lee, J. T. Nguyen, M. Barbisin, N. L. Xu, V. R. Mahuvakar, M. R. Andersen, K. Q. Lao, K. J. Livak, and K. J. Guegler. Real-time quantification of microrna by stem-loop rt-pcr. *Nucleic Acids Res*, 33(20):e179, 2005.

[60] F. Tang, P. Hajkova, S. C. Barton, K. Lao, and M. A. Surani. Microrna expression profiling of single whole embryonic stem cells. *Nucleic Acids Res*, 34(2):e9, 2006.

[61] F. Tang, P. Hajkova, S. C. Barton, D. O'Carroll, C. Lee, K. Lao, and M. A. Surani. 220-plex microrna expression profile of a single cell. *Nat Protoc*, 1(3):1154–9, 2006.

[62] L. Warren, D. Bryder, I. L. Weissman, and S. R. Quake. Transcription factor profiling in individual hematopoietic progenitors by digital rt-pcr. *Proc Natl Acad Sci U S A*, 103(47):17807–12, 2006.

[63] B. J. Hindson, K. D. Ness, D. A. Masquelier, P. Belgrader, N. J. Heredia, A. J. Makarewicz, I. J. Bright, M. Y. Lucero, A. L. Hiddessen, T. C. Legler, T. K. Kitano, M. R. Hodel, J. F. Petersen, P. W. Wyatt, E. R. Steenblock, P. H. Shah, L. J. Bousse, C. B. Troup, J. C. Mellen, D. K. Wittmann, N. G. Erndt, T. H. Cauley, R. T. Koehler, A. P. So, S. Dube, K. A. Rose, L. Montesclaros, S. Wang, D. P. Stumbo, S. P. Hodges, S. Romine, F. P. Milanovich, H. E. White, J. F. Regan, G. A. Karlin-Neumann, C. M. Hindson, S. Saxonov, and B. W. Colston. High-throughput droplet digital pcr system for absolute quantitation of dna copy number. *Anal Chem*, 83(22):8604–10, 2011.

[64] L. B. Pinheiro, V. A. Coleman, C. M. Hindson, J. Herrmann, B. J. Hindson, S. Bhat, and K. R. Emslie. Evaluation of a droplet digital polymerase chain reaction format for dna copy number quantification. *Anal Chem*, 84(2):1003–11, 2012.

[65] M. A. Unger, H. P. Chou, T. Thorsen, A. Scherer, and S. R. Quake. Monolithic microfabricated valves and pumps by multilayer soft lithography. *Science*, 288(5463):113–6, 2000.

[66] T. Thorsen, S. J. Maerkl, and S. R. Quake. Microfluidic large-scale integration. *Science*, 298(5593):580–4, 2002.

[67] C. E. Sims and N. L. Allbritton. Analysis of single mammalian cells on-chip. *Lab Chip*, 7(4):423–40, 2007.

[68] V. Lecault, A. K. White, A. Singhal, and C. L. Hansen. Microfluidic single cell analysis: from promise to practice. *Curr Opin Chem Biol*, 16(3-4):381–90, 2012.

[69] J. S. Marcus, W. F. Anderson, and S. R. Quake. Parallel picoliter rt-pcr assays using microfluidics. *Anal Chem*, 78(3):956–8, 2006.

[70] J R Rettig and A Folch. Large-scale single-cell trapping and imaging using microwell arrays. *Anal Chem*, 77:5628–5634, 2005.

[71] D Di Carlo, N Aghdam, and L P Lee. Single-cell enzyme concentrations, kinetics, and inhibition analysis using high-density hydrodynamic cell isolation arrays. *Anal Chem*, 78:4925–4930, 2006.

[72] D. Di Carlo, L. Y. Wu, and L. P. Lee. Dynamic single cell culture array. *Lab Chip*, 6(11):1445–9, 2006.

[73] P. J. Lee, P. J. Hung, V. M. Rao, and L. P. Lee. Nanoliter scale microbioreactor array for quantitative cell biology. *Biotechnol Bioeng*, 94(1):5–14, 2006.

[74] X. Li and P. C. Li. Microfluidic selection and retention of a single cardiac myocyte, on-chip dye loading, cell contraction by chemical stimulation, and quantitative fluorescent analysis of intracellular calcium. *Anal Chem*, 77(14):4315–22, 2005.

[75] A. R. Wheeler, W. R. Throndset, R. J. Whelan, A. M. Leach, R. N. Zare, Y. H. Liao, K. Farrell, I. D. Manger, and A. Daridon. Microfluidic device for single-cell analysis. *Anal Chem*, 75(14):3581–6, 2003.

[76] S. Kobel, A. Valero, J. Latt, P. Renaud, and M. Lutolf. Optimization of microfluidic single cell trapping for long-term on-chip culture. *Lab Chip*, 10(7):857–63, 2010.

[77] P. C. Li, L. de Camprieu, J. Cai, and M. Sangar. Transport, retention and fluorescent measurement of single biological cells studied in microfluidic chips. *Lab Chip*, 4(3):174–80, 2004.

[78] N. Bontoux, L. Dauphinot, T. Vitalis, V. Studer, Y. Chen, J. Rossier, and M. C. Potier. Integrating whole transcriptome assays on a lab-on-a-chip for single cell gene profiling. *Lab Chip*, 8(3):443–50, 2008.

[79] J. S. Marcus, W. F. Anderson, and S. R. Quake. Microfluidic single-cell mrna isolation and analysis. *Anal Chem*, 78(9):3084–9, 2006.

[80] H. Wu, A. Wheeler, and R. N. Zare. Chemical cytometry on a picoliter-scale integrated microfluidic chip. *Proc Natl Acad Sci U S A*, 101(35):12809–13, 2004.

[81] A. M. Skelley, O. Kirak, H. Suh, R. Jaenisch, and J. Voldman. Microfluidic control of cell pairing and fusion. *Nat Methods*, 6(2):147–52, 2009.

[82] S. Koster, F. E. Angile, H. Duan, J. J. Agresti, A. Wintner, C. Schmitz, A. C. Rowat, C. A. Merten, D. Pisignano, A. D. Griffiths, and D. A. Weitz. Drop-based microfluidic devices for encapsulation of single cells. *Lab Chip*, 8(7):1110–5, 2008.

[83] J. F. Edd, D. Di Carlo, K. J. Humphry, S. Koster, D. Irimia, D. A. Weitz, and M. Toner. Controlled encapsulation of single-cells into monodisperse picolitre drops. *Lab Chip*, 8(8):1262–4, 2008.

[84] J. Voldman, M. L. Gray, M. Toner, and M. A. Schmidt. A microfabrication-based dynamic array cytometer. *Anal Chem*, 74(16):3984–90, 2002.

[85] A Ashkin. The study of cells by optical trapping and manipulation of living cells using infrared laser beams. *ASGSB Bull*, 4:133–146, 1991.

[86] A Ashkin, J M Dziedzic, and T Yamane. Optical trapping and manipulation of single cells using infrared laser beams. *Nature*, 330:769–771, 1987.

[87] H. Zhang and K. K. Liu. Optical tweezers for single cells. *J R Soc Interface*, 5(24):671–90, 2008.

[88] Z. C. Landry, S. J. Giovanonni, S. R. Quake, and P. C. Blainey. Optofluidic cell selection from complex microbial communities for single-genome analysis. *Methods Enzymol*, 531:61–90, 2013.

[89] J. F. Zhong, Y. Chen, J. S. Marcus, A. Scherer, S. R. Quake, C. R. Taylor, and L. P. Weiner. A microfluidic processor for gene expression profiling of single human embryonic stem cells. *Lab Chip*, 8(1):68–74, 2008.

[90] G. Guo, M. Huss, G. Q. Tong, C. Wang, L. Li Sun, N. D. Clarke, and P. Robson. Resolution of cell fate decisions revealed by single-cell gene expression analysis from zygote to blastocyst. *Dev Cell*, 18(4):675–85, 2010.

[91] K.H. Kazim H Narsinh, Ning Sun, Veronica Sanchez-Freire, Andrew S A.S. Lee, Patricia Almeida, Shijun Hu, Taha Jan, Kitchener D K.D. Wilson, Denise Leong, Jarrett Rosenberg, others, Mylene Yao, Robert C Robbins, and Joseph C Wu. Single cell transcriptional profiling reveals heterogeneity of human induced pluripotent stem cells. *Gene Expression*, 121:1217, 2011.

[92] L. Flatz, R. Roychoudhuri, M. Honda, A. Filali-Mouhim, J. P. Goulet, N. Kettaf, M. Lin, M. Roederer, E. K. Haddad, R. P. Sekaly, and G. J. Nabel. Single-cell gene-expression profiling reveals qualitatively distinct cd8 t cells elicited by different gene-based vaccines. *Proc Natl Acad Sci U S A*, 108(14):5724–9, 2011.

[93] K. J. Livak, Q. F. Wills, A. J. Tipping, K. Datta, R. Mittal, A. J. Goldson, D. W. Sexton, and C. C. Holmes. Methods for qpcr gene expression profiling applied to 1440 lymphoblastoid single cells. *Methods*, 59(1):71–9, 2013.

[94] P. Dalerba, T. Kalisky, D. Sahoo, P. S. Rajendran, M. E. Rothenberg, A. A. Leyrat, S. Sim, J. Okamoto, D. M. Johnston, D. Qian, M. Zabala, J. Bueno, N. F. Neff, J. Wang, A. A. Shelton, B. Visser, S. Hisamori, Y. Shimono, M. van de Wetering, H. Clevers, M. F. Clarke, and S. R. Quake. Single-cell dissection of transcriptional heterogeneity in human colon tumors. *Nat Biotechnol*, 29(12):1120–7, 2011.

[95] M. Diehn, R. W. Cho, N. A. Lobo, T. Kalisky, M. J. Dorie, A. N. Kulp, D. Qian, J. S. Lam, L. E. Ailles, M. Wong, B. Joshua, M. J. Kaplan, I. Wapnir, F. M. Dirbas, G. Somlo, C. Garberoglio, B. Paz, J. Shen, S. K. Lau, S. R. Quake, J. M. Brown, I. L. Weissman, and M. F. Clarke. Association of reactive oxygen species levels and radioresistance in cancer stem cells. *Nature*, 458(7239):780–3, 2009.

[96] N. M. Toriello, E. S. Douglas, N. Thaitrong, S. C. Hsiao, M. B. Francis, C. R. Bertozzi, and R. A. Mathies. Integrated microfluidic bioprocessor for single-cell gene expression analysis. *Proc Natl Acad Sci U S A*, 105(51):20173–8, 2008.

[97] P. Mary, L. Dauphinot, N. Bois, M. C. Potier, V. Studer, and P. Tabeling. Analysis of gene expression at the single-cell level using microdroplet-based microfluidic technology. *Biomicrofluidics*, 5(2):24109, 2011.

[98] Y. Gong, A. O. Ogunniyi, and J. C. Love. Massively parallel detection of gene expression in single cells using subnanolitre wells. *Lab Chip*, 10(18):2334–7, 2010.

[99] R. Sandberg. Entering the era of single-cell transcriptomics in biology and medicine. *Nat Methods*, 11(1):22–4, 2014.

[100] B. Treutlein, D. G. Brownfield, A. R. Wu, N. F. Neff, G. L. Mantalas, F. H. Espinoza, T. J. Desai, M. A. Krasnow, and S. R. Quake. Reconstructing lineage hierarchies of the distal lung epithelium using single-cell rna-seq. *Nature*, 509(7500):371–5, 2014.

[101] A. Zeisel, A. B. Munoz-Manchado, S. Codeluppi, P. Lonnerberg, G. La Manno, A. Jureus, S. Marques, H. Munguba, L. He, C. Betsholtz, C. Rolny, G. Castelo-Branco, J. Hjerling-Leffler, and S. Linnarsson. Brain structure. cell types in the mouse cortex and hippocampus revealed by single-cell rna-seq. *Science*, 347(6226):1138–42, 2015.

[102] A. M. Streets, X. Zhang, C. Cao, Y. Pang, X. Wu, L. Xiong, L. Yang, Y. Fu, L. Zhao, F. Tang, and Y. Huang. Microfluidic single-cell whole-transcriptome sequencing. *Proc Natl Acad Sci U S A*, 111(19):7048–53, 2014.

[103] 2nd Wadsworth, M. H., T. K. Hughes, and A. K. Shalek. Marrying microfluidics and microwells for parallel, high-throughput single-cell genomics. *Genome Biol*, 16(1):129, 2015.

[104] S. Bose, Z. Wan, A. Carr, A. H. Rizvi, G. Vieira, D. Pe'er, and P. A. Sims. Scalable microfluidics for single-cell rna printing and sequencing. *Genome Biol*, 16(1):120, 2015.

[105] M. T. Guo, A. Rotem, J. A. Heyman, and D. A. Weitz. Droplet microfluidics for high-throughput biological assays. *Lab Chip*, 12(12):2146–55, 2012.

[106] E. Z. Macosko, A. Basu, R. Satija, J. Nemesh, K. Shekhar, M. Goldman, I. Tirosh, A. R. Bialas, N. Kamitaki, E. M. Martersteck, J. J. Trombetta, D. A.

Weitz, J. R. Sanes, A. K. Shalek, A. Regev, and S. A. McCarroll. Highly parallel genome-wide expression profiling of individual cells using nanoliter droplets. *Cell*, 161(5):1202–14, 2015.

[107] A. M. Klein, L. Mazutis, I. Akartuna, N. Tallapragada, A. Veres, V. Li, L. Peshkin, D. A. Weitz, and M. W. Kirschner. Droplet barcoding for single-cell transcriptomics applied to embryonic stem cells. *Cell*, 161(5):1187–201, 2015.

[108] J. H. Lee, E. R. Daugharthy, J. Scheiman, R. Kalhor, J. L. Yang, T. C. Ferrante, R. Terry, S. S. Jeanty, C. Li, R. Amamoto, D. T. Peters, B. M. Turczyk, A. H. Marblestone, S. A. Inverso, A. Bernard, P. Mali, X. Rios, J. Aach, and G. M. Church. Highly multiplexed subcellular rna sequencing in situ. *Science*, 343(6177):1360–3, 2014.

[109] J. H. Lee, E. R. Daugharthy, J. Scheiman, R. Kalhor, T. C. Ferrante, R. Terry, B. M. Turczyk, J. L. Yang, H. S. Lee, J. Aach, K. Zhang, and G. M. Church. Fluorescent in situ sequencing (fisseq) of rna for gene expression profiling in intact cells and tissues. *Nat Protoc*, 10(3):442–58, 2015.

[110] R. N. Zare and S. Kim. Microfluidic platforms for single-cell analysis. *Annu Rev Biomed Eng*, 12:187–201, 2010.

[111] H G Schulze, S O Konorov, N J Caron, J M Piret, M W Blades, and R F Turner. Assessing differentiation status of human embryonic stem cells noninvasively using raman microspectroscopy. *Anal Chem*, 82:5020–5027, 2010.

[112] O. Adewumi, B. Aflatoonian, L. Ahrlund-Richter, M. Amit, P. W. Andrews, G. Beighton, P. A. Bello, N. Benvenisty, L. S. Berry, S. Bevan, B. Blum, J. Brooking, K. G. Chen, A. B. Choo, G. A. Churchill, M. Corbel, I. Damjanov, J. S. Draper, P. Dvorak, K. Emanuelsson, R. A. Fleck, A. Ford, K. Gertow, M. Gertsenstein, P. J. Gokhale, R. S. Hamilton, A. Hampl, L. E. Healy, O. Hovatta, J. Hyllner, M. P. Imreh, J. Itskovitz-Eldor, J. Jackson, J. L. Johnson, M. Jones, K. Kee, B. L. King, B. B. Knowles, M. Lako, F. Lebrin, B. S. Mallon, D. Manning, Y. Mayshar, R. D. McKay, A. E. Michalska, M. Mikkola, M. Mileikovsky, S. L. Minger, H. D. Moore, C. L. Mummery, A. Nagy, N. Nakatsuji, C. M. O'Brien, S. K. Oh, C. Olsson, T. Otonkoski, K. Y. Park, R. Passier, H. Patel, M. Patel, R. Pedersen, M. F. Pera, M. S. Piekarczyk, R. A. Pera, B. E.

Reubinoff, A. J. Robins, J. Rossant, P. Rugg-Gunn, T. C. Schulz, H. Semb, E. S. Sherrer, H. Siemen, G. N. Stacey, M. Stojkovic, H. Suemori, J. Szatkiewicz, T. Turetsky, T. Tuuri, S. van den Brink, K. Vintersten, S. Vuoristo, D. Ward, T. A. Weaver, L. A. Young, and W. Zhang. Characterization of human embryonic stem cell lines by the international stem cell initiative. *Nat Biotechnol*, 25(7):803–16, 2007.

[113] T. E. Ludwig, V. Bergendahl, M. E. Levenstein, J. Yu, M. D. Probasco, and J. A. Thomson. Feeder-independent culture of human embryonic stem cells. *Nat Methods*, 3(8):637–46, 2006.

[114] B. Tinland, A. Pluen, J. Sturm, and G. Weill. Persistence length of single-stranded dna. *Macromolecules*, 30(19):5763–5765, 1997.

[115] J. Lu, G. Getz, E. A. Miska, E. Alvarez-Saavedra, J. Lamb, D. Peck, A. Sweet-Cordero, B. L. Ebert, R. H. Mak, A. A. Ferrando, J. R. Downing, T. Jacks, H. R. Horvitz, and T. R. Golub. Microrna expression profiles classify human cancers. *Nature*, 435(7043):834–8, 2005.

[116] B. B. Lozzio, C. B. Lozzio, E. G. Bamberger, and A. S. Feliu. A multipotential leukemia cell line (k-562) of human origin. *Proc Soc Exp Biol Med*, 166(4):546–50, 1981.

[117] J. Y. Yuan, F. Wang, J. Yu, G. H. Yang, X. L. Liu, and J. W. Zhang. Microrna-223 reversibly regulates erythroid and megakaryocytic differentiation of k562 cells. *J Cell Mol Med*, 13(11-12):4551–9, 2009.

[118] P. Landgraf, M. Rusu, R. Sheridan, A. Sewer, N. Iovino, A. Aravin, S. Pfeffer, A. Rice, A. O. Kamphorst, M. Landthaler, C. Lin, N. D. Socci, L. Hermida, V. Fulci, S. Chiaretti, R. Foa, J. Schliwka, U. Fuchs, A. Novosel, R. U. Muller, B. Schermer, U. Bissels, J. Inman, Q. Phan, M. Chien, D. B. Weir, R. Choksi, G. De Vita, D. Frezzetti, H. I. Trompeter, V. Hornung, G. Teng, G. Hartmann, M. Palkovits, R. Di Lauro, P. Wernet, G. Macino, C. E. Rogler, J. W. Nagle, J. Ju, F. N. Papavasiliou, T. Benzing, P. Lichter, W. Tam, M. J. Brownstein, A. Bosio, A. Borkhardt, J. J. Russo, C. Sander, M. Zavolan, and T. Tuschl. A mammalian microrna expression atlas based on small rna library sequencing. *Cell*, 129(7):1401–14, 2007.

[119] N. Xu, T. Papagiannakopoulos, G. Pan, J. A. Thomson, and K. S. Kosik. Microrna-145 regulates oct4, sox2, and klf4 and represses pluripotency in human embryonic stem cells. *Cell*, 137(4):647–58, 2009.

[120] J. Huft, D. J. Da Costa, D. Walker, and C. L. Hansen. Three-dimensional large-scale microfluidic integration by laser ablation of interlayer connections. *Lab Chip*, 10(18):2358–65, 2010.

[121] P. J. Murphy, B. R. Cipriany, C. B. Wallin, C. Y. Ju, K. Szeto, J. A. Hagarman, J. J. Benitez, H. G. Craighead, and P. D. Soloway. Single-molecule analysis of combinatorial epigenomic states in normal and tumor cells. *Proc Natl Acad Sci U S A*, 110(19):7772–7, 2013.

[122] M. Kantlehner, R. Kirchner, P. Hartmann, J. W. Ellwart, M. Alunni-Fabbroni, and A. Schumacher. A high-throughput dna methylation analysis of a single cell. *Nucleic Acids Res*, 39(7):e44, 2011.

[123] J. Tischler and M. A. Surani. Investigating transcriptional states at single-cell-resolution. *Curr Opin Biotechnol*, 24(1):69–78, 2013.

[124] Y. Taniguchi, P. J. Choi, G. W. Li, H. Chen, M. Babu, J. Hearn, A. Emili, and X. S. Xie. Quantifying e. coli proteome and transcriptome with single-molecule sensitivity in single cells. *Science*, 329(5991):533–8, 2010.

[125] V. Lecault, M. Vaninsberghe, S. Sekulovic, D. J. Knapp, S. Wohrer, W. Bowden, F. Viel, T. McLaughlin, A. Jarandehei, M. Miller, D. Falconnet, A. K. White, D. G. Kent, M. R. Copley, F. Taghipour, C. J. Eaves, R. K. Humphries, J. M. Piret, and C. L. Hansen. High-throughput analysis of single hematopoietic stem cell proliferation in microfluidic cell culture arrays. *Nat Methods*, 8(7):581–6, 2011.

[126] D. Falconnet, A. Niemisto, R. J. Taylor, M. Ricicova, T. Galitski, I. Shmulevich, and C. L. Hansen. High-throughput tracking of single yeast cells in a microfluidic imaging matrix. *Lab Chip*, 11(3):466–73, 2011.

[127] F. Notta, S. Doulatov, E. Laurenti, A. Poeppl, I. Jurisica, and J. E. Dick. Isolation of single human hematopoietic stem cells capable of long-term multilineage engraftment. *Science*, 333(6039):218–21, 2011.

[128] D. G. Kent, M. R. Copley, C. Benz, S. Wohrer, B. J. Dykstra, E. Ma, J. Cheyne, Y. Zhao, M. B. Bowie, Y. Zhao, M. Gasparetto, A. Delaney, C. Smith, M. Marra, and C. J. Eaves. Prospective isolation and molecular characterization of hematopoietic stem cells with durable self-renewal potential. *Blood*, 113(25):6342–50, 2009.

[129] A. K. White, M. VanInsberghe, O. I. Petriv, M. Hamidi, D. Sikorski, M. A. Marra, J. Piret, S. Aparicio, and C. L. Hansen. High-throughput microfluidic single-cell rt-qpcr. *Proc Natl Acad Sci U S A*, 108(34):13999–4004, 2011.

[130] F. Tang, K. Lao, and M. A. Surani. Development and applications of single-cell transcriptome analysis. *Nat Methods*, 8(4 Suppl):S6–11, 2011.

[131] P. Mestdagh, T. Feys, N. Bernard, S. Guenther, C. Chen, F. Speleman, and J. Vandesompele. High-throughput stem-loop rt-qpcr mirna expression profiling using minute amounts of input rna. *Nucleic Acids Res*, 36(21):e143, 2008.

[132] A. Diercks, H. Kostner, and A. Ozinsky. Resolving cell population heterogeneity: real-time pcr for simultaneous multiplexed gene detection in multiple single-cell samples. *PLoS One*, 4(7):e6326, 2009.

[133] K. A. Heyries, C. Tropini, M. Vaninsberghe, C. Doolin, O. I. Petriv, A. Singhal, K. Leung, C. B. Hughesman, and C. L. Hansen. Megapixel digital pcr. *Nat Methods*, 8(8):649–51, 2011.

[134] K. A. Heyries and C. L. Hansen. Parylene c coating for high-performance replica molding. *Lab Chip*, 11(23):4122–5, 2011.

[135] E. Park, B. Williams, B. J. Wold, and A. Mortazavi. Rna editing in the human encode rna-seq data. *Genome Res*, 22(9):1626–33, 2012.

[136] F Goreaud and R Plissier. On explicit formulas of edge effect correction for ripley's kfunction. *Journal of Vegetation Science*, 10:433–438, 1999.

[137] S. Bhat, J. Herrmann, P. Armishaw, P. Corbisier, and K. R. Emslie. Single molecule detection in nanofluidic digital array enables accurate measurement of dna copy number. *Anal Bioanal Chem*, 394(2):457–67, 2009.

[138] S. Dube, J. Qin, and R. Ramakrishnan. Mathematical analysis of copy number variation in a dna sample using digital pcr on a nanofluidic device. *PLoS One*, 3(8):e2876, 2008.

[139] D. Ling and P. M. Salvaterra. Robust rt-qpcr data normalization: validation and selection of internal reference genes during post-experimental data analysis. *PLoS One*, 6(3):e17762, 2011.

[140] M. Verma, E. G. Karimiani, R. J. Byers, S. Rehman, H. V. Westerhoff, and P. J. Day. Mathematical modelling of mirna mediated bcr.abl protein regulation in chronic myeloid leukaemia vis-a-vis therapeutic strategies. *Integr Biol (Camb)*, 5(3):543–54, 2013.

[141] D. Sayed and M. Abdellatif. Micrornas in development and disease. *Physiol Rev*, 91(3):827–87, 2011.

[142] D. P. Bartel. Micrornas: target recognition and regulatory functions. *Cell*, 136(2):215–33, 2009.

[143] C. C. Pritchard, H. H. Cheng, and M. Tewari. Microrna profiling: approaches and considerations. *Nat Rev Genet*, 13(5):358–69, 2012.

[144] N. R. Christoffersen, A. Silahtaroglu, U. A. Orom, S. Kauppinen, and A. H. Lund. mir-200b mediates post-transcriptional repression of zfhx1b. *RNA*, 13(8):1172–8, 2007.

[145] E. Barrey, G. Saint-Auret, B. Bonnamy, D. Damas, O. Boyer, and X. Gidrol. Pre-microrna and mature microrna in human mitochondria. *PLoS One*, 6(5):e20220, 2011.

[146] M. Wu, M. Piccini, C. Y. Koh, K. S. Lam, and A. K. Singh. Single cell microrna analysis using microfluidic flow cytometry. *PLoS One*, 8(1):e55044, 2013.

[147] Encode Project Consortium. An integrated encyclopedia of dna elements in the human genome. *Nature*, 489(7414):57–74, 2012.

[148] LA Luigi A Warren, JA Joshua A Weinstein, and Stephen R SR Quake. The digital array response curve, 2007.

[149] N. Farago, A. K. Kocsis, S. Lovas, G. Molnar, E. Boldog, M. Rozsa, V. Szemenyei, E. Vamos, L. I. Nagy, G. Tamas, and L. G. Puskas. Digital pcr to determine the number of transcripts from single neurons after patch-clamp recording. *Biotechniques*, 54(6):327–36, 2013.

[150] A. Kumari, C. Brendel, A. Hochhaus, A. Neubauer, and A. Burchert. Low bcr-abl expression levels in hematopoietic precursor cells enable persistence of chronic myeloid leukemia under imatinib. *Blood*, 119(2):530–9, 2012.

[151] Y. Chen, B. Zhang, H. Feng, W. Shu, G. Y. Chen, and J. F. Zhong. An automated microfluidic device for assessment of mammalian cell genetic stability. *Lab Chip*, 12(20):3930–5, 2012.

[152] A. Stahlberg, C. Thomsen, D. Ruff, and P. Aman. Quantitative pcr analysis of dna, rnas, and proteins in the same single cell. *Clin Chem*, 58(12):1682–91, 2012.

[153] K. A. Whitehead, R. Langer, and D. G. Anderson. Knocking down barriers: advances in sirna delivery. *Nat Rev Drug Discov*, 8(2):129–38, 2009.

[154] B. L. Davidson and Jr. McCray, P. B. Current prospects for rna interference-based therapies. *Nat Rev Genet*, 12(5):329–40, 2011.

[155] M. DiFiglia, M. Sena-Esteves, K. Chase, E. Sapp, E. Pfister, M. Sass, J. Yoder, P. Reeves, R. K. Pandey, K. G. Rajeev, M. Manoharan, D. W. Sah, P. D. Zamore, and N. Aronin. Therapeutic silencing of mutant huntingtin with sirna attenuates striatal and cortical neuropathology and behavioral deficits. *Proc Natl Acad Sci U S A*, 104(43):17204–9, 2007.

[156] S. D. Li, Y. C. Chen, M. J. Hackett, and L. Huang. Tumor-targeted delivery of sirna by self-assembled nanoparticles. *Mol Ther*, 16(1):163–9, 2008.

[157] G. J. Hannon and J. J. Rossi. Unlocking the potential of the human genome with rna interference. *Nature*, 431(7006):371–8, 2004.

[158] X. Su, J. Fricke, D. G. Kavanagh, and D. J. Irvine. In vitro and in vivo mrna delivery using lipid-enveloped ph-responsive polymer nanoparticles. *Mol Pharm*, 8(3):774–87, 2011.

[159] G. Cannon and D. Weissman. Rna based vaccines. *DNA Cell Biol*, 21(12):953–61, 2002.

[160] A. J. Geall, A. Verma, G. R. Otten, C. A. Shaw, A. Hekele, K. Banerjee, Y. Cu, C. W. Beard, L. A. Brito, T. Krucker, D. T. O'Hagan, M. Singh, P. W. Mason, N. M. Valiante, P. R. Dormitzer, S. W. Barnett, R. Rappuoli, J. B. Ulmer, and C. W. Mandl. Nonviral delivery of self-amplifying rna vaccines. *Proc Natl Acad Sci U S A*, 109(36):14604–9, 2012.

[161] L. Warren, P. D. Manos, T. Ahfeldt, Y. H. Loh, H. Li, F. Lau, W. Ebina, P. K. Mandal, Z. D. Smith, A. Meissner, G. Q. Daley, A. S. Brack, J. J. Collins, C. Cowan, T. M. Schlaeger, and D. J. Rossi. Highly efficient reprogramming to pluripotency and directed differentiation of human cells with synthetic modified mrna. *Cell Stem Cell*, 7(5):618–30, 2010.

[162] J. R. Plews, J. Li, M. Jones, H. D. Moore, C. Mason, P. W. Andrews, and J. Na. Activation of pluripotency genes in human fibroblast cells by a novel mrna based approach. *PLoS One*, 5(12):e14397, 2010.

[163] Anonymous. Is this really the rnaissance? *Nat Biotechnol*, 32(3):201, 2014.

[164] E. P. Thi, C. E. Mire, A. C. Lee, J. B. Geisbert, J. Z. Zhou, K. N. Agans, N. M. Snead, D. J. Deer, T. R. Barnard, K. A. Fenton, I. MacLachlan, and T. W. Geisbert. Lipid nanoparticle sirna treatment of ebola-virus-makona-infected nonhuman primates. *Nature*, 521(7552):362–5, 2015.

[165] L. Timmerman. Merck joins messenger rna frenzy, betting $100m on moderna therapeutics. *Forbes*, (September 7, 2015), 2015.

[166] T. Kawai and S. Akira. The role of pattern-recognition receptors in innate immunity: update on toll-like receptors. *Nat Immunol*, 11(5):373–84, 2010.

[167] K. Kariko, M. Buckstein, H. Ni, and D. Weissman. Suppression of rna recognition by toll-like receptors: the impact of nucleoside modification and the evolutionary origin of rna. *Immunity*, 23(2):165–75, 2005.

[168] M. S. Kormann, G. Hasenpusch, M. K. Aneja, G. Nica, A. W. Flemmer, S. Herber-Jonat, M. Huppmann, L. E. Mays, M. Illenyi, A. Schams, M. Griese,

I. Bittmann, R. Handgretinger, D. Hartl, J. Rosenecker, and C. Rudolph. Expression of therapeutic proteins after delivery of chemically modified mrna in mice. *Nat Biotechnol*, 29(2):154–7, 2011.

[169] N. Desai. Challenges in development of nanoparticle-based therapeutics. *AAPS J*, 14(2):282–95, 2012.

[170] S. C. Semple, A. Akinc, J. Chen, A. P. Sandhu, B. L. Mui, C. K. Cho, D. W. Sah, D. Stebbing, E. J. Crosley, E. Yaworski, I. M. Hafez, J. R. Dorkin, J. Qin, K. Lam, K. G. Rajeev, K. F. Wong, L. B. Jeffs, L. Nechev, M. L. Eisenhardt, M. Jayaraman, M. Kazem, M. A. Maier, M. Srinivasulu, M. J. Weinstein, Q. Chen, R. Alvarez, S. A. Barros, S. De, S. K. Klimuk, T. Borland, V. Kosovrasti, W. L. Cantley, Y. K. Tam, M. Manoharan, M. A. Ciufolini, M. A. Tracy, A. de Fougerolles, I. MacLachlan, P. R. Cullis, T. D. Madden, and M. J. Hope. Rational design of cationic lipids for sirna delivery. *Nat Biotechnol*, 28(2):172–6, 2010.

[171] A. Sridharan, C. Patel, and J. Muthuswamy. Voltage preconditioning allows modulated gene expression in neurons using pei-complexed sirna. *Mol Ther Nucleic Acids*, 2:e82, 2013.

[172] B. Urban-Klein, S. Werth, S. Abuharbeid, F. Czubayko, and A. Aigner. Rnai-mediated gene-targeting through systemic application of polyethylenimine (pei)-complexed sirna in vivo. *Gene Ther*, 12(5):461–6, 2005.

[173] P. Kumar, H. Wu, J. L. McBride, K. E. Jung, M. H. Kim, B. L. Davidson, S. K. Lee, P. Shankar, and N. Manjunath. Transvascular delivery of small interfering rna to the central nervous system. *Nature*, 448(7149):39–43, 2007.

[174] E. Song, P. Zhu, S. K. Lee, D. Chowdhury, S. Kussman, D. M. Dykxhoorn, Y. Feng, D. Palliser, D. B. Weiner, P. Shankar, W. A. Marasco, and J. Lieberman. Antibody mediated in vivo delivery of small interfering rnas via cell-surface receptors. *Nat Biotechnol*, 23(6):709–17, 2005.

[175] A. Akinc, W. Querbes, S. De, J. Qin, M. Frank-Kamenetsky, K. N. Jayaprakash, M. Jayaraman, K. G. Rajeev, W. L. Cantley, J. R. Dorkin, J. S. Butler, L. Qin, T. Racie, A. Sprague, E. Fava, A. Zeigerer, M. J. Hope, M. Zerial, D. W. Sah, K. Fitzgerald, M. A. Tracy, M. Manoharan, V. Koteliansky, Ad Fougerolles,

and M. A. Maier. Targeted delivery of rnai therapeutics with endogenous and exogenous ligand-based mechanisms. *Mol Ther*, 18(7):1357–64, 2010.

[176] J. Sparks, G. Slobodkin, M. Matar, R. Congo, D. Ulkoski, A. Rea-Ramsey, C. Pence, J. Rice, D. McClure, K. J. Polach, E. Brunhoeber, L. Wilkinson, K. Wallace, K. Anwer, and J. G. Fewell. Versatile cationic lipids for sirna delivery. *J Control Release*, 158(2):269–76, 2012.

[177] N. M. Belliveau, J. Huft, P. J. Lin, S. Chen, A. K. Leung, T. J. Leaver, A. W. Wild, J. B. Lee, R. J. Taylor, Y. K. Tam, C. L. Hansen, and P. R. Cullis. Microfluidic synthesis of highly potent limit-size lipid nanoparticles for in vivo delivery of sirna. *Mol Ther Nucleic Acids*, 1:e37, 2012.

[178] T. S. Zimmermann, A. C. Lee, A. Akinc, B. Bramlage, D. Bumcrot, M. N. Fedoruk, J. Harborth, J. A. Heyes, L. B. Jeffs, M. John, A. D. Judge, K. Lam, K. McClintock, L. V. Nechev, L. R. Palmer, T. Racie, I. Rohl, S. Seiffert, S. Shanmugam, V. Sood, J. Soutschek, I. Toudjarska, A. J. Wheat, E. Yaworski, W. Zedalis, V. Koteliansky, M. Manoharan, H. P. Vornlocher, and I. MacLachlan. Rnai-mediated gene silencing in non-human primates. *Nature*, 441(7089):111–4, 2006.

[179] M. Frank-Kamenetsky, A. Grefhorst, N. N. Anderson, T. S. Racie, B. Bramlage, A. Akinc, D. Butler, K. Charisse, R. Dorkin, Y. Fan, C. Gamba-Vitalo, P. Hadwiger, M. Jayaraman, M. John, K. N. Jayaprakash, M. Maier, L. Nechev, K. G. Rajeev, T. Read, I. Rohl, J. Soutschek, P. Tan, J. Wong, G. Wang, T. Zimmermann, A. de Fougerolles, H. P. Vornlocher, R. Langer, D. G. Anderson, M. Manoharan, V. Koteliansky, J. D. Horton, and K. Fitzgerald. Therapeutic rnai targeting pcsk9 acutely lowers plasma cholesterol in rodents and ldl cholesterol in nonhuman primates. *Proc Natl Acad Sci U S A*, 105(33):11915–20, 2008.

[180] A. D. Stroock, S. K. Dertinger, A. Ajdari, I. Mezic, H. A. Stone, and G. M. Whitesides. Chaotic mixer for microchannels. *Science*, 295(5555):647–51, 2002.

[181] I. V. Zhigaltsev, N. Belliveau, I. Hafez, A. K. Leung, J. Huft, C. Hansen, and P. R. Cullis. Bottom-up design and synthesis of limit size lipid nanoparticle systems with aqueous and triglyceride cores using millisecond microfluidic mixing. *Langmuir*, 28(7):3633–40, 2012.

[182] A. K. Leung, I. M. Hafez, S. Baoukina, N. M. Belliveau, I. V. Zhigaltsev, E. Afshinmanesh, D. P. Tieleman, C. L. Hansen, M. J. Hope, and P. R. Cullis. Lipid nanoparticles containing sirna synthesized by microfluidic mixing exhibit an electron-dense nanostructured core. *J Phys Chem C Nanomater Interfaces*, 116(34):18440–18450, 2012.

[183] Y. Pei, P. J. Hancock, H. Zhang, R. Bartz, C. Cherrin, N. Innocent, C. J. Pomerantz, J. Seitzer, M. L. Koser, M. T. Abrams, Y. Xu, N. A. Kuklin, P. A. Burke, A. B. Sachs, L. Sepp-Lorenzino, and S. F. Barnett. Quantitative evaluation of sirna delivery in vivo. *RNA*, 16(12):2553–63, 2010.

[184] M. T. Abrams, M. L. Koser, J. Seitzer, S. C. Williams, M. A. DiPietro, W. Wang, A. W. Shaw, X. Mao, V. Jadhav, J. P. Davide, P. A. Burke, A. B. Sachs, S. M. Stirdivant, and L. Sepp-Lorenzino. Evaluation of efficacy, biodistribution, and inflammation for a potent sirna nanoparticle: effect of dexamethasone co-treatment. *Mol Ther*, 18(1):171–80, 2010.

[185] S. Mukherji, M. S. Ebert, G. X. Zheng, J. S. Tsang, P. A. Sharp, and A. van Oudenaarden. Micrornas can generate thresholds in target gene expression. *Nat Genet*, 43(9):854–9, 2011.

[186] J. Gilleron, W. Querbes, A. Zeigerer, A. Borodovsky, G. Marsico, U. Schubert, K. Manygoats, S. Seifert, C. Andree, M. Stoter, H. Epstein-Barash, L. Zhang, V. Koteliansky, K. Fitzgerald, E. Fava, M. Bickle, Y. Kalaidzidis, A. Akinc, M. Maier, and M. Zerial. Image-based analysis of lipid nanoparticle-mediated sirna delivery, intracellular trafficking and endosomal escape. *Nat Biotechnol*, 31(7):638–46, 2013.

[187] G. Sahay, W. Querbes, C. Alabi, A. Eltoukhy, S. Sarkar, C. Zurenko, E. Karagiannis, K. Love, D. Chen, R. Zoncu, Y. Buganim, A. Schroeder, R. Langer, and D. G. Anderson. Efficiency of sirna delivery by lipid nanoparticles is limited by endocytic recycling. *Nat Biotechnol*, 31(7):653–8, 2013.

[188] L. Warren, Y. Ni, J. Wang, and X. Guo. Feeder-free derivation of human induced pluripotent stem cells with messenger rna. *Sci Rep*, 2:657, 2012.

[189] N. J. Caron, B. K. Gage, M. D. O'Connor, C. J. Eaves, T. J. Kieffer, and

J. M. Piret. A human embryonic stem cell line adapted for high throughput screening. *Biotechnol Bioeng*, 110(10):2706–16, 2013.

[190] R. L. Rungta, H. B. Choi, P. J. Lin, R. W. Ko, D. Ashby, J. Nair, M. Manoharan, P. R. Cullis, and B. A. Macvicar. Lipid nanoparticle delivery of sirna to silence neuronal gene expression in the brain. *Mol Ther Nucleic Acids*, 2:e136, 2013.

[191] A. K. White, K. A. Heyries, C. Doolin, M. Vaninsberghe, and C. L. Hansen. High-throughput microfluidic single-cell digital polymerase chain reaction. *Anal Chem*, 85(15):7182–90, 2013.

[192] P. C. Blainey and S. R. Quake. Digital mda for enumeration of total nucleic acid contamination. *Nucleic Acids Res*, 39(4):e19, 2011.

[193] K. A. Janes, C. C. Wang, K. J. Holmberg, K. Cabral, and J. S. Brugge. Identifying single-cell molecular programs by stochastic profiling. *Nat Methods*, 7(4):311–7, 2010.

[194] J. P. Junker, E. S. Noel, V. Guryev, K. A. Peterson, G. Shah, J. Huisken, A. P. McMahon, E. Berezikov, J. Bakkers, and A. van Oudenaarden. Genome-wide rna tomography in the zebrafish embryo. *Cell*, 159(3):662–75, 2014.

[195] N. Crosetto, M. Bienko, and A. van Oudenaarden. Spatially resolved transcriptomics and beyond. *Nat Rev Genet*, 16(1):57–66, 2015.

[196] S. Fredriksson, M. Gullberg, J. Jarvius, C. Olsson, K. Pietras, S. M. Gustafsdottir, A. Ostman, and U. Landegren. Protein detection using proximity-dependent dna ligation assays. *Nat Biotechnol*, 20(5):473–7, 2002.

[197] S. C. Bendall, E. F. Simonds, P. Qiu, A. D. Amir el, P. O. Krutzik, R. Finck, R. V. Bruggner, R. Melamed, A. Trejo, O. I. Ornatsky, R. S. Balderas, S. K. Plevritis, K. Sachs, D. Pe'er, S. D. Tanner, and G. P. Nolan. Single-cell mass cytometry of differential immune and drug responses across a human hematopoietic continuum. *Science*, 332(6030):687–96, 2011.

[198] A. A. Khan, D. Betel, M. L. Miller, C. Sander, C. S. Leslie, and D. S. Marks. Transfection of small rnas globally perturbs gene regulation by endogenous micrornas. *Nat Biotechnol*, 27(6):549–55, 2009.

[199] J. Wang and S. R. Quake. Rna-guided endonuclease provides a therapeutic strategy to cure latent herpesviridae infection. *Proc Natl Acad Sci U S A*, 111(36):13157–62, 2014.

[200] M. K. White, W. Hu, and K. Khalili. The crispr/cas9 genome editing methodology as a weapon against human viruses. *Discov Med*, 19(105):255–62, 2015.

Appendix A

Design Considerations

A.1 Single-Cell Digital PCR Prototype with Alternative Approach to Mixing

Digital PCR requires template molecules to be randomly distributed among reaction chambers in order to accurately infer the number of molecules in the array from the number of reaction chambers with PCR amplification. If the number of molecules in the array is significantly less than the number of chambers compartmentalizing the solution, then most of the chambers will contain either one or zero template molecules. In this case, the number of positive wells (with amplified product) at the end of PCR gives a count of the number of molecules in the sample to a close approximation. However, if the number of template molecules is not small compared to the number of chambers, many chambers will contain more than one template molecule. This results in the number of positive reaction chambers being significantly less than the number of molecules in the sample. However, as long as the array is not fully saturated, template abundance can still be estimated based on the statistical relationship between the number of molecules and the expected number of positive wells.

In integrating digital PCR with the cell processing previously established, one of the challenges is ensuring the sample is thoroughly mixed prior to dPCR compartmentalization. In conventional dPCR, a solution that is already completely mixed is simply injected into a dPCR array, or partitioned into droplets. In our single-cell RT-qPCR device, chemical reactions are assembled on-chip by diluting a sample into a larger chamber with the required reagent. Some mixing of solutions occurs through advection, however the majority of the combined solution is mixed by diffusion. An initial prototype attempted to solve this problem by pushing template solution with PCR reagent into a dPCR array consisting of a bifurcating structure of channels that can partitioned with valves into dPCR chambers. However, prior to compart-

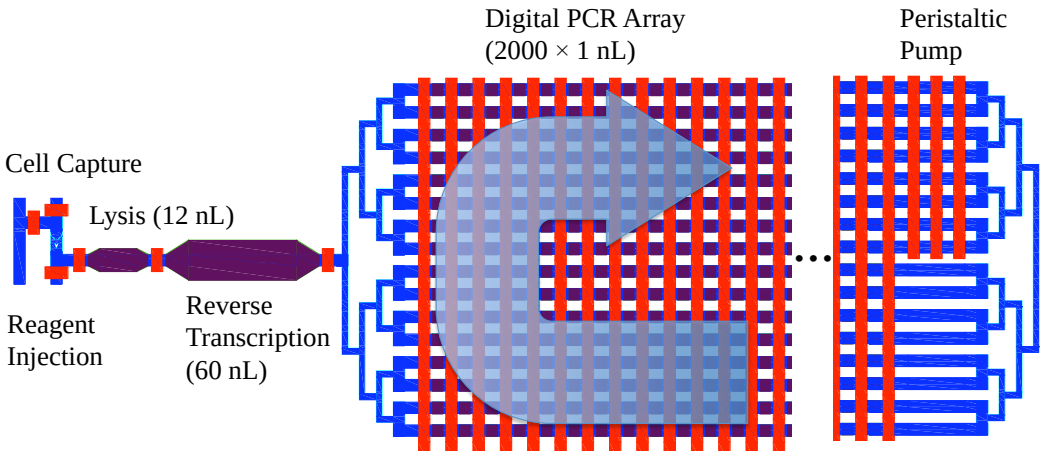

Figure A.1: Design schematic of an early prototype single cell digital PCR device. This design is based on physical valve partitioning of channels into digital PCR chambers, and requires a much larger footprint compared to the surface tension partitioning with oil strategy presented in Chapter 3. This architecture incorporates a peristaltic pump to create a rotary mixer in the array to completely mix the solution before partitioning. Valve (or 'control') channels are indicated in red.

mentalization, the injected PCR and template solution can be mixed by using valves to pump the solution around the ring of dPCR channels (Figure A.1). This rotary mixing reduces diffusion times by wrapping the template and PCR solutions within each other to decrease characteristic diffusion distances. In practice, this approach still required long mixing times and was further limited in dPCR chamber density as it used mechanical valves to partition the channels into dPCR chambers.

The high-density planar emulsion dPCR arrays previously developed by Heyries et al. overcome the large footprint of conventional valve-based dPCR arrays. However, this approach requires a pre-mixed PCR/template solution to be injected as the dPCR array is dead-end filled, preventing any rotary mixing and imposing long diffusion distances between far chambers of the array. In order to incorporate high-density planar emulsion dPCR arrays, the prototype single-cell dPCR device mixes PCR solution with template by diffusion in a 50 nL chamber (see Chapter 3). This mixed PCR solution is then pushed (with unmixed PCR reagent) into an array of 1020 × 25 pL dPCR chambers which accommodates approximately half of the mixed PCR/template solution. This strategy of sampling half of the pre-mixed PCR/template solution, and the architecture of the mixing chamber, accomplishes injection of a completely mixed

PCR solution into the dPCR array. The disadvantage of this approach is the entire content of the cell is not analyzed, limiting the precision and sensitivity of the device, particularly in cases where transcript abundance is less than 6 copies per cell. Potentially, the mixed PCR/template solution may be pushed with an immiscible phase fluid such as oil or a gas in order to facilitate fluid transfer between chambers without dilution or an unmixed front of solution.

Appendix B

Protocols[1]

B.1 Fabrication

After fabricating the molds described in the methods section of chapter 2, multilayer soft lithography is used to create microfluidic devices. This protocol uses polydimethylsiloxane (PDMS): specifically RTV615. The device uses a 'push-up' geometry, with the valve/control channels in the layer underneath the flow channels (for sample and reagents). This information is contained in Chapter 2, however is presented here in expanded form with greater detail.

Before coating with PDMS, treat wafers with TMCS (trichloromethylsilande). Seal wafers in a box containing a beaker of TMCS. TMCS is volatile and will coat wafer to prevent PDMS from sticking to the photoresist (features).

B.1.1 Flow Layer

1. Mix Flow layer (thick) (5:1 A:B). Use 50 g A and 10 g B per wafer.
2. Pour 5:1 mixture on the top layer wafer in foiled dish.
3. Use pipette tips with bigger side down to centre flow wafer and push it down to release bubbles from under wafer
4. Degas the mixture/wafer by placing in vacuum for minimum 1 hour.

B.1.2 Control and Blank Layer(s)

1. While degassing, mix Control and blank layers (thin) (20:1 A:B). Use 20g A and 1g B per wafer (40 g A and 2 g B for both control and blank if being used)
2. Place control wafer on spinner and pour 20:1 mixture on about 2/3 of wafer.

[1]Parts of this protocol are reproduced from *Microfluidic Technology for High-Throughput Single Cell Gene Expression Analysis*, by Adam White, University of British Columbia, 2010.

3. Spin cycle:
    - Ramp 10s to 500 rpm, hold 5s
    - Ramp 5s to 1800 rpm, hold 60s
    - Ramp 5s to 0 rpm
4. When finished spinning, place in a dish and close lid (can put wafer on lid because its flatter)
5. Repeat for blank(s) and then set aside blank layer.

B.1.3 Bake Flow and Control Layers

1. When there are only a few bubbles left on flow layer, remove from vacuum chamber, use pipette tip to drag bubbles off the features, and push wafer to bottom.
2. Bake Flow Layer 80°C, 60 Min.
3. Wait 15 min and then bake Control Layer 80°C, 45 Min (this way you can remove both layers from oven at the same time)

B.1.4 Align Flow Layer to Control Layer

1. Remove both layers from oven and allow to cool for a couple minutes
2. Cut on the inside of the flow wafer for a clean lift off. Cut multiple times to ensure there is no debris that might fold under flow layer and prevent proper bonding to control layer. Peel flow layer off of wafer.
3. Immediately after peeling flow layer, place it on top of control layer to minimize chance of debris getting between the 2 layers.
4. Align flow layer to control layer (still on wafer).
5. Use tape (scotch) to clean off top of the chip
6. Bake Flow and Control layers for 1 hour at 80°C.

B.1.5 Ports

1. Peel combined flow and control layers off of wafer. Make multiple cuts to ensure a clean lift off.
2. Punch holes in devices (bonded Control and Flow layers).
3. When you think you are 45 min away from finishing punching holes, bake blank layer for 45 min at 80°C
4. Clean bottom of bonded layers vigorously with tape. Remove blank layer from oven and place bonded layers control and flow layers onto the blank layer. Be sure the control (thin) layer of the bonded layers is down. Check for collapsed valves and use syringe to suck them out if necessary. Try to avoid bubbles. Clean top surface with tape.
5. Cook overnight at 80°C. Mimimum 3 hours.

B.1.6 Mounting Individual Devices

1. Dice Chips
2. Place chips on glass slides. Be sure to clean slides with water and IPA first. Clean chips with tape (bottom before fastening to slide, top after fastening). Make sure plug holes are up (blank and thin on the bottom, thick on top)
3. Bake slides with chips at 80°C over night. Be sure to label the slides with information about chip, fabrication date, etc.

B.1.7 General Considerations

1. RTV stands for room temperature vulcanization. Do not let RTC A:B sit for too long (greater than 4 hours).
2. RTV A : RTV B, 10:1 is the stoichiometrically equivalent ratio.
3. Use Nitrile gloves since Latex gloves contain sulfur that may react with Pt catalyst in RTV.
4. Check that layers have baked properly before alignment (touch edge of wafers with a tweezer.

B.2 Device Operation

The first device operation protocol presented is for a heat lysis, followed by a 2-step RT-qPCR with seperate reverse transcription (RT) and qPCR steps. This protocol was used with miRNA and mRNA assays. Alternatively, a chemical lysis followed by 1-step RT-qPCR protocol is also presented. This protocol is faster, however did not work for miRNA assays, and was applied to measurements of GAPDH and SNV measurements. Krytox oil is used as the fluid in the control lines.

B.2.1 Cell Loading, Washing, and Heat Lysis

1. Device is primed with PBS containing 0.5 mg/mL BSA and 0.5 U/μL RNase Inhibitor. The bovine serum albumin (BSA) prevents cells from sticking to channel walls.

2. Cells loaded into device suspended in culture media (directly from culture). Optional off-chip wash. Cell suspensions may be drawn into microcapillery pipette tips, and plugged into the sample inlet ports. The pipette tip is released from the pipette and air pressure is applied to opening. We used PDMS plugs to seal the pipette tips around the applied air pressure line. Alternatively, the cell suspension may be drawn into tygon tubing with a steel pin on the end of it, which is in turn plugged into the microfluidic device. Cell loading works best at concentrations between 5x10^5 and 1x10^6 cells/mL. Lower concentrations will work but it will take longer to achieve high occupancy of trapped single cells. Higher concentrations may lead to clogging in the inlet port or at the traps. Load cells at approximately 2 psi. Optionally, the peristaltic pump may be used for gentler and controlled cell loading.

3. After loading cells, perform on-chip wash to remove untrapped cells and extracellular RNA. Cells are washed with the same solution that primes the device.

4. Close valves to partition cell loading channel in order to isolate cells in capture chambers.

5. Using microscope, confirm and count which chambers contain cells (enter into spreadsheet).

6. Acutate valves to isolate cell capture chamber. Place device on flatbed thermocycler for heat lysis at 85°C for 7 minutes; followed by 4°C hold.

B.2.2 Reverse Transcription

1. Using the ABI High Capacity Reverse Transcription kit, the RT solution prepared as below (modified from ABI protocol).

   - 10x RT Buffer: 2.00 μL
   - 5x RT primer: 4.00 μL
   - dNTPs: 1.00 μL
   - Multiscribe RT Enzyme: 1.34 μL
   - RNase Inhibitor: 0.26 μL
   - Tween 20 (1%): 2.0 μL
   - H20: 9.4 μL

2. Reverse transcription mix is loaded into the device and flushed through the reagent injection channels.

3. RT reagent is injected into the reaction by opening the valve connecting the cell chamber to the RT chamber, and the valve connecting the cell chamber to the reagent injection line. RT chamber is dead-end filled, and then the reagent the connection to the reagent injection line is closed.

4. The device is placed on a flatbed thermocycler for a pulsed temperature RT protocol.

   - 16°C x 2 min
   - 60 cycles of (20°C x 30 s, 42°C x 30 s, 50°C x 1 s)
   - 85°C x 5 min
   - Hold 4°C

B.2.3 Real-Time Polymerase Chain Reaction

1. The reagent mix for the PCR reaction is prepared using the ABI Taqman Universal Master Mix.

- 2x Taqman Universal Master Mix (ABI): 25.0 μL
- 20x Real-Time Primer/Probe: 2.50 μL
- Tween 20 (1%): 5.0 μL
- Water: 7.5 μL
- RT product (already in device): 10.0 μL

2. Flush reagent injection lines prior to injecting PCR reagent into reaction chambers (similar to RT injection). Input pressure may be increased to increase dead-end filling rate. Pressure should not be decreased as this may result in back-flow from the reaction chambers, and could lead to cross-contamination.

3. One the PCR reaction chamber is filled, the valves closing the PCR chambers are actuated. The rest of the control lines may be removed (cut away or unplugged) to facilitate placing the device into the custom flatbed thermocycler apparatus for imaging the qPCR reaction.

4. The thermocycler controls termperature cycling for the PCR protocol

   - 95°C Hot Start for 10 mins
   - 50 cycles of 95°C x 15 s (denature) and 60°C x 1 min (anneal/extend)

B.2.4 Chemical Lysis and One-Step RT-qPCR

The chemical lysis followed by one-step RT-qPCR protocol is based on the Ivitrogen CellsDirect One-Step RT-qPCR Kit.

1. For device priming and cell loading, follow steps 1-5 from the heat lysis protocol.

2. The lysis buffer is prepared following the CellsDirect kit instructions.

   - Resuspension buffer: 30 μL
   - Lysis enhancer solution: 3 μL

3. The lysis buffer is injected into the 10 nL chambers used for reverse transcription in the other protocol. This follows the same procedure of flushing the reagent injection lines prior to opening valves to permit dead-end filling.

4. Incubate lysis reaction for 10 minutes at room temperature.

5. Place device on flatbed thermocycler for heat inactivation of lysis reagent, 10 minutes at 75°C.

6. Prepare RT-qPCR reagent as instructed in CellsDirect kit, with addition of Tween 20 surfactant.

    - SuperScript III RT/Platinum Taq Mix: 1.0 μL
    - 2X Reaction Mix (with ROX Reference Dye): 25 μL
    - 20X Taqman Primers/Probes 2.5 μL
    - Magnesium Sulphate: 1.0 μL
    - Tween (1%): 5.0 μL
    - Water: 5.5 μL
    - Lysate (already in device): 10 μL (equivalent)

7. RT-qPCR reagent is injected into device similar to final PCR steps in the heat lysis protocol presented above, and the device is placed in the custom flatbed thermocycler and imaging apparatus.

8. A one-step RT-qPCR reaction is performed by RT followed by qPCR without interruption or addition of reagents.

    - 50°C for 15 minutes
    - 95°C for 2 minutes
    - 40-50 cycles of 95°C x 15 seconds and 60°C x 30 seconds